INFORMATION TO USERS

This manuscript has been reproduced from the microfilm master. UMI films the text directly from the original or copy submitted. Thus, some thesis and dissertation copies are in typewriter face, while others may be from any type of computer printer.

The quality of this reproduction is dependent upon the quality of the copy submitted. Broken or indistinct print, colored or poor quality illustrations and photographs, print bleedthrough, substandard margins, and improper alignment can adversely affect reproduction.

In the unlikely event that the author did not send UMI a complete manuscript and there are missing pages, these will be noted. Also, if unauthorized copyright material had to be removed, a note will indicate the deletion.

Oversize materials (e.g., maps, drawings, charts) are reproduced by sectioning the original, beginning at the upper left-hand corner and continuing from left to right in equal sections with small overlaps.

ProQuest Information and Learning
300 North Zeeb Road, Ann Arbor, MI 48106-1346 USA
800-521-0600

THE INFLUENCE OF COMPETING SORBENTS ON THE DYNAMICS AND MECHANISMS OF METAL REACTIONS IN NATURAL SYSTEMS: A MULTI-SCALE APPROACH

by

Maarten Nachtegaal

A dissertation submitted to the Faculty of the University of Delaware in partial fulfillment of the requirements for the degree of Doctor of Philosophy in Plant and Soil Sciences

Summer 2003

THE INFLUENCE OF COMPETING SORBENTS ON THE DYNAMICS AND MECHANISMS OF METAL REACTIONS IN NATURAL SYSTEMS: A MULTI-SCALE APPROACH

by

Maarten Nachtegaal

Approved: Donald L. Sparks

Donald L. Sparks, Ph.D.
Chair of the Department of Plant and Soil Sciences

Approved: Robin W. Morgan

Robin Morgan, Ph.D.
Dean of the College of Agriculture and Natural Resources

Approved:

Conrado M. Gempesaw II, Ph.D.
Vice Provost for Academic Programs and Planning

I certify that I have read this dissertation and that in my opinion it meets the academic and professional standard required by the University as a dissertation for the degree of Doctor of Philosophy.

Signed: Donald L. Sparks

Donald L. Sparks, Ph.D.
Professor in charge of dissertation

I certify that I have read this dissertation and that in my opinion it meets the academic and professional standard required by the University as a dissertation for the degree of Doctor of Philosophy.

Signed: Yan Jin

Yan Jin, Ph.D.
Member of dissertation committee

I certify that I have read this dissertation and that in my opinion it meets the academic and professional standard required by the University as a dissertation for the degree of Doctor of Philosophy.

Signed: George W. Luther III

George W. Luther III, Ph.D.
Member of dissertation committee

I certify that I have read this dissertation and that in my opinion it meets the academic and professional standard required by the University as a dissertation for the degree of Doctor of Philosophy.

Signed: Andreas C. Scheinost

Andreas C. Scheinost, Ph.D.
Member of dissertation committee

I certify that I have read this dissertation and that in my opinion it meets the academic and professional standard required by the University as a dissertation for the degree of Doctor of Philosophy.

Signed: 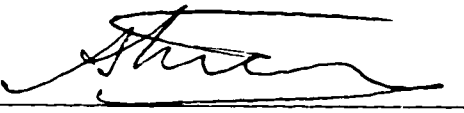

Andrew Teplyakov, Ph.D.
Member of dissertation committee

ACKNOWLEDGMENTS

In the summer of 1999 I landed as a foreigner on American soil. Much has changed in 4 years. I have made Delaware my home away from home. At the same time I started to appreciate the beauty of dirt and slowly but surely made soil science my field of expertise. This would never have happened as it was not for the great friendships and professional relations I built with many people at the University of Delaware. I owe an intense amount to Dr. Sparks for giving me the opportunity to earn my PhD degree in soil chemistry and advising and mentoring me for four years. These four years at the University of Delaware formed me not only as a researcher but also as a person. Dr. Sparks has built an excellent learning and research environment, in which students, postdocs and visiting scientist work closely together. I would also like to thank Jerry for his support and friendship for the last 4 years and for showing us the part of America we will miss the most. I would never have been able to write this dissertation without the feedback and scientific input of my fellow students and friends: Eef, Darryl, Derek, Chris and Kirk when I arrived at UD and Stefan, Markus, Dave, Kristin, Laura, Kristian and Jeff during the later part of my graduate studies.

Several people outside the University of Delaware have helped me collecting and understanding my data. My friend, Jeroen Sonke at the national high magnetic field lab, who helped collecting ICP-MS data and discussing results. During the numerous trips to the different national labs, Sue Wirrick and Chris Jacobsen at X1A, Kaumundi Pandya at X11A and Tony Lanzirotti at X26 made the trips to the NSLS a worthwhile and enjoyable experience. Matthew Marcus at the ALS helped me

tremendously with collecting and interpreting micro-EXAFS data. A big thanks to Ken Livi at John Hopkins.for helping me with the microprobe analysis and Raul Lobo with providing me with time on his XRD machine.

I would like to thank my friends and family at home who supported us throughout the years. Loes, Theo, Els, Bas, Wim and Dukke, thanks (bedankt) for your unending love and support. Thanks also to the new friends we made in Delaware, which made these four years in Delaware a worthwhile experience we will never forget.

Lastly, I am forever grateful to Magriet, my wife. It has been an incredible adventure for the two of us: moving to the states away from our families, adjusting to a new culture, earning our degrees, being apart during many meetings, beamline trips and visa problems, building new friendships and maintaining old ones. And we had a great time, thanks to your incredible positive energy and never ending love and support!

TABLE OF CONTENTS

LIST OF TABLES

LIST OF FIGURES

ABSTRACT

There is a gap in our current understanding of metal sorption mechanisms in multi-sorbent systems, where several competing mechanisms are available for metal uptake. In order to develop accurate risk assessments and effective remediation strategies, insights in the reaction pathways between first row transition elements and soils is of utmost importance. In this study, molecular scale spectroscopic and microscopic techniques were combined with macroscopic sorption and desorption studies to elucidate the intrinsic metal sorption mechanisms to soils and common reactive soil constituents, clay minerals, organic matter and iron oxides.

In a study to investigate the effect of humic acid coatings on the intrinsic Ni sorption mechanisms to the kaolinite surface, extended X-ray absorption fine structure (EXAFS) spectroscopic studies revealed that organic coatings do affect metal sorption, but do not change the intrinsic metal uptake mechanisms of the underlying clay mineral. At the pH of this study, 7.5, Ni was found to be incorporated into stable precipitates, formed at the kaolinite surface. A nickel hydroxide was formed in the presence of a 5-wt% organic coating, whereas in the presence of a 1-wt% organic coating, a more stable Ni-Al layered double hydroxide (LDH) was formed. Similarly, the mechanisms governing Zn uptake in a goethite coated kaolinite system were studied as a function of pH. Using EXAFS spectroscopy as a molecular tool to determine the Zn reaction mechanisms under conditions representative of natural soil and geochemical environments, it was found that at pH 5, Zn was mainly bound to the kaolinite edge sites. At pH 7, both the extent of the iron oxide coating and the reaction

time, determined the Zn sorption complex formed at the goethite-coated kaolinite interface. The dominant sorption mechanism was found to change from the initial formation of inner-sphere complexes with the goethite coating to the formation of a Zn-Al LDH surface precipitate at the kaolinite surface with increasing reaction time.

Speciation of Zn in a smelter contaminated soil was directly identified using state of the art molecular spectroscopic and microscopic tools. Comparison of the Zn speciation in the non-treated soil and the aluminosilicate- and compost- treated soil revealed no significant differences in speciation between the treated and non-treated soils 12 yrs after the application of the additives. Amorphous, neo-formed, Zn containing surface precipitates, Zn-Al LDH and Zn-phyllosilicates, made up 60 % of the total Zn fraction in these smelter contaminated soils. This finding is extremely important, since surface precipitates have not been previously considered when modeling Zn speciation in such multi-sorbent systems. Desorption studies however indicated that Zn-containing surface precipitates are only stable at near neutral pH and therefore the formation of metal containing surface precipitates did not lead to a permanent immobilization of the metal.

Synchrotron based X-ray microscopy, combined with C1s-near edge X-ray absorption fine structure (NEXAFS) spectroscopy, was applied to study the interactions of natural biopolymers with metals *in situ* and with high chemical and spatial sensitivity. It was learned that changes in the position of the C 1s(C=O) $\rightarrow$ $1\pi^*_{C=O}$ electronic transitions in the NEXAFS spectra could well be used to qualitatively describe metal interactions with specific functional groups of the biopolymers. These results can be used to assist in predicting the fate of metals in complex ligand mixtures.

Chapter 1

INTRODUCTION

1.1 RESEARCH MOTIVATION

Transition elements, Mn, Fe, Ni, Co and Zn in particular, are important nutrients when present at trace levels in the soil solution (Fráusto da Silva and Williams, 1991). At higher availabilities, these elements are often detrimental to the environment (Chaney, 1993). The flux by which transition elements are introduced into the environment by anthropogenic sources currently equals or exceeds the natural flux (Nriagu and Pacyna, 1988). The fate of potentially toxic metals in the environment is greatly dependent on their speciation in soils. It is often difficult to assess the speciation of a metal contaminant in a soil environment directly and thus many remediation efforts are based on the total contaminant metal burden or on sequential extractions which extract 'specific' metal fractions. Predictions based on this total or 'specific' metal fraction might not reflect the true speciation of the metal. Consequently, the mechanisms by which metals are sorbed/released in soils over time are not understood and often, technically and economically sound remediation strategies based on such predictions cannot be developed. Therefore, determining contaminant speciation is of utmost importance to insure the implementation of sound remediation strategies, to be able to predict contaminant stability in the soil over time, and to successfully model the fate of contaminants in the environment.

The (bio)availability of trace metals is dictated by reactions taking place at the soil solution-particle interface. Therefore, a complete understanding of long term trace element availability depends on knowing the adsorption and desorption reactions taking place at the soil particle surfaces. Adsorption reactions may involve electrostatic attractions between a solution ion and a charged surface (outer-sphere complex), a ligand exchange process, where a direct coordinative bond with surface functional groups is formed (inner-sphere complex) or the formation of a polynuclear metal cluster (Scheidegger et al. 1997).

Research predominantly done in the last decade has shown that when the amount of a metal cation on a surface increases to a high surface coverage, a precipitate of the cation can form with the ions of the mineral. When the precipitate covers the entire surface it is referred to as a "surface precipitate" and when the precipitate grows away from the surface before covering it, the term "surface cluster" is used (Sparks, 1995).

Laboratory sorption experiments, combined with state of the art synchrotron based X-ray absorption spectroscopy (XAS) to delineate the structure of the sorbed metal on the atomic scale, have shown that the incorporation of first row transition metals, i.e. Cr, Mn, Fe, Ni, Co, Cu and Zn in brucite like precipitates, formed on surfaces of clay minerals and Al oxides may play an important role in the immobilization of these metals in non-acidic soils (Fendorf et al. 1994; Junta et al. 1994; O'Day et al. 1994; Manceau et al. 1999; Scheidegger et al. 1997; Scheinost et al. 1999; Thompson et al. 1999; Ford et al. 2000; Schlegel et al. 2001). The structural

formula of these brucite like precipitates is generally written as $[Me^{2+}_{1-x}Me^{3+}_{x}(OH)_2]^{x+} \cdot (x/n)\ A^{n-} \cdot mH_2O$, where the metals (Me) occupy the octahedral layers and anions (A) in the interlayer are needed to compensate for the positive charge of the octahedral layers. These precipitates form below saturation conditions with respect to the formation of a bulk precipitate in solution and below theoretical monolayer coverage (Scheidegger 1997). An increased stability of the precipitate has been observed with increasing aging time (Ford et al. 1999; Scheckel et al. 2000) and thus the incorporation of first row transition elements in stable surface precipitates might lead to a long-term removal of the metal from the soil solution.

However, our ability to generalize the significance of this process in soils is limited to laboratory sorption studies only, where fractionated, well characterized clay mineral surfaces are used. In the soil environment mineral surfaces are often coated with organic or oxide coatings. These coatings may interfere with the intrinsic metal sorption mechanisms on clay minerals in several ways: First of all, the presence of organic or oxide coatings may alter the reactivity of the underlying clay mineral surface, by forming inner-sphere complexes with the highly reactive aluminol groups at the clay mineral edge sites and by modifying the electrical properties of the clay mineral-water interface (Templeton et al. 2001). Second of all, formation of metal organic complexes can reduce the availability of these metals for the formation of a precipitate phase. On the contrary, enhanced mineral dissolution by organic acids can lead to a larger availability of metals for the stabilization of a surface precipitate. Additionally, the metal uptake capacity of the coated clay mineral is significantly

higher than that of the clay mineral surface itself, due to the larger surface area and cation exchange capacity (CEC) of the coated complex.

An additional problem with organic coatings is that very little is actually known on soil organic matter (SOM) itself, including its macromolecular structure and genesis, and on how SOM reacts with metals, i.e. what functional groups are involved in metal binding and what is their binding affinity for metals.

To successfully model and predict the fate of metals in soils and sediments on which sound remediation strategies can be based, insights into the effects of organic and oxide coatings on the intrinsic metal sorption to the kaolinite surface and into larger scale (field scale) processes are crucial. Additionally, a fundamental insight into metal complexation by SOM is still largely needed.

The remainder of this chapter consists of four sections. In section 1.2 the general mechanisms by which transition metals are sorbed to individual soil components will be briefly discussed, including the experimental setup, which is defined by the solid phase/metal combination, the experimental conditions (e.g. metal concentration, type and concentration of the background electrolyte, pH), and the time scale employed at which the different sorption complexes are formed. Emphasis will be placed on the mechanisms and kinetics of surface precipitate formation, since the incorporation of transition metals into stable precipitate phases can potentially reduce the long-term bioavailability of these metals. In section 1.3 the limited studies on metal sorption in multi-sorbent systems will be reviewed. In the next section the

application of synchrotron based XAS as a spectroscopic tool to study metal sorption complexes formed in multi-sorbent systems will be reviewed. In section 1.5, the objectives of this dissertation research will be presented.

1.2 Metal speciation in single sorbent systems

As stated earlier, understanding metal availability in soils depends on knowing the speciation (the chemical form) of the metal in the soil solution. The speciation of metals in soils is mainly determined by the solution conditions (i.e. pH, ionic strength, Eh and presence of other cations/anions in solution) and by interactions of the metals with solid particles. Metals can be freely available and in different oxidation states in the soil solution. At certain pH and ionic strength conditions, metals may form complexes with anions from the soil solution, such as $Me(OH)_2$ (neutral complex), $Me(OH)^+$ (positive complex), MeL^- (negative complex), etc. (Stumm and Morgan, 1996).

One can distinguish between the following sorption mechanisms: absorption, adsorption, bulk precipitation and surface precipitation. Sorption is a general term that should be used when the retention mechanism at a surface is not known (Sparks, 1995).

Absorption of a trace metal can be defined as the retention of a metal within a particle. Absorption plays a major role in sorption of metals by soil organic matter

(SOM) and hydrous ferric oxides, where the metals can diffuse into inter-particle voids (Stevenson, 1994; Schwertmann et al., 1985).

Adsorption of a trace metal is defined as the accumulation of the metal at an interface between the solid surface and the bathing soil solution. Both physical and chemical forces are involved in adsorption of metals from solution. Physical forces include van der Waals forces (e.g. partitioning) and electrostatic outer-sphere complexes (e.g. ion exchange). Chemical forces result from short-range interactions that include inner-sphere complexation (ligand exchange, covalent bonding and hydrogen bonding) (Stumm and Morgan, 1996).

1.2.1 Metal partitioning to clay minerals

In soil science, the term "cation exchange" is used to characterize the replacement of one adsorbed, readily exchangeable cation by another (Sposito, 1989). Cation exchange is not a chemical reaction in the usual sense, since the bonds broken and formed are long-range electrostatic bonds of low energy (McBride, 1994). Electrostatic bonding of metal ions to clay minerals occurs mainly at planar sites of permanent structural charge and is therefore pH independent. Only for clay minerals with low structural charge (e.g. kaolinite or pyrophyllite) does significant electrostatic bonding at the clay edge sites of variable charge take place. In these systems electrostatic bonding is pH dependent (Stumm and Morgan, 1996; Sparks, 1995)

The Me^{n+}-Na^{+} exchange, where Me^{n+} is a metal cation with valence n, can be described as (McBride, 1994):

$$Me^{n+} + nNa^{+}\text{-clay} \leftrightarrow Me^{n+}\text{-clay} + nNa^{+} \quad (1)$$

The selectivity coefficient (K_s) can be written:

$$K_s = ([Na]^n (N_{Me}) / ([Me](N_{Na})^n) \quad (2)$$

where [Na] and [Me] represent the molarity of the metals in solution, and N_{Na} and N_{Me} symbolize the fraction of clay exchange sites occupied by Na^+ and Me^{n+}. Equation (1) shows that multivalent cations effectively replace monovalent cations from clay exchange sites when the monovalent cation concentration is low.

Ion exchange reactions at surface sites exposed to solution are extremely fast. In fact, the kinetics of cation exchange has not generally been accessible to measurements by conventional methods. Cation exchange on clays without narrow interlayer regions (e.g. kaolinite) appears to be instantaneous (McBride 1994). With 2:1 clay minerals that contain both external and internal exchange sites, particularly with vermiculite and micas where partially collapsed interlayer sites exist, the kinetics are slower (Sparks, 1995). This is due to the presence of exchange sites of low accessibility on these clay minerals; the actual "chemical" process of cation exchange itself, however, is fast also on these sites.

Chemisorption (also called specific sorption) involves the formation of a covalent bond between a metal and the clay surface and leads to the formation of an inner-sphere metal complex. The edges of layer silicate clays provide surface sites for the chemisorption of transition and heavy metals. The sorption site presented to the metal in solution is a valence-unsatisfied OH^- or H_2O ligand bound to a metal ion

(Al^{3+} or Si^{4+}). For example, on the octahedral aluminum sites, a trace metal, Me, may bind according to the reaction:

$$[>Al\text{-}OH]^{-1/2} + Me(H_2O)_6{}^{n+} \rightarrow [>Al\text{-}O\text{-}Me(H2O)_5]^{(n-3/2)+} + H_3O^+ \quad (3)$$

This reaction has at least four features that distinguish it from cation exchange (McBride, 1994):

1. Release of n H^+ ions for each Me^{n+} cation chemisorbed
2. A high degree of specificity shown by particular minerals for particular trace metals
3. Tendency toward irreversibility, or at least a desorption rate that is orders of magnitude slower than the adsorption rate
4. A change in the measured surface charge toward a more positive value.

This last feature implies that the adsorbed metal and its charge become part of the mineral surface, thereby shifting the point of zero charge (PZC) to higher pH.

Chemisorption of metals generally becomes more specific as the solution pH increases; i.e., formation of inner-sphere complexes is favored at elevated pH and ionic strength (Elzinga, 1999; Koppelman, 1977; Scheidegger, 1998; Strawn, 1998). Chemisorption of metal cations on clay minerals is slower than cation exchange, often increasing gradually over several days. Trace metal cations chemisorbed on clays gradually lose much of their initial lability (as measured by diminishing self-exchange

rates) over a period of days. Consequently, trace metal chemisorption on clay minerals is considered to be highly irreversible (McBride, 1994).

Precipitation is defined as the process of depositing a substance from the soil solution (Sparks, 2000). As the concentration of an ion in a solution is increased, precipitation of a new solid phase will not occur until the solubility product of that phase has been exceeded (McBride, 1994). The status of the solution phase with respect to precipitation can be quantified by comparing the ion productivity product (IAP) to the thermodynamic solubility product of the crystalline phase, K_{SO}. When $IAP/K_{SO} < 1$, the solution is undersaturated with respect to the solid phase; when $IAP/K_{SO} > 1$ the solution is oversaturated with respect to the solid phase (Stumm and Morgan, 1996). Some degree of supersaturation is required for precipitation to occur because crystal nuclei can only be formed after an energy barrier is overcome. In clay and soil solutions, the energy barrier to nucleation is reduced because mineral surfaces can act as seed crystals. This reduces the extent of supersaturation necessary for precipitation to be initiated (Stumm and Morgan, 1996; McBride, 1994).

Macroscopically, chemisorption reactions, which are two-dimensional surface processes, can rarely be separated experimentally from the three-dimensional precipitation reactions. Precipitation reactions are often much slower than sorption reactions so that time dependent sorption of metals and other ions is often characteristic of precipitation in soils (McBride, 1994).

When the amount of a metal cation or anion (negatively charged metal complex) on a surface increases to a high surface coverage, a precipitate of the cation or anion can form with the ions of the mineral. This three-dimensional growth mechanism is known as surface precipitation (Sparks, 1995). At low surface coverages surface complexation dominates, when surface coverage increases nucleation occurs or distinct entities or aggregates form on the surface.

Surface induced precipitation occurs below monolayer coverage of the surface and at solution conditions undersaturated with respect to homogeneous precipitation. A proposed pathway for the formation and stabilization of Ni surface precipitates on clay minerals is the following. Initially a Ni-hydroxide phase forms at the mineral surface, well below super saturation. Or when Al is present in solution, Al co-precipitation with Ni is thermodynamically preferred. This precipitation may be explained by the combination of several processes (Yamaguchi et al., 2001). First, the electric field of the mineral surface attracts Ni ions through adsorption, leading to a local supersaturation at the mineral-water interface. Second, the solid phase may act as a nucleation center for polyhydroxy species and catalyze the precipitation process (McBride, 1994). Third, the physical properties of water molecules adsorbed at the mineral surface are different from those of free water (Sposito, 1989), potentially causing a lower solubility of metal hydroxides at the mineral-water interface.
With time Al, which is released by weathering of the mineral surface, slowly diffuses into the octahedral layer and partly replaces Ni in the octahedral sites. A so-called Ni-Al layered double hydroxide (LDH) is formed, which is thermodynamically favored

over α-Ni hydroxide. This Ni-Al LDH is more resistant to weathering than the Ni-hydroxide originally formed.

Further stabilization of the precipitate can occur by diffusion of Si polymers in the interlayer space of the LDH, thereby replacing the anions. Polymerization and condensation of the interlayer Si polymers slowly transforms the LDH into a precursor Me-Al phyllosilicate, which might further develop into a tri-octahedral clay. Stabilization also occurs in precipitates formed on Al-free substrates. This stabilization is contributed to increasing crystallinity with time, so called Ostwald ripening (Ford et al., 1999).

Insights on the mechanisms of surface precipitate formation and stabilization have been gained from batch and molecular scale sorption studies with only one sorbent present. A shortcoming of the current studies is that little is known on how organic matter or oxides interfere with this sorption process. These sorbents are ubiquitous in soils, have a high surface area and metal binding capacity, and occur often as coatings on clay minerals. For these reasons these sorbents are major competitors for metal sorption on clay mineral surfaces.

1.2.2. Metal partitioning to SOM

SOM, or humic substances (HS) or biopolymers, are described as the total of high molecular weight organic compounds in soils excluding undecayed plant and animal tissues, their "partial decomposition" products, and the soil biomass

(Stevenson, 1994). As this definition suggests, very little is actually known about humic substances, including the macromolecular or 'backbone' structure of HS and its genesis (Stevenson, 1994; Sparks, 1995). Humic substances however make up 0.5-5 wt% in mineral soils and almost 100 wt% in peat (Sparks, 1995). The surface area and cation exchange capacity (CEC) of SOM are higher than those of clay minerals. It has been estimated that up to 80% of the CEC of soils is due to organic matter (Stevenson, 1994). The point of zero charge (pzc), defined as the pH at which the colloidal particle has no net charge, is low, about 3, therefore SOM is negatively charged at pH values greater than 3. HS often occur as coatings on mineral surfaces, thereby masking the mineral surface from solution. And HS play an important role in colloid facilitated transport. These points illustrate that any increase in our fundamental understanding of the macromolecular structure of HS, and their reactivity towards contaminants could greatly enhance our understanding of contaminants in the environment.

Historically, HS are operationally divided into humic acids, fulvic acids and humin. The organic matter fraction, which can be isolated from a soil by treating the soil with a light base solution and then acidifying the supernatant so that a precipitate formed, is called humic acid. The fraction which remains in solution, even after acidifying, is called fulvic acid. The organic matter fraction, which stays in soils after these treatments, is called humin. Humic acids are by far the largest fraction of humic substances. Humic substances provide slow release sources of N, P and S for plants. In addition they contribute to cation retention on the soil (Stevenson 1994).

A successful approach to understanding the reactivity of HS towards metals, independent of the overall macromolecular structure of HS, is based on the functional group content of the HS, since functional groups can be determined and ultimately determine the reactivity of the HS. Traditionally the functional group content of HS has been determined by wet chemical methods; recently nuclear magnetic resonance (NMR) spectroscopy has become available for (semi-) quantitative analysis of the functional groups of HS. A variety of functional groups, of both acidic and basic nature have been reported in humic substances. Due to their acidic nature and abundance, carboxylic and phenolic groups are the most important metal complexing sites on HS (Stevenson, 1994).

An attempt to predict the types of interactions between metal ions and organic ligands is based on the concept of 'hardness' and 'softness' of metals and electron-donor atoms of complexing sites (Pearson, 1963; Buffle and Stumm, 1994). Hard cations, such as alkali and alkaline earth metals interact via electrostatic, ionic reactions, while soft cations, such as Pb^{2+}, Cu^{+}, Zn^{2+} and Cd^{2+} react to form covalent bonds. Metals such as Mn^{2+}, Fe^{2+}, Co^{2+}, Ni^{2+} and Cu^{2+} form complexes of intermediate strength. The degree of hardness can be determined from the term Z^2/r, where Z and r are the charge and radius of the cation, respectively. The preference of hard metals for ligand atoms decreases in the following order: F > O > N ~Cl > Br > I > S. This order is reversed for soft metal ions. Thus hard donor atoms such as F and O prefer hard metal ions, while soft donor atoms such as I and S prefer soft metals.

These predictions only partly hold true in explaining the observed metal partitioning to HS. Decades of research have produced a wealth of data on metal partitioning to HS, using a range of macroscopic and spectroscopic techniques. Every technique has its advantages and disadvantages. Thermodynamic modeling of metal titration curves for example is difficult, since the complex ligand mixture produces no sharp equivalence points (Purdue 1985). Almost any function will fit the data points in a typical metal titration curve. Electron paramagnetic resonance (EPR) spectroscopy was the first spectroscopic technique applied to study metal complexation with HS (McBride 1987). Only a few metals, Cu, Mn and Fe are paramagnetic. Senesi and co-workers (1988, 1991) found, using EPR, that Fe^{III} binds more strongly to carboxylic groups than Cu^{II} which binds much stronger than Mn^{II}. Extended X-ray absorption fine structure (EXAFS) spectroscopy has also been applied to study metal partitioning to HS (Xia et al. 1997). The disadvantage of studying heavy metal – HS interactions with EXAFS spectroscopy is that C/N/S are weak backscatterers for heavy metal atoms and thus second shell features are not very well resolved (Nachtegaal and Sparks, 2003). NMR has been largely applied to study carbon group functionalities in HS. NMR can however not be used to study HA *in situ*, i.e. in the natural environment, because the presence of paramagnetic elements, such as Fe leads to broadening of the spectra. And as is true for all of these techniques, no simultaneous information on the chemistry and the spatial distribution of functional groups or the metal can be obtained.

Based on the disadvantages of the currently available techniques to study HS-metal complexation, it is worthwhile to explore the possibilities of a relatively new spectroscopic technique, synchrotron-based near edge X-ray absorption fine structure (NEXAFS) spectroscopy, to answer some of the fundamental questions on HS. Similarly to NMR, NEXAFS has capabilities of probing the main functional groups of HS, with no metals such as Fe adversely influencing the spectral quality. C1s-NEXAFS spectroscopy has been applied to study the bonding environment of C in complex macromolecules, such as polymers, coal and humic acid (Myneni 2003). The C-NEXAFS inner-shell spectrum reveals the manifold of excited states available for the photoexcited electrons. These excited states are well described by the lowest unoccupied molecular orbitals (LUMOs) of organic functional groups. Combining NEXAFS spectroscopy with X-ray microscopy gives the added advantage of being able to study the distribution of C containing functional groups in solution.

1.2.3 Metal partitioning to iron oxides

Iron oxides (ferrihydrite, hematite and goethite) are major components in most soils (Jambor, 1998; Schwertmann et al., 1985). Due to the large surface area of these oxides (~60-200 m^2/g), many internal surface sites, the presence of these oxides as coatings on clay particles, and high reactivity, these oxides are a potential competitor for the formation of surface precipitates as a sink for heavy metals.

Iron oxides can sorb metals both by adsorption and by incorporation of the metals in the crystal structure upon aging. Ford et al. (1997) for example, studied

metal partitioning during hydrous iron oxide aging. They found that coprecipitated Ni and Mn became less extractable after ferrihydrite transformation to goethite, while Pb and Cd showed net desorption with aging, and sorption reversibillity remained essentially unchanged. Martinez and McBride (1998) studied the coprecipitation of Cd, Cu, Pb and Zn in iron oxides. Although the experimental conditions employed were favorable for the homogeneous distribution of metals throughout the coprecipitate, Electron Microscope Analyses (EMPA) suggest that Cu and Zn segregation within aggregates of aged hydrous ferric oxides (to goethite and hematite) occurs.

In a few studies (Grossl et al., 1997; Lützenkirchen et al., 1997), metal adsorption to crystalline iron oxides such as goethite and hematite has been found to be independent of ionic strength, thus suggesting inner-sphere complexation. Pressure-jump relaxation (Grossl et al., 1994, 1995, 1997) and XAS (Bargar et al., 1998, Schlegel et al., 1997, Trivedi et al. 2001) studies, employed to elucidate the reaction kinetics and mechanisms for metal adsorption to the goethite surface confirmed that inner sphere sorption complexes are being formed. Overall, metal affinities for goethite follow the following order Cu > Pb > Zn > Cd > Co > Ni > Mn > Ca > (Coughlin and Stone, 1995; McKenzie, 1980; Schwertmann et al., 1989), which is consistent with the trend in electronegativity of the metals (Schwertmann et al., 1989).

Coughlin and Stone (1995) found an increasingly stable fraction of Co, Ni and Cu sorbed to goethite with aging. It was proposed that, similar to the formation of Me-

Al LDH precipitates on clay mineral surfaces, microscale formation of metal spinels, $(Me^{2+}, Fe^{2+})Fe^{3+}{}_2O_4$, at the goethite surface may have caused the net increase in sorption and the subsequent decrease in the ability to desorb partitioned metals.

1.3 Metal speciation in multi-sorbent systems

The degree to which heavy metals partition to clay minerals, organic matter and metal oxides ultimately controls their fate and bioavailability in the soil system. The sorption behavior of the individual soil components, under different reaction conditions is reasonably well understood. However, soils are highly heterogeneous systems. Prediction of the fate of a contaminant in real soil systems based on the sorption studies to single sorbent systems is highly questionable, since in most mineral soils, organic matter and hydrous ferric and manganese oxides are intimately associated with the clay minerals. Accordingly, clay and organic matter function more as a unit than as separate entities and the relative contribution of organic and inorganic surfaces to adsorption will depend on the extent to which the clay is coated with organic substances. For soils with similar clay and organic matter contents, the contribution of organic matter to the binding of trace elements was found to be highest when the predominant clay mineral is kaolinite and lowest when montmorillonite is the main clay mineral (Stevenson, 1994).

Only a few studies exist that used spectroscopic techniques to elucidate metal sorption mechanisms in multi sorbent systems. Martinez and McBride (1999) investigated metal sorption to both the invidual sorbents iron oxide and HA (extracted from leaf compost) and their mixture using EPR spectroscopy. After aging for 200 days, Cd and Zn were equally well retained by the iron oxide and the mixture, while initially they were sorbed better by the oxides than by the mixture. Cu solubility decreased in the ferric oxide and increased in the organic matter system upon aging. Lead solubility remained very low in all systems. Pb and Cu were mostly complexed by the nonlabile organo complexes, while Zn and Cd were found more in the labile fraction. Using XAS as spectroscopic tool to elucidate the sorption complexes formed at a HA coated goethite surface, Alcacio et al. (2001) found that Cu(II) sorbs to both goethite and HA at low HA concentrations and to the organic groups of the HA at higher coating levels.

Yamaguchi et al. (2001) studied the sorption of Ni to gibbsite and pyrrophyllite in the presence of citrate and salicylate. These small organic acids suppressed both Ni removal from solution and the formation of a surface precipitate at pH 7.5, which was attributed to strong complexation of the metals by the small organic acids. The small organic acids are used as substitute for humic substances, which are complex organic molecules. Interestingly, a study by Zachara et al. (1994) on Co^{2+} sorption by a subsurface mineral separate showed that the presence of a humic acid coating augmented, rather than changed the intrinsic adsorption behavior of the mineral sorbents. This indicates that humic substances, especially when coated onto mineral

surfaces might have a different impact on Ni uptake behavior than small organic molecules.

A study on Ni sorption on the clay fraction of a Matapeake silt loam, with and without a small organic fraction (~ 1 wt%), suggested that Ni-Al layered double hydroxides (Ni-Al LDH) can be formed in soils (Roberts, 1999). In these experiments, formation of a Ni surface precipitate was not observed at pH 6 in contrast to systems aged at pH 6.8 and 7.5. These results stress the importance of verifying the potential for surface precipitation in soils. However, identification of these phases in whole soils may be difficult, due to limitations of the spectroscopic techniques employed to separate different phases in multi component systems. The ability to ascertain the generality of the formation of these stable phases can be improved by examining the effect of competitive surfaces in the soil matrix.

1.4 The role of (micro focused) XAS in elucidating metal sorption mechanisms

X-ray absorption spectroscopy (XAS) is commonly divided into the extended X-ray absorption fine structure (EXAFS) region (> 30 eV above the absorption edge) and the X-ray absorption near edge spectroscopy (XANES) or near-edge X-ray absorption fine structure (NEXAFS) (region between 30eV below and above absorption edge). There is no fundamental distinction between the physics of EXAFS and XANES other than the complexity of the spectra arising from the dominant electronic processes in each region. For this reason EXAFS and XANES are referred to jointly under the terms

XAS. The primary role of synchrotron based XAS in environmental studies is to help delineate the different sorption complexes formed at the particle-solution interfaces. Information obtained from XAS analysis include the oxidation state of the target metal, identification of nearest neighbours around the central metal atom, and coordination number and bond distances to the nearest neighbours. The major advantage of XAS over other spectroscopic techniques such as XPS and energy dispersive spectroscopy (EDS) is that samples can be studied *in situ*, without any sample alteration.

When attempting to study metal speciation in heterogeneous systems using XAS, one must realize that standard (bulk) XAFS probes an area of several millimeters in a sample, where Zn could be present in multiple phases. When Zn is present in multiple phases, the atomic shells from the different species overlap so that one cannot separate them out when there is a mixture (Manceau et al. 2003). With the advent of high-brilliance synchrotron radiation sources, it is now possible to identify metal species in dilute concentrations with high spatial resolution, using μ-focused extended EXAFS. When probing only a small area of a sample, typically several square micrometers, one can minimize the number of species contributing to the overall spectrum. By treating the μ-EXAFS spectra of the unknown sample as a whole, i.e. fitting linear combinations of reference spectra to the unknown spectra, one can than deconvolute up to three major species contributing to the overall spectrum. The success of such a fitting approach depends on the availability of all unknown species in the reference database. Even when a large database of reference spectra is available and a good fit is

achieved, there is some doubt whether a unique solution is achieved (Wasserman 1999). By collecting a great number of spectra of the sample one can use principal component analysis (PCA) to determine how many independent components are needed to reproduce the complete dataset.

Although μ-focused EXAFS has great potential to probe the Zn speciation in soils, it has only been applied in some limited cases. Both bulk and μ-focused XAFS analyses were performed on the surface and subsurface layers of a smelter contaminated soil (Roberts et al., 2002). These soils did not receive any pretreatments and the pH was around 5. XAFS revealed that the Zn distribution in the surface soil consisted of approximately 66% franklinite and 34% sphalerite (ZnS), material aerially deposited from the smelter. Zn in the subsurface soil was dominated by sorption complexes to Al-bearing minerals and to a lesser extent to Fe oxides. More labile outer-sphere complexes were also present in this sample.

By collecting polarized EXAFS spectra of a separated soil clay fraction, Manceau et al. (2000) found that Zn is partly incorporated into neo-formed phyllosilicate phases formed in an area near a former Zn smelter in Belgium. This is the first and only study so far, indicating that Zn surface precipitation can be an important sorption mechanism of metals in heavily contaminated areas.

Soils around the historic Maatheide smelting facility in Belgium have been exposed to deposition of metals for years. The soils in the vicinity around the smelter were contaminated with Zn in concentrations up to several thousand parts per million

and thus provide an ideal place to study the importance of surface precipitates. Severe phytoxicity and subsequent soil erosion have resulted in 135 ha of bare land, after 80 years of Zn smelting. Twelve years ago, a remediation project was started to *in situ* remediate the soil (Vangronsveld et al. 1995). This is one of the longest running *in situ* remediation projects in the world, which makes it a perfect place to study the importance of surface precipitates in reducing the bioavailability of Zn.

1.5 OBJECTIVES OF DISSERTATION RESEARCH

The goal of my dissertation research was to obtain a fundamental understanding of the reactions that first row transition metals undergo in multi-sorbent systems, in which a variety of sorption mechanisms are available for metal uptake. To successfully model and predict the fate of metals in soils and sediments, insights into the competiveness of available sorption mechanisms is crucial. Emphasis is placed on understanding the formation and stabilization mechanisms of metal containing surface precipitates in such heterogeneous systems, since these surface precipitates might contribute to a significant reduction of the bioavailability of the metal in the environment. The overall strategy for this research was to combine macroscopic adsorption and desorption experiments with *in situ* spectroscopic and microscopic techniques to gain molecular-scale insight into metal sorption mechanisms.

Specifically the objectives of this dissertation research were:

1) To determine the effect of two coatings, an organic (humic acid) and an iron oxide (goethite) coating, on intrinsic metal (Ni and Zn) sorption mechanisms, including surface precipitation, to the underlying kaolinite surface.
2) To determine the Zn speciation and presence of surface precipitates in remediated and non remediated Zn contaminated smelter soils using state of the art micro-focused spectroscopic analysis.
3) To ascertain the mechanisms of metal-humic substance interactions using novel scanning transmission X-ray microscopy and C-NEXAFS spectroscopy.

1.6 REFERENCES

Alcacio T.E., D. Hesterberg, J.W. Chou, J.D.Martin, S. Beauchemin and D.E. Sayers. 2001. Molecular scale characteristics of Cu(II) bonding in goethite-humate complexes. *Geoch. Cosmochim. Acta* **65:** 1355-1366.

Bargar, J.R., G.E. Brown Jr. and G.A Parks. 1998. Surface complexation of Pb(II) at oxide-water ineterfaces, III XAFS determination of Pb(II) and Pb(II)-chloro adsorption complexes on goethite and alumina. *Geochim. Cosmochim. Acta* **62:** 193-207.

Buffle, J. and W. Stumm. 1994. General chemistry of aquatic systems, *In*: J. Buffle and RR. DeVitre (eds). Biological regulation of aquatic systems. CRC Press, Boca Raton, Fl.

Chaney, R.L. 1993. *In*: Robson, A.D. (eds). p. 135. Zinc in Soils and Plants. Kluwer Academic Publishers, the Netherlands.

Coughlin, B.R. and A.T. Stone. 1995. Nonreversible adsorption of divalent metal ions (MnII, CoII, NiII, and PbII) onto goethite, effects of acidification, FeII addition, and picolinic acid addition. *Environ. Sci. Technol.* **29:** 2445-2450.

Elzinga, E.J. and D.L. Sparks. 1999. Nickel sorption mechanisms in a pyrophyllite – montmorillonite mixture. *J. Colloid Interface Sci.* **213:** 506-512.

Fendorf, S.E., G.E. Lamble, M.G. Stapleton, M.J. Kelley and D.L. Sparks. 1994. Mechanisms of chromium (III) sorption on silica. 1. Cr(III) surface structure derived by extended X-ray absorption fine structure spectroscopy. *Environ. Sci. Technol.* **28:** 284-289.

Ford, R.G., P.M. Bertsch, and K.J. Farley. 1997. Changes in transition and heavy metal partitioning during hydrous iron oxide aging. *Environ. Sci. Technol.* **31:** 2028-2033.

Ford, R.G., A.C. Scheinost, K.G. Scheckel and D.L. Sparks. 1999. The link between clay mineral weathering and the stabilization of Ni surface precipitates. *Environ. Sci. Technol.* **33:** 3140-3144.

Ford, R.G., and Sparks, D.L. (2000) The nature of Zn precipitates formed in the presence of pyrophyllite. *Environ. Sci. Technol.* **34,** 2479-2483.

Fráusto da Silva, J.J.R. and R.J.P. Williams. 1991. The biological chemistry of the elements. Oxford University Press Inc.. New York.

Grossl, P.R., and D.L. Sparks. 1994. Rapid kinetics of Cu(II) adsorption/desorption on goethite. *Environ. Sci. Technol.* **28:** 1422-1429.

Grossl, P.R., and D.L. Sparks 1995. Evaluation of ion adsorption/desorption kinetics on goethite using pressure-jump relaxation kinetics. *Geoderma* **67:** 87-95.

Grossl, P.R., M. Eick, D.L. Sparks and C.C. Ainsworth. 1997. Evaluation of contaminant ion adsorption/desorption kinetics on goethite. 2. Kinetic evaluation using a pressure-jump relaxation technique. *Environ. Sci. Technol.* **31:** 321-329.

Jambor, J.L. and J.E. Dutrizac. 1998. Occurrence and constitution of natural and synthetic ferrihydrite, a widespread iron oxyhydroxide. *Chem. Rev.* **98:** 2549-2585.

Junta, J.L. and M.F. Hochella Jr. 1994. Manganese(II) oxidation at mineral surfaces: A microscopic and spectroscopic study. *Geochim. Cosmochim. Acta* **58:** 4985-4999.

Koppelman, M.H. and J.G. Dillard. 1977. A study of the adsorption of Ni(II) and Cu(II) by clay minerals. *Clay Clay Minerals* **25:** 457-462.

Lützenkirchen, J. 1997. Ionic strength effects on cation sorption to oxides, macroscopic observations and their significance in microscopic interpretation. *J. Colloid Interface Sci.* **195:** 149-155.

Manceau, A., M. Schlegel, K.L. Nagy and L. Charlet. 1999. Evidence for the formation of trioctahedral clay upon sorption of Co^{2+} on Quartz. *J. Colloid Interface Sci.* **220:** 191-197.

Manceau, A., B. Lanson, M.L. Schlegel, J.C. Hargré, M. Musso, L. Eybert-Bérard, J.-L. Hazemann, D. Chateigner and G.M. Lamble. 2000. Quantitative Zn speciation in smelter-contaminated soils by EXAFS Spectroscopy. *Am. J. Sci.* **300:** 280-343.

Manceau A., M.A. Marcus and N. Tamura. 2003. Quantitative speciation of heavy metals in soils and sediments by synchrotron X-ray techniques. *In* N.C. Sturchio, P. Fenter, S.R. Sutton and M.L. Rivers (eds.) Applications of Synchrotron Radiation in Low-Temperature Geochemistry and Environmental Science. Reviews in Mineralogy. Mineralogical Society of America. Washington. D.C.

Martinez, C.E. and M.B. McBride. 1998. Coprecipitates of Cd, Cu, Pb and Zn in iron oxides: Solid phase transformation and metal solubility after aging and thermal treatment. *Clays Clay Miner.* **46:** 537-545.

Martinez, C.E. and M.B. McBride. 1999. Dissolved and labile concentrations of Cd, Cu, Pb, and Zn in aged ferrihydrite-organic mater systems. *Environ. Sci. Technol.* **33:** 745-750.

McBride M.B. 1994. Environmental Chemistry of Soils. Oxford University Press. New York.

McKenzie, M.B. 1980. The adsorption of lead and other heavy metals on oxides of manganese and iron. *Aust. J. Soil. Res.* **18:** 61-72.

Myneni S.C.B. 2003. Soft X-ray spectroscopy and spectromicroscopy studies of organic molecules in the environment. *In* N.C. Sturchio, P., S.R. Fenter, M.L. Sutton and M.L. Rivers (eds.) Applications of Synchrotron Radiation in Low-Temperature Geochemistry and Environmental Science. Reviews in Mineralogy. Mineralogical Society of America. Washington. D.C.

Nachtegaal, M. and D.L. Sparks. 2003a. Nickel sequestration in a kaolinite-humic acid complex. *Environ. Sci. Technol.* **37:** 529-534.

Nriagu J.O., and J.M. Pacyna. 1988. Quantitative assessment of worldwide contamination of air, water and soils by trace metals. *Nature* **333:** 134-139

O'Day, P.A., G.A. Parks and G.E. Brown Jr.. 1994. Molecular structure and binding sites of cobalt(II) surface complexes on kaolinite from X-ray absorption spectroscopy. *Clays Clay Miner.* **42:** 337-355.

Pearson, R.G. 1963. Hard and soft acids and bases. *J. Am. Chem. Soc.* **85:** 3533-3539.

Perdue, E.M. and C.R. Lytle. 1983. Distribution model for binding of protons and metal ions by humic substances. *Environ. Sci. Technol.* **17:** 654-660.

Roberts, D.R., A.M. Scheidegger and D.L. Sparks. 1999. Kinetics of mixed Ni-Al precipitate formation on a soil clay fraction. *Environ. Sci. Technol.* **33:** 3749-3754.

Roberts, D.R., A.C. Scheinost and D.L. Sparks. 2002. Zinc speciation in a smelter-contaminated soil profile using bulk and microspectroscopic techniques. *Environ. Sci. Technol.* **36**: 1742-1750.

Scheckel K.G., A.C. Scheinost, R.G. Ford and D.L. Sparks. 2000. Stability of layered Ni hydroxide surface precipitates - A dissolution kinetics study. *Geochim. Cosmochim. Acta* **64**: 2727-2735.

Scheidegger A. M., G. M. Lamble and D. L. Sparks. 1997. Spectroscopic evidence for the formation of mixed-cation hydroxide phases upon metal sorption on clays and aluminum oxides. *J. Colloid Interface Sci.* **186:** 118-128.

Scheidegger, A.M., D.G. Strawn, G.M. Lamble and D.L. Sparks. 1998. The kinetics of mixed Ni-Al hydroxide formation on clay and aluminum oxide minerals: A time-resolved XAFS study. *Geochim. Cosmochim. Acta* **62:** 2233-2245.

Scheinost, A.C., R.G. Ford and D.L. Sparks. 1999. The role of Al in the formation of secondary Ni precipitates on pyrophyllite, gibbsite, talc, and amorphous silica: a DRS study. *Geochim. Cosmochim. Acta* **63:** 3193-3203.

Schlegel, M.L., A. Manceau and L. Charlet. 1997. EXAFS study of Zn and ZnEDTA sorption at the goethite (α-FeOOH)/water interface. *J. Phys. IV* **7**: 823-824.

Schlegel, M.L., A. Manceau, L. Charlet and J.-L. Hazemann. 2001. Adsorption mechanisms of Zn on hectorite as a function of time, pH, and ionic strength. *Am. J. Sci.* **301:** 798-830.

Schwertmann, U. and R.M. Taylor 1989. Minerals in Soil Environments, 2nd edition. SSSA book series no.1. Soil Science Society of America, Wisconsin, WI.

Senesi, N. and G. Calderoni. 1988. Structural and chemical characterization of copper, iron and manganese complexes formed by paleosol humic acids. *Org. Geochem.* **13:** 1145-1152.

Senesi N., G. Spostio, G.R. Bradford and K.M. Holtzclaw. 1991. Residual metal reactivity of humic acids extracted from soil amended with sewage-sludge. *Water Air Soil Pol.* **55:** 409-425.

Sparks D.L. 1995. Environmental Soil Chemistry. Academic Press, Inc. London.

Sposito, G.A. 1984. The surface chemistry of soils. New York, Oxford University Press.

Stevenson, F.J. 1994. Humus chemistry, genesis, composition, reactions. Wiley & Sons Inc.

Strawn, D.G., A.M. Scheidegger and D.L. Sparks. 1998. Kinetics and mechanisms of Pb(II) sorption and desorption at the aluminum oxide-water interface. *Environ. Sci. Technol.* **32:** 2596-2602.

Stumm, W. and J.J. Morgan. 1996. Aquatic Chemistry. Wiley. New York.

Templeton, A.S., T.P. Trainor, S.J. Traina, A.M. Spormann and G. E. Brown Jr.. 2001. Pb(II) distributions at biofilm-metal oxide interfaces. *P. Natl. Acad. Sci. USA* **244:** 11897-11902.

Thompson, H.A., G.A. Parks and G.E. Brown Jr.. 1999. Dynamic interactions of dissolution, surface adsorption, and precipitation in an aging cobalt(II)-clay-water system. *Geochim. Cosmochim. Acta* **64:** 1767-1779.

Trivedi, P., L. Axe and T.A. Tyson. 2001. An analysis of zinc sorption to amorphous versus crystalline iron oxides using XAS. *Colloid Interface Sci.* **244:** 230-238.

Vangronsveld J., F. Van Assche and H. Clijsters. 1995. Reclamation of a bare industrial area contaminated by non-ferrous metals: *in situ* metal immobilization and fixation. *Environ. Pol.* **87:** 51-59.

Wasserman S.R., P.G. Allen, D.K. Shuh, J.J. Bucher and N.M. Edelstein. 1999. EXAFS and principal component analysis: A new shell game. *J. Synchrotron Rad.* **6:** 284-286.

Xia, K., W. Bleam and P.A. Helmke. 1997. Studies of the nature of Cu^{2+} and Pb^{2+} binding sites in soil humic substances using X-ray absorption spectroscopy. *Geochim. Cosmochim. Acta* **61:** 2211-2221.

Yamaguchi, N.U., A.C. Scheinost and D.L. Sparks. 2001. Surface-induced nickel hydroxide precipitation in the presence of citrate and salicylate. *Soil. Sci. Soc. Am. J.* **65:** 729-736.

Zachara, J.M., C.T. Resch and S.C. Smith. 1994. Influence of humic substances on Co^{2+} sorption by a subsurface mineral separate and its mineralogic components. *Geochim. Cosmochim. Acta* **58:** 553-556.

Chapter 2

NICKEL SEQUESTRATION IN A KAOLINITE-HUMIC ACID MIXTURE

2.1 ABSTRACT

Incorporation of first row transition metals into stable surface precipitates can play an important role in reducing the bioavailability of these metals in neutral and alkaline soils. Organic coatings may interfere with this sorption mechanism by changing the surface characteristics and by masking the mineral surface from metal sorptives. In this study, kinetic sorption and desorption experiments were combined with extended x-ray absorption fine structure (EXAFS) spectroscopy, to elucidate the effect of humic acid (HA) coatings on the formation and stabilization of nickel precipitates at the kaolinite-water interface. Initial Ni uptake (pH = 7.5, $[Ni]_i$ = 3mM and I = 0.02 M $NaNO_3$) increased with greater amounts of HA coated onto the kaolinite surface. Ni uptake continued over an extended period of time without reaching an apparent equilibrium. EXAFS analysis of the Ni sorption complex structures formed over time (up to 7 months) revealed the formation of a Ni-Al layered double hydroxide (LDH) precipitate at the kaolinite surface in the absence of HA. Humic acid alone formed an inner-sphere complex with Ni (with 2 Carbon atoms at an average radial distance of 2.85 Å). A Ni-Al LDH precipitate phase was formed at the kaolinite surface in the presence of a 1wt% HA coating. However, with 5-wt% HA coated at the kaolinite surface, the formation of a surface precipitate was slowed down significantly and the precipitate formed was similar in structure to $Ni(OH)_2$ (s). The $Ni(OH)_2$ precipitate

was not resistant to proton dissolution, while the Ni-Al LDH precipitate was. These results augment earlier findings that the incorporation of Ni and other first row transition metals into stable surface precipitates is an important sequestration pathway for toxic metals in the environment, despite the presence of ubiquitous coating materials such as humic acids.

2.2 INTRODUCTION

The mobility and bioavailability of trace metals in soils is largely dictated by reactions taking place at the soil solution-particle interfaces (Hochella 1990, Sparks 1995). Therefore, a complete understanding of long-term metal availability depends on knowing the adsorption and desorption reactions taking place at the soil particle surfaces. Laboratory studies of metal partitioning identified the incorporation of Cr, Ni, Co, Cu and Zn into a neoformed surface precipitate as the primary sorption mechanism for these potentially toxic metals at pH > 6.0 (Fendorf et al. 1994, Scheidegger et al. 1997, O'Day et al. 1994, Towle et al. 1997, Xia et al. 1997, Cheah et al. 1998, Schlegel et al. 1999, Ford and Sparks 2000). Depending on the reaction conditions, time and the absorbent phase present, either a metal hydroxide, a mixed layered double hydroxide (LDH) or a phyllosilicate formed at the mineral surfaces (Thompson et al. 1999a, Thompson et al. 1999b, Manceau et al. 1999, Ford et al. 1999, Scheinost and Sparks 2000). These neo-formed phases form well below theoretical monolayer coverage and in a pH range at which metal hydroxide precipitates would not be expected to form according to their thermodynamic

solubility product. The precipitates are stabilized upon aging (Ford et al. 1999, Scheckel et al. 2000). This stabilization has been attributed to the transformation of a mixed layered double hydroxide phase into a more stable phyllosilicate phase and/or to Ostwald ripening. Identification of the potential of surface precipitate formation in non-acidic soils is important, since this sorption process might lead to the long-term removal of potentially hazardous first row transition metals from the soil solution.

Zn-containing surface precipitates have recently been identified in soils close to smelter facilities (Morin et al. 1999, Manceau et al. 2000). The conditions in these soils are favorable for the formation of precipitates, with high concentrations of metal (weight percent) present, alkaline pH, and relatively small amounts of organic matter. Organic matter and particularly humic substances (HS), the stable organic pool in soils, can strongly compete for metal uptake with the mineral surface and may mask the mineral surface from metals in the solution phase (Stevenson 1994, Vermeer et al. 1999, Pétrović et al. 1999). Humic substances are ubiquitous in soils, and are often intimately associated with clay minerals (Stevenson 1994). A study on Ni sorption mechanisms on the clay fraction of a Matapeake silt loam, with and without a small organic fraction (~1-wt%) present, suggested that Ni-Al layered double hydroxides formed in soils with low organic matter content (Roberts et al. 1999). However, identification of Ni sorption complexes that have formed in whole soils is challenging, due to the limitations of current available spectroscopic techniques in separating a broad array of sorption sites, each with a unique spectroscopic signature.

Our understanding of the relative importance of surface precipitate formation in natural systems can be improved by examining the effect of individual competitive sorbents on the mechanism of surface precipitate formation. Elzinga and Sparks (1999) studied the competition between Ni adsorption onto montmorillonite and Ni surface precipitate formation on pyrophyllite, and found that neither mechanism was dominating. Yamaguchi et al. (2001) studied the influence of small organic acids, i.e. citrate and salicylate, on Ni sorption onto gibbsite and pyrophyllite. These organic acids suppressed Ni removal from solution and the formation of a surface precipitate. These results were attributed to strong metal complexation by the small organic acids in solution. Conversely, a study by Zachara et al. (1994) on Co^{2+} sorption by a subsurface mineral separate showed that the presence of a humic acid coating augmented, rather than changed the intrinsic sorption behavior of the mineral sorbents. This suggests that humic substances, especially when coated onto mineral surfaces, may have a different effect on Ni uptake behavior than do small organic molecules in solution.

In the present study, macroscopic Ni sorption and desorption kinetic studies are combined with extended x-ray absorption fine structure (EXAFS) spectroscopy to characterize the structure and stability of the sorption complex formed on kaolinite coated with humic acid (HA). The objective of the present work is to elucidate the effects of HA coatings on mechanisms of Ni surface precipitate formation and stabilization. A range of organic matter contents representative of those found in soils is used as coatings (Sparks 1995). The HA coatings may interfere with the intrinsic Ni

sorption mechanisms to kaolinite in several ways: First of all, formation of Ni and Al organic complexes can reduce the availability of these metals for the formation of a precipitate phase. On the contrary, enhanced mineral dissolution by organic acids can lead to a larger availability of Al and Si for the stabilization of the precipitate. Second of all, the metal uptake capacity of the coated kaolinite is significantly higher than that of kaolinite, due to the larger surface area and cation exchange capacity (CEC) of the HA coated kaolinite. Additionally, the presence of organic coatings may alter the reactivity of the underlying kaolinite surface, by forming inner-sphere complexes with the highly reactive aluminol groups of the kaolinite edge sites and by modifying the electrical properties of the kaolinite-water interface (Templeton 2001).

2.3 MATERIALS AND METHODS

2.3.1 Materials

The kaolinite used in this study is a well-crystallized Georgia kaolinite, Clay Mineral Society source clay (KGa-1). The kaolinite was treated for the possible presence of carbonates, organic matter and manganese/iron oxides using standard procedures (Jackson 1956). Carbonates and exchangeable divalent ions were removed by reaction with a NaOAc buffer at pH 5 in a near boiling warm water bath. Organic matter was removed by treatment of the kaolinite with 30% H_2O_2. Iron oxides were removed with a dithionite-citrate-bicarbonate mixture in a 80°C warm water bath. The resulting kaolinite was washed twice with a 1.0 M NaCl solution, and twice with DI water. The

<0.2 μm fraction was separated by centrifugation, dialyzed against milli-Q H_2O, and freeze-dried.

A well characterized HA isolated from a bog-soil collected in the White Mountain National Forest in Rumney, New Hampshire, was supplied by Drs. G. Davies and E.A. Ghabbour (Northeastern University, Boston, MA, USA). The isolation procedure and characterization of the HA are outlined elsewhere (Davies et al. 1997). Essentially the soil was pre-treated with mild solvents (a benzene-methanol mixture). After pre-extraction the humic substances were extracted with aqueous base. The ash content of this HA is 0.25 wt%. The supernatant was brought to pH 1.0 with concentrated HCl. The remaining HA gel was washed and freeze-dried before any further use.

Humic acid coated kaolinite samples containing 1 and 5 wt.% of humic acid were prepared by dissolving 0.01 g (1-wt%) and 0.05 g (5-wt%) HA in 50 mL of a N_2 purged 0.05 M NaOH solution. The HA solution was brought to pH 7.5 prior to mixing with 1 g of kaolinite. The pH of the kaolinite-humic acid suspension was brought to 3.5. This mixture was shaken for 48h and brought to 200 mL, pH = 7.5 and I = 0.02 M $NaNO_3$ prior to the sorption experiments. For all experiments, the mass of kaolinite was maintained constant (5 g L^{-1}) while the fraction of organic matter was varied.

The cation exchange capacity (CEC) of the solids was determined by Ba-Mg exchange, without pH buffering. The specific surface area of the solids was

determined by a five point N_2 Brunauer-Emmett-Teller (BET) gas adsorption isotherm method. The CEC and the specific surface area of the mixtures and individual components are given in Table 2.1.

2.3.2 Nickel sorption experiments.

The kinetics of Ni partitioning to kaolinite (hydrated in the background solution for 48h), 5-wt% HA (dissolved in 0.05 M NaOH, precipitated at pH 3.0, after which the pH was raised to pH 7.5), and kaolinite coated with 1 and 5-wt% HA were studied in batch reactors. Experiments were carried out in a 0.02 M $NaNO_3$ background solution and at pH 7.5, since previous research (Scheidegger et al. 1997, Scheinost and Sparks 2000) indicated that Ni-Al precipitates do form at this pH in the absence of competing sorbent surfaces. The systems were purged with N_2, and milli-Q H_2O was used throughout to minimize the formation of carbonates. Nickel from a 0.1 M $Ni(NO_3)_2$ stock solution was added in one mL aliquots to achieve an initial [Ni] of 3 mM. The solution was undersaturated with respect to homogeneous precipitation of $Ni(OH)_2$ (*29*). The pH was kept constant at 7.5 using a Radiometer pH-stat titrator (Westlake, OH) for the first two days and afterwards by weekly manual readjustments using 0.1 M NaOH. Samples (10 mL) were periodically collected from the suspension and filtered through a 0.2 μm membrame filter. Filtered supernatants were analyzed for dissolved Ni by inductively coupled plasma optical emission spectroscopy (ICP-OES). Solid samples were collected after 4 days, 2 weeks, 1 month and 7months for characterization using XAFS spectroscopy. Solids were isolated under vacuum

filtration and transferred to a polyethylene holder. The wet paste was sealed into the holder with 0.0005-in. Kapton polymide tape (CHR Industries, type K-104) to avoid moisture loss during analysis.

	CEC(meq.100g $^{-1}$)†	BET-surface area
Kaolinite	9.37 (pH 6.0)	14.01 m^2g^{-1}
1-wt% HA-kaolinite	25.80 (pH 5.5)	13.42 m^2g^{-1}
5-wt% HA-kaolinite	29.62 (pH 5.5)	11.68 m^2g^{-1}
Humic acid	83.83 (pH 3.6)	1.25 m^2g^{-1}

† = Cation Exchange Capacity, determined by Ba-Mg exchange, unbuffered

Table 2.1. Summary of the physicochemical characteristics of the solids used in this study.

2.3.3 Desorption experiments.

The effect of a 5-wt% HA coating on the reversibility of Ni sorption to kaolinite was studied using a replenishment technique. Thirty (30) mL aliquots of suspension were separated from the kaolinite and 5wt% HA-kaolinite sorption experiments after 7 months of reaction. These aliquots were centrifuged at 2500 g for 10 min. The supernatants were collected for ICP-OES analysis, the remaining solids were resuspended in either the $NaNO_3$ background electrolyte solution used in the sorption experiments (pH = 7.5, I = 0.02 M $NaNO_3$), in a $CaCl_2$ solution (pH=6.0, I=0.01 M $CaCl_2$) or in a 0.1 M HNO_3 solution (pH = 4.0). The solids were resuspended using a Vortex stirrer, shaken for 24h at 25 °C in a reciprocal shaker, and centrifuged at 2500 g for 10 min. This replenishment was repeated 14 times.

2.3.4. XAFS data collection and analyses.

X-ray absorption spectra were collected at beamline X-11A of the National Synchrotron Light Source (NSLS), Brookhaven National Laboratory. The electron storage ring operated at 2.8 GeV with an average beam current of 180 mA. The monochromator consisted of two parallel Si (111) crystals with an entrance slit of 0.5mm. Higher order harmonics were suppressed by detuning 25% from the maximum beam intensity. The monochromator position was calibrated by assigning the first inflection point on the K-edge of a nickel metal foil to 8333.0 eV. The spectra were collected in fluorescence mode using an Ar-filled Lytle detector. A 6μm-Co filter and

soller slits were placed between the sample and the detector to reduce elastic scattering. The incoming beam was measured with a N_2-filled ion chamber. All spectra were collected at room temperature and at least three scans were collected per sample to improve the signal to noise ratio.

XAFS data reduction was performed using WinXAS 2.1 following standard procedures (Eick and Fendorf 1998, Scheinost and Sparks 2000). The χ function was extracted from the raw data by fitting a linear function to the pre-edge region and a spline function to the post-edge region, and normalizing the edge jump to unity. The energy axis (eV) was converted to photoelectron wave vector units ($Å^{-1}$) by assigning the origin, E_o, to the first inflexion point of the absorption edge. The resulting $\chi(k)$ functions were weighted with k^3 to compensate for the dampening of the XAFS amplitude with increasing k and were Fourier-transformed to obtain radial structure functions (RSF). A Bessel window with a smoothing parameter of 4 was used to suppress artifacts due to the finite Fourier filtering range between Δk = 1.5-13.8 $Å^{-1}$. The two major peaks below 3.5 $Å^{-1}$ in the Fourier transformed curves were isolated and backtransformed. An R range of ≈ 1.07-2.04 $Å^{-1}$ was used for the first peak and an R range of ≈ 2.04-3.28 $Å^{-1}$ for the second. These backtransformed peaks were fit in k space. Structural parameters were extracted with fits to the standard EXAFS equation. *Ab initio* Ni-O and Ni-Ni/Al (or Ni-C for the HA containing samples) scattering paths were generated using the FEFF 7.02 code from the refinement of the structure of

lizardite where Ni was substituted for Mg in octahedral positions (Mellini 1982). After each of the individual peaks in the Fourier transform spectra were backtransformed and fit, multishell fitting was done in R space over the range of the first two shells (ΔR = 1.07-3.30) using the same parameters. Optimization of the parameters was then performed again, with the E_o shifts constrained to be equal. The amplitude reduction factor, $(S_o)^2$, was fixed at 0.85. A good fit was determined on the basis of the minimum residual error.

2.4 RESULTS AND DISCUSSION

2.4.1 Solid characteristics

The physicochemical characteristics of the solids used in this study are collected in Table 2.1. The CEC was determined by Ba-Mg exchange and without the presence of a pH buffer, since these organic pH buffers could potentially interact with HA. The CEC's of the (coated) kaolinite samples were all determined at pH ~ 5.5. The CEC increases significantly when kaolinite is coated with increasing amounts of HA. The CEC of the HA was determined at a much lower pH ~3.6. Most carboxyl groups deprotonate between pH 4 and 6. Therefore the CEC of HA is expected to be much higher at pH 5.5. Cation exchange capacities ranging from 300 to 1400 $cmol.kg^{-1}$ have been reported for HA in the literature (Sparks 1995).

The BET surface area values reported in Table 2.1 compare with values reported in the literature (Pennell 1995, deJonge 1996) and are an indication of the small pore size of

HA, rather then the external surface area. The reason for this is that nitrogen is subject to molecular sieving at 77 K due to activated diffusion in micropores of HA (deJonge 1996). The large HA surface area determined by the ethylene glycol monomethyl ether (EGME) method and reported in the literature, is a consequence of polar interactions between HA and EGME. No reliable methods are currently available to determine the precise surface area of humic substances and subsequently the total surface loadings could not be reported in this study. The decreasing BET surface area with increasing amounts of HA coated at the kaolinite surface indicates that a significant portion of the kaolinite surface is being covered by the HA.

2.4.2 Adsorption kinetics

The adsorption of Ni as a function of time was investigated on pristine kaolinite and HA, and on 1 and 5 wt% HA coated kaolinite (Figure 2.1a,b). Only 8% of the initial Ni concentration was retained by the pristine kaolinite surface after 60 hrs of reaction, while approximately 40% was retained by the HA only system, indicating that HA has a much higher reactive surface area than kaolinite. After 60 hours, the 1 and 5 wt% HA coated kaolinite retained approximately 18 and 25% of initial Ni concentrations, respectively. Increasing metal sorption with increasing amounts of HA coated on the mineral surface, has also been reported for cobalt sorption to organic matter – mineral complexes (Zachara 1994).

The 5 wt% HA has a higher sorption capacity than when the same amount of HA is coated at the kaolinite surface. This suggests that a significant amount of the nickel

sorption sites on both kaolinite (edge sites) and HA (mainly carboxylic and phenolic functional groups) have become unavailable as a result of the formation of chemical bonds between the kaolinite and the humic acid.

The release of Ni by the HA after about 30 h of reaction may be caused by the partial dissolution of HA at the basic pH employed in this study. The release of Ni is not observed in the HA-coated kaolinite samples. This is due to a stabilization of HA when it is bound to clay minerals (Stevenson 1994, Ghabbour et al. 1998).

Nickel sorption to kaolinite and kaolinite coated with 1-wt% HA is initially fast and is followed by a slow continued Ni uptake (Figure 2.1b). A slow continued Ni uptake can be observed to a lesser extent for the 5 wt% HA-kaolinite. This two-step sorption process is characteristic of heavy metal sorption on clays and oxide surfaces (Benjamin 1981, Scheidegger 1997). Several mechanisms have been proposed for the slow continued metal uptake by clays and oxide surfaces, including: adsorption of metals onto sites that have relatively large activation energies (Scheidegger et al. 1997, Strawn and Sparks 2000, Papelis 1995), diffusion into micro-pores of the minerals (Strawn and Sparks 2000, Axe and Trivedi 2002), and a continuous growth of a surface precipitate away from the sorbent surface (Eick and Fendorf 1998). EXAFS studies indicated the formation of Ni-Al LDH at the kaolinite surface under the reaction conditions employed in this study and in the absence of organic matter (Scheidegger 1997, Eick and Fendorf 1998). Therefore it is likely that the growth of a surface precipitate away from the kaolinite surface is responsible for the continued Ni uptake by the kaolinite. Driving forces for a continuous growth of a surface precipitate

include the continued presence of Ni in solution, and the increase in surface area due to the formation of a precipitate phase. It is likely that several sorption mechanisms are involved in the Ni uptake by the HA coated kaolinite systems, since several different sorption sites are available in these systems. The higher initial Ni sorption in the HA coated systems and the slower continued Ni uptake (about 12 % of the initial Ni sorption in 9000h) compared to the pristine kaolinite (almost double the initial Ni sorption), indicate that, besides the formation of a surface precipitate, the formation of sorption complexes with the functional groups of HA play an important role in the sequestration of Ni (see also EXAFS discussion later in this chapter).

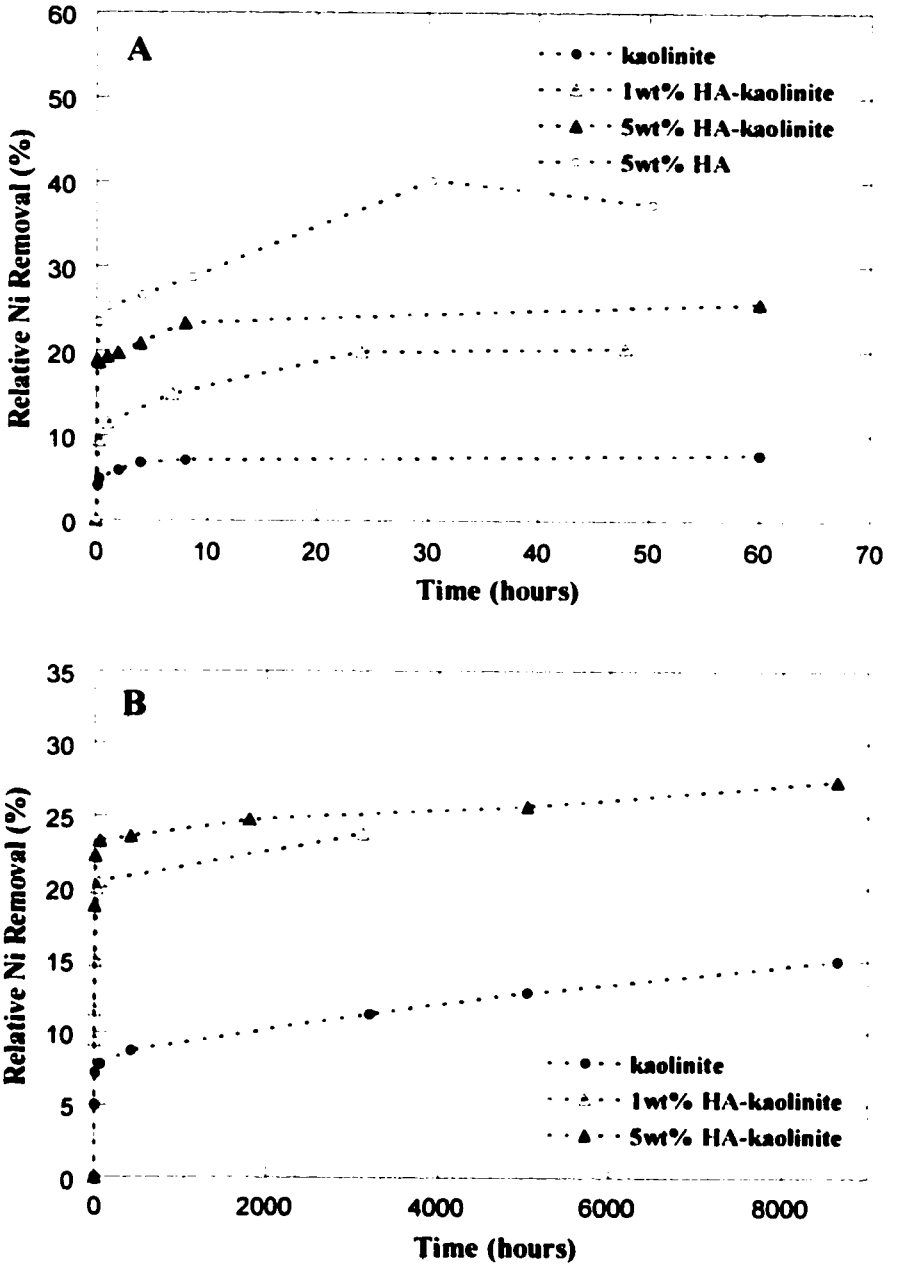

Figure 2.1. Ni sorption kinetics a) within the first 60 hours (initial sorption conditions: pH = 7.5, I=0.02 M $NaNO_3$, $[Ni]_i$= 3 mM) and b) Ni sorption kinetics over the entire reaction range.

2.4.3 *Desorption behavior*

To compare the stability of the sorption complexes formed at the kaolinite-water and the kaolinite-HA coating-water interfaces, desorption experiments were carried out. Three desorption agents were employed: a background electrolyte solution (pH = 6.0, I= 0.02 M), a calcium chloride solution pH=6.0, I=0.1M) and a nitric acid (pH = 4.0) solution. The background solution is most likely to remove any weakly held outer sphere complexes. The calcium solution, which is two orders higher in concentration than the nickel solution, can out compete for Ni at HA binding sites where electrostatic interactions dominate (Naylor and Overstreet 1969, Mandal et al. 2000) and is expected to remove most electrostatically bound Ni from the HA. Nitric acid can remove Ni from both the HA, by proton competition, and from a precipitate phase by proton dissolution. Proton dissolution is especially effective when a less stable nickel-hydroxide is being formed (Scheckel and Sparks 2001).

The relative amount of Ni remaining on the surface is plotted versus the number of replenishments (Figure 2.2). Nickel desorption behavior from the kaolinite surface changed little as the number of desorption replenishments is increased. Only HNO_3 slowly released Ni with each replenishment. The initial 30 % Ni released from the kaolinite sample with the first replenishment included some Ni entrapped in the wet paste after centrifugation and weak, electrostatically bound Ni. The remaining 70% could not be desorbed from the kaolinite surface with the $CaCl_2$ or the $NaNO_3$ background solutions. Similar results for desorption of Ni, after 6 months of contact time with mineral surfaces, were observed by others (Ford et al. 1999, Scheckel and

Sparks 2001). The presence of this resistant fraction has been attributed to the formation and subsequent stabilization of a surface precipitate. Nickel desorption form HA-coated kaolinite was markedly different than what was observed for the pristine kaolinite system. The $CaCl_2$ solution was more effective in removing a small nickel fraction than the $NaNO_3$ solution, suggesting that a small Ni portion (~35%) is bound directly to the HA. However, a stable Ni fraction (~65%) could not be desorbed by either the $CaCl_2$ or $NaNO_3$ background solutions. The HNO_3 solution desorbed essentially all Ni from the HA coated kaolinite samples with 14 replenishments. This slow, yet total Ni release has been found to be characteristic of Ni release from nickel hydroxide phases, which are not stable to proton dissolution (Scheckel and Sparks 2001).

From the sorption and desorption studies it may be concluded that the HA coating almost tripled the total Ni uptake, but the sorption complex formed in the presence of this coating is less stable to proton promoted dissolution than the sorption complex formed in the absence of the coating.

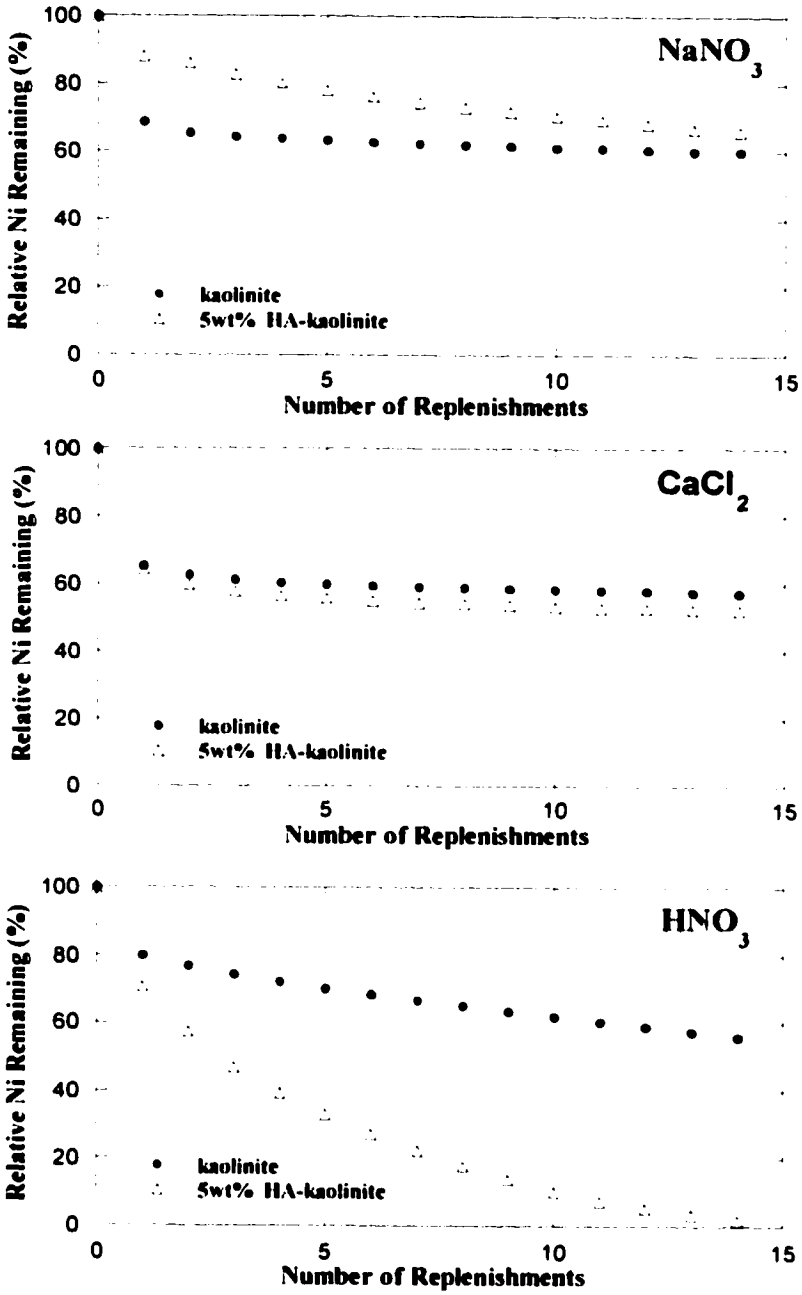

Figure 2.2. Percentage Ni remaining at the kaolinite or the 5-wt% HA-kaolinite surface after desorption with a) the background electrolyte (pH=7.5, I= 0.02 M $NaNO_3$) or b) a calcium chloride solution (pH=6.0, I=0.1 M $CaCl_2$) or c) a nitric acid solution (pH=4.0).

2.4.4 *EXAFS spectroscopy*

The structure of the dominant Ni sorption complex formed at the different solid-water interfaces can be inferred from EXAFS analysis. Figure 2.3a shows the background subtracted k^3 weighted χ functions of the Ni reacted kaolinite, HA, and kaolinite coated with 1 and 5-wt% HA. The Fourier transformed radial structure functions (RSF), which are uncorrected for phase shifts, are plotted in Figure 2.3b. The solid lines represent the magnitude and imaginary part and the dotted lines the best fits resulting from multiple shell fitting. The first peak in the RSF at ~1.8 Å is indicative of backscattering from the first ligand shell, and the second peak at ~2.8 Å indicates backscattering from the first metal shell. This metal shell could be fit with Ni in the case of the 12 days reacted kaolinite and the HA coated kaolinite samples and a combination of Ni and Al in the 7 months reacted kaolinite. The Ni-Ni/Al peak increases in intensity over time in both the kaolinite and the coated kaolinite systems. This increase in intensity of the second shell qualitatively indicates the growth of a Ni containing precipitate phase.

In Table 2.2, the structural parameters, derived from EXAFS analysis, are shown. The coordination number (CN) of the Ni-O shell is approximately equal to six for all samples, indicating that Ni is in an octahedral environment in all sorption complexes. The Ni-O bond distance is the same in all samples, except for the HA sample where the Ni-O bond distance is slightly higher and closer to Ni-O bond distances of Ni in aqueous solutions (Pandya et al. 1990). The Ni-Ni bond distances of the surface precipitates are around 3.06 Å, which are significantly shorter than that of a pure Ni

hydroxide phase (β-$NiOH_2$), 3.12 Å, and of a nickel hydroxide with 50% vacancies in the octahedral layer (α- $NiOH_2$), 3.09 Å (Table 2.2). This contraction in bond length has been attributed to several factors, including the presence of both Al and Ni in the octahedral layers, where the smaller Al atom forces the Ni-Ni bond length to contract (Scheinost and Sparks 2000). The low Ni-Ni coordination number in the 5-wt% HA-kaolinite mixtures indicates that in these samples the development of a surface precipitate phase is still in an initial phase after 7 months.

The presence of a high frequency beat in the Ni-HA χ function (Figure 2.3a) indicates the presence of higher order shells. A small Fourier peak around ~ 2.3 Å could only be fit with a Ni-C scattering path at 2.85 Å and with a CN of ~ 1.8 (Table 2.2). Xia et al. (1997) found similar results for a Ni reacted HA, with two carbon atoms at an average radial distance of 2.93 Å. These results indicate that under the reaction conditions applied, Ni forms a bidentate inner-sphere complex with carbon containing functional groups of HA. Carboxylic and phenolic functional groups are the most likely candidates to bond with Ni, because of their abundance and reactivity at the pH employed (Stevenson 1994). However, weak backscattering contributions from low Z elements beyond the first shell prevent a more detailed analysis (Davies et al 1997). The absence of a Ni-Ni shell in the Ni-reacted HA sample confirms that these systems were not supersaturated with respect to bulk precipitation of a Ni hydroxide/carbonate phase under the reaction conditions of this study.

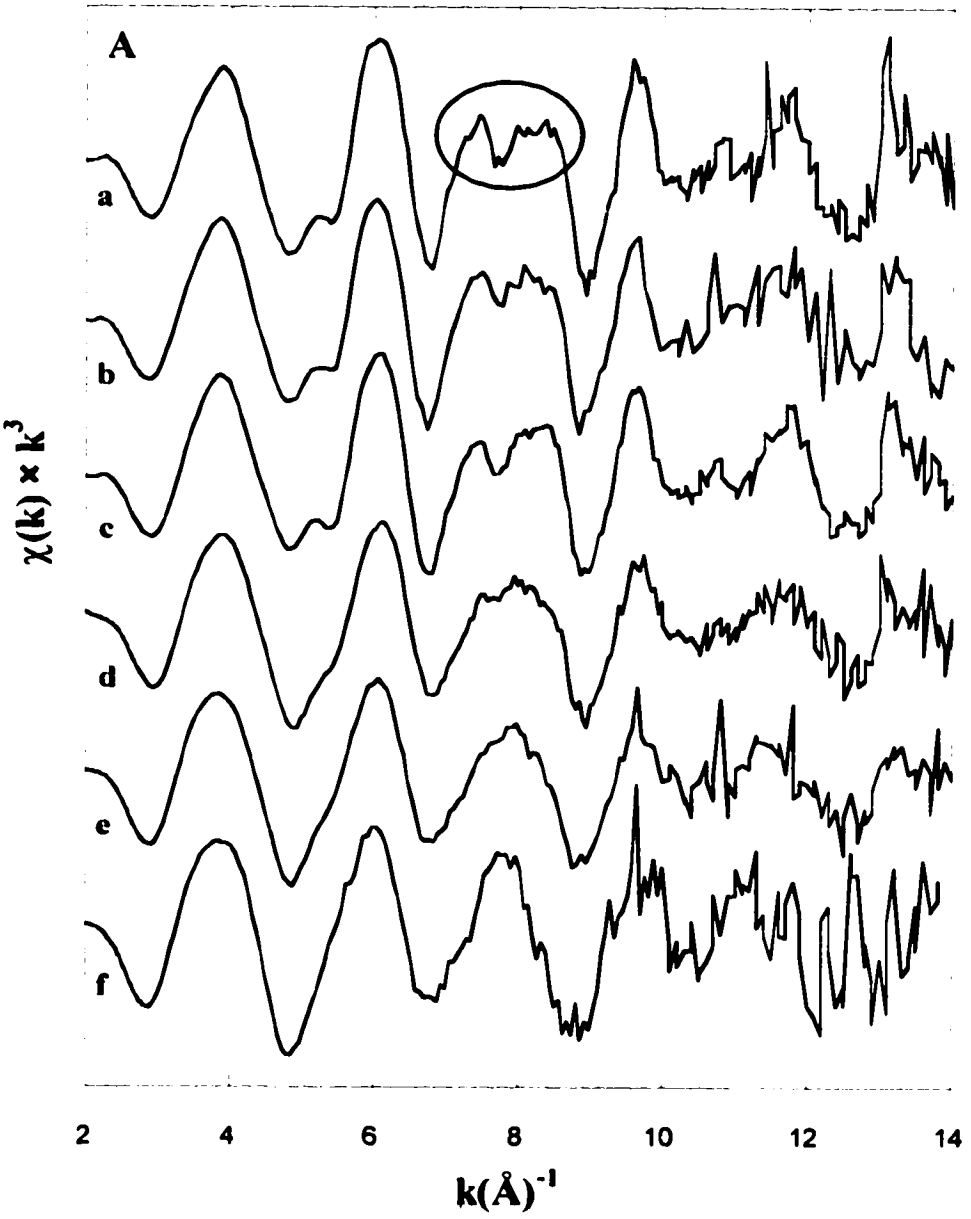

Figure 2.3a. The k^3 weighted Ni-K_α EXAFS spectra of kaolinite reacted with Ni for 7 months (a) and 12 days (b), 1-wt% HA coated kaolinite reacted with Ni for 4 days (c), 5-wt% HA coated kaolinite reacted with Ni for 7 months (d) and 27 days (e), and HA reacted with Ni for 2 days (f).

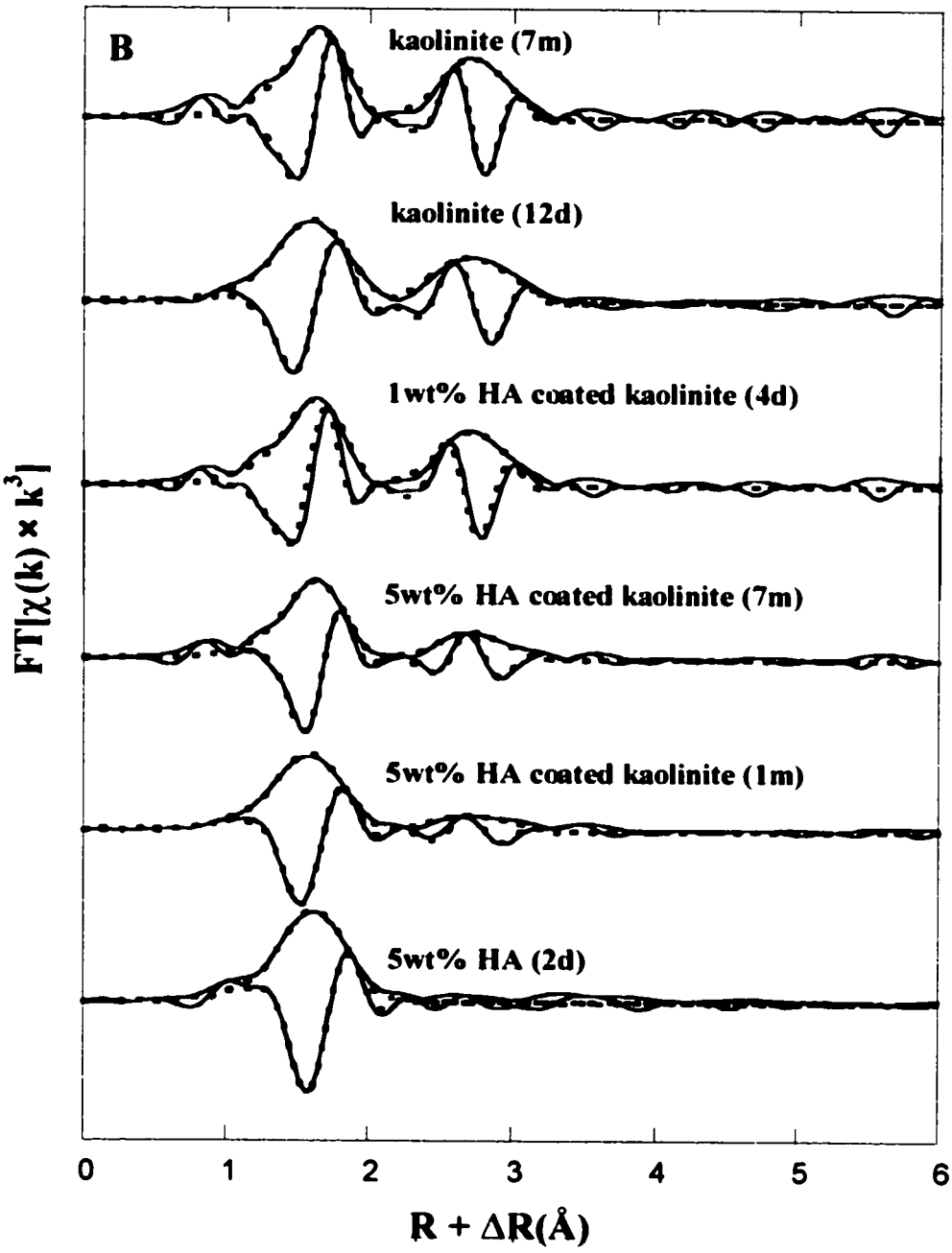

Figure 2.3b The Fourier transforms of the Ni-K_α EXAFS spectra (uncorrected for phase shifts), with solid lines indicating the magnitude and imaginary part and the dotted symbols the best fits.

The precipitate formed at the kaolinite surface after 12 days of reaction contains three Ni atoms at an average radial distance of 3.06 Å. After 7 months of reaction, the precipitate contains three Ni atoms at 3.06 Å and ~ three Al atoms at 3.20 Å. Similar results have been found for Co (Thompson et al. 1999a, Thompson et al. 1999b) and Ni (Scheidegger et al. 1997, Eick et al. 1998) containing precipitates formed at the kaolinite surface and indicate that the initial Ni hydroxide transforms into a more stable mixed Ni-Al layered double hydroxide (LDH) over time. The fit for the 7 month reacted kaolinite significantly improved when an Al path was included in the fit (Table 2.2), suggesting the presence of both Ni and Al in the octahedral layer of the precipitate phase. No meaningful fits were obtained in other samples when Al was included. Due to similar Ni-Ni and Ni-Al bond distances in Ni-Al LDH and the weak backscattering of Al compared to Ni, this inability to fit Al in the octahedral layer is not necessarily a proof of the absence of Al in the octahedral layer. Information on the presence of Al in the precipitate can be obtained from the χ functions (Figure 2.3a). A characteristic beat pattern at 8-9 $Å^{-1}$ has been found by Scheinost and Sparks (2000) to be solely produced by the presence of second shell Al. This characteristic beat pattern is present in the kaolinite and the kaolinite coated with 1-wt% HA samples, indicating the formation of a mixed Ni-Al LDH in these samples. The absence of this characteristic beat pattern in the 5-wt% HA coated kaolinite spectra indicates that the precipitate formed is a $NiOH_2$ phase rather than a mixed LDH. These results complement the desorption studies and show that a stable Ni-Al LDH is formed at the kaolinite surface and at the kaolinite surface in the presence of a 1-wt% organic

		Ni-O			Ni-Ni/C/Al					
	rt	CN	R(Å)	$\sigma^2(Å)^2$	Atom	CN	R(Å)	$\sigma^2(Å)^2$	ΔE_0(eV)	%res
Single components										
HA	48h	6.0	2.06	0.004					-1.93	2.52
HA	48h	5.8	2.05	0.005	C	1.8	2.85	0.010	-2.93	2.13
Kaolinite	12d	6.3	2.05	0.006	Ni	3.2	3.06	0.007	-2.04	5.44
Kaolinite	7m	5.9	2.04	0.005	Ni	4.0	3.06	0.006	-2.06	6.63
Kaolinite	7m	5.4	2.04	0.004	Ni	3.5	3.06	0.007	-2.81	
					Al	3.2	3.20	0.020	-2.81	4.82
Coated samples										
1wt% HA-kaolinite	4d	5.2	2.04	0.005	Ni	3.0	3.05	0.006	-2.26	12.91
5wt% HA-kaolinite	27d	5.5	2.04	0.005	Ni	1.4	3.06	0.005	-2.75	8.63
5wt% HA-kaolinite	7m	5.7	2.04	0.006	Ni	1.9	3.06	0.006	-1.81	20.30
References (*13*)										
α-Ni hydroxide		5.5	2.04	0.005	Ni	5.6	3.09	0.006		
LDH Ni/Al=1.3		5.4	2.05	0.004	Ni	2.8	3.06	0.004		

rt = Reaction time
CN = Coordination Number (± 20% (*O'Day et al. 1994*))
R = Inter-atomic distance (± 0.02Å (*O'Day et al. 1994*))
$\sigma^2(Å^2)$ = Debye Waller factor
ΔE_0 = Phase shift
%res = Residual error

Table 2.2. Best-fit structural parameters derived from EXAFS analysis.

coating, while a less stable (with respect to proton dissolution) Ni hydroxide is being formed in the presence of a 5-wt% organic coating.

The goodness of the fit (% residual in Table 2.2) is not as good for the coated samples as for the individual components. This indicates that, apart from a nickel containing precipitate, another nickel sorption complex is present, which dilutes the EXAFS signal from the precipitate phase. The dissolution studies indicated that about 40% of the nickel is bound to the HA, whereas 60% is included in a precipitate phase. Therefore the dilution of the EXAFS signal from the Ni-Ni shell by a Ni-C path is expected, but this Ni-C path could not be fit. This is not very surprising, since low Z elements hardly contribute to the EXAFS signal.

2.5 SUMMARY AND CONCLUSIONS

This research shows that a Ni containing precipitate phase is formed at the kaolinite surface, even in the presence of a 5-wt% organic coating. Ni uptake kinetics and capacity increases with the amount of HA coated at the kaolinite surface, but the formation of a surface precipitate is slowed down significantly with a higher amount of HA coating. The precipitate formed in the presence of a 5-wt% HA coating is nickel hydroxide, whereas in the presence of a 1wt% HA coating a more stable Ni-Al LDH is formed. Both precipitates are resistant to desorption with mild desorption agents, but the nickel hydroxide precipitate is not stable with respect to proton dissolution. These results show that organic coatings do affect metal sorption, but do not change the intrinsic metal uptake of the underlying clay mineral. This information

should be considered when included in any complexation model and may be of value in developing sound remediation strategies for soils contaminated with toxic first row transition metals.

2.6 REFERENCES

Axe, L. and P. Trivedi. 2002. Intraparticle surface diffusion of metal contaminants and their attenuation in microporous amorphous Al, Fe, and Mn oxides. *J. Colloid Interface Sci.* **247:** 259-265.

Benjamin, M.M. and J.O. Leckie. 1981. Multiple-site adsorption of Cd, Cu, Zn and Pb on amorphous iron oxyhydrixuide. *J. Colloid Interface Sci.* **79:** 209-221.

Cheah, S.F., G.E. Brown Jr. and G.A. Parks. 1998. XAFS spectroscopy study of Cu(II) sorption on amorphous SiO2 and gamma-Al2O3: Effect of substrate and time on sorption complexes. *J. Colloid Interface Sci.* **208:** 110-128.

Davies, G., A. Fataftah, A. Cherkasskly, E. A. Ghabbour, A. Radwan, S. A. Jansen, S. Kolla, M. D. Paciolla, L. T. Sein Jr., W. Buermann, M. Balasubramanian, J. Budnick and B. Xing. 1997. Tight metal binding by humic acids and its role in biomineralization. *J. Chem. Soc., Dalton Transactions.* **21:** 4047-4060.

Eick, M. J. and S. E. Fendorf. 1998. Reaction sequence of Nickel(II) with kaolinite: Mineral dissolution and surface complexation and precipitation. *Soil Sci. Soc. Am. J.* **62:** 1257-1267.

Elzinga, E. J. and D. L. Sparks. 1999. Nickel sorption mechanisms in a pyrophyllite-montmorillonite mixture. *J. Colloid Interface Sci.* **213:** 506-512.

Fendorf, S. E., G. M. Lamble, M. G. Stapleton, M. J. Kelley and D. L. Sparks. 1994. Mechanisms of chromium(III) sorption on silica. 1. Cr(III) surface-structure derived by extended X-ray-absorbtion fine-structure spectroscopy. *Environ. Sci. Technol.* **28:** 284-289.

Ford, R. G., A. C. Scheinost, K. G. Scheckel and D. L Sparks. 1999. The link between clay mineral weathering and the stabilization of Ni surface precipitates. *Environ. Sci. Technol.* **33:** 3140-3144.

Ford, R.G. and D.L. Sparks. 2000. The nature of Zn precipitates formed in the presence of pyrophyllite. *Environ. Sci. Technol.* **34:** 2479-2483.

Ghabbour, E. A., G. Davies, K. O'Donaughy, T.L. Smith and M. E. Goodwillie. 1998. *In* Humic Substances. Structures, Properties and Uses. Davies, G. and E. A. Ghabbour (Eds.) The Royal Society of Chemistry: Cambridge.

Hochella, M.F. 1990. Atomic-structure, microtopography, composition, and reactivity of mineral surfaces. *In* Mineral-Water Interface Geochemistry. Hochella, M.F. and A.F. White Jr. (Eds.) Mineralogical Society of America: Washington. DC. Vol. **23:** 87-132.

Jackson, M.L. 1956. Soil chemical analysis-advanced course. University of Wisconsin. Madison. Wisconsin.

deJonge, H. and M.C. Mittelmeijer-Hazeleger. 1996. Adsorption of CO2 and n(2) on soil organic matter: Nature of porosity, surface area, and diffusion mechanisms. *Environ. Sci. Technol.*, **30:** 408-413.

Manceau, A., M. Schlegel, K. L. Nagy, L. Charlet. 1999. Evidence for the formation of trioctahedral clay upon sorption of Co2+ on quartz. *J. Colloid Interface Sci.* **220:** 181-197.

Manceau, A., B. Lanson, M.L. Schlegel, J.C. Hargré, M. Musso, L. Eybert-Bérard, J.-L. Hazemann, D. Chateigner and G.M. Lamble. 2000. Quantitative Zn speciation in smelter-contaminated soils by EXAFS spectroscopy. *Am. J. Sci.* **300:** 289-343.

Mandal, R., M.S.A. Salam, J. Murimboh, N.M. Hassan, C.L. Chakrabarti, M.H. Back and D.C. Grégoire. 2000. Competition of Ca(II) and Mg(II) with Ni(II) for binding by a well-characterized fulvic acid in model solutions. *Environ. Sci. Technol.* **34:** 2201-2208.

Mattigod, S. V., D. Rai, A. R. Felmy and L.F. Rao. 1997. Solubility and solubility product of crystalline Ni(OH)(2). *J. Solution Chem.* **26:** 391-403.

Mellini, M. 1982. The crystal-structure of lizardite 1T - hydrogen-bonds and polytypism. *Am. Mineral.* **67:** 587-598.

Morin, G., J.D. Ostergren, F. Juillot, P. Ildefonse, G. Calas and G.E. Brown Jr.. 1999. XAFS determination of the chemical form of lead in smelter-contaminated soils and mine tailings: Importance of adsorption processes. *Am. Mineral.* **84:** 420-434.

Naylor, D.V. and R. Overstreet. 1969. Sodium-calcium exchange behavior in organic soils. *Soil Sci. Soc. Am. J.*, **33:** 848-851.

O'Day, P. A., G. E. Brown Jr. and G. A. Parks. 1994. X-ray absorption spectroscopy of cobalt(II) multinuclear surface complexes and surface precipitates on kaolinite. *J. Colloid Interface Sci.* **165:** 269-289.

O'Day, P. A., J. J. Rehr, S. I. Zabinsky and G. E. Brown Jr.. 1994. Extended X-ray-absorption fine-structure (EXAFS) analysis of disorder and multiple-scattering in complex crystalline solids. *J. Am. Chem. Soc.* **116:** 2938-2949.

Pandya, K.I., W.E. O'Grady, D.A. Corrigan, J. McBreen and R.W. Hoffman. 1990. Extended X-ray absorption fine-structure investigations of nickel hydroxides. *J. Phys. Chem.* **94:** 21-26

Papelis, C. 1995. X-ray photoelecttron spectroscopic studies of cadmium and selenite adsorption on aluminum oxides. *Environ. Sci. Technol.* **29:** 1526-1533.

Pennell, K.D., S.A. Boyd and L.M. Abriola, 1995. Surface-area of soil organic-matter reexamined. *Soil Sci. Soc. Am. J.* **59:** 1012-1018.

Pétrović, M., M. Kaštelan-Macan, A.J.M. Horvat. 1999. Interactive sorption of metal ions and humic acids onto mineral particles. *Wat. Air, Soil Pol.* **111:** 41-56

Roberts, D.R., A.M. Scheidegger and D.L. Sparks. 1999. Kinetics of mixed Ni-Al precipitate formation on a soil clay fraction. *Environ. Sci. Technol.* **33:** 3749-3754.

Scheckel K.G., A.C. Scheinost, R.G. Ford and D.L. Sparks. 2000. Stability of layered Ni hydroxide surface precipitates - A dissolution kinetics study. *Geochim. Cosmochim. Acta* **64**: 2727-2735.

Scheckel, K. G. and D. L.Sparks. 2001. Dissolution kinetics of nickel surface precipitates on clay mineral and oxide surfaces. *Soil Sci. Soc. Am. J.* **65:** 685-694.

Scheinost, A. C. and D. L. Sparks. 2000. Formation of layered single- and double-metal hydroxide precipitates at the mineral/water interface: A multiple-scattering XAFS analysis. *J. Colloid Interface Sci.* **223:** 167-178.

Scheidegger A. M., G. M. Lamble and D. L. Sparks. 1997. Spectroscopic evidence for the formation of mixed-cation hydroxide phases upon metal sorption on clays and aluminum oxides. *J. Colloid Interface Sci.* **186:** 118-128.

Schlegel, M. L., L. Charlet and A. Manceau. 1999. Sorption of metal ions on clay minerals - II. Mechanism of Co sorption on hectorite at high and low ionic strength and impact on the sorbent stability. *J. Colloid Interface Sci.* **220:** 392-405.

Sparks D.L. 1995. Environmental Soil Chemistry. Academic Press, Inc. London.

Strawn, D. G. and D. L Sparks. 2000. Effects of soil organic matter on the kinetics and mechanisms of Pb(II) sorption and desorption in soil. *Soil Sci. Soc. Am. J.* **64:** 144-156.

Stevenson, F.J. 1994. Humus chemistry, genesis, composition, reactions. Wiley & Sons Inc.

Templeton, A.S., T.P. Trainor, S.J. Traina, A.M. Spormann and G. E. Brown Jr.. 2001. Pb(II) distributions at biofilm-metal oxide interfaces. *P. Natl. Acad. Sci. USA* **244:** 11897-11902.

Thompson, H. A., G. A. Parks and G. E . Brown Jr.. 1999a. Ambient-temperature synthesis, evolution, and characterization of cobalt-aluminum hydrotalcite-like solids. *Clays Clay Miner.* **47:** 425-438.

Thompson, H.A., G.A. Parks and G.E. Brown Jr.. 1999b. Dynamic interactions of dissolution, surface adsorption, and precipitation in an aging cobalt(II)-clay-water system. *Geochim. Cosmochim. Acta* **64:** 1767-1779.

Towle, S. N., J. R. Bargar, G. E. Brown Jr. and G.A. Parks. 1997. Surface precipitation of Co(II)(aq) on Al2O3. *J. Colloid Interface Sci.* **187:** 62-82.

Vermeer, A.W.P., J.K. McCulloch, W.H. Van Riemsdijk and L.K. Koopal. 1999. Metal ion adsorption to complexes of humic acid and metal oxides: Deviations from the additivity rule. *Environ. Sci. Technol.* **33:** 3892-3897.

Xia, K., W. Bleam and P. A. Helmke. 1997. Studies of the nature of binding sites of first row transition elements bound to aquatic and soil humic substances using X-ray absorption spectroscopy. *Geochim. Cosmochim. Acta* **61:** 2223-2235.

Xia, K., W. Bleam and P.A. Helmke. 1997. Studies of the nature of Cu^{2+} and Pb^{2+} binding sites in soil humic substances using X-ray absorption spectroscopy. *Geochim. Cosmochim. Acta* **61:** 2211-2221.

Xia, K., A. Mehadi, R.W. Taylor and W.F. Bleam. 1997. X-ray absorption and electron paramagnetic resonance studies of Cu(II) sorbed to silica: Surface-induced precipitation at low surface coverages *J. Colloid Interface Sci.*, **185:** 252-257.

Yamaguchi, N.U., A.C. Scheinost and D.L. Sparks. 2001. Surface-induced nickel hydroxide precipitation in the presence of citrate and salicylate. *Soil. Sci. Soc. Am. J.* **65:** 729-736.

Zachara, J.M., C.T. Resch and S.C. Smith. 1994. Influence of humic substances on Co^{2+} sorption by a subsurface mineral separate and its mineralogic components. *Geochim. Cosmochim. Acta* **58:** 553-556.

Chapter 3

EFFECT OF IRON OXIDE COATINGS ON ZINC SORPTION MECHANISMS AT THE MINERAL/WATER INTERFACE

3.1 ABSTRACT

Oxide surface coatings are ubiquitous in the environment, but their effect on the intrinsic metal uptake mechanism by the underlying mineral surface is poorly understood. In this study, the zinc (Zn) sorption complexes formed at the kaolinite, goethite and goethite coated kaolinite surfaces, were systematically studied using extended x-ray absorption fine structure (EXAFS) spectroscopy as a function of pH, aging time, surface loading, and the extent of goethite coating,. At pH 5.0, Zn partitions to all sorbents by specific chemical binding to hydroxyl surface sites. At pH 7.0, the dominant sorption mechanism changes with reaction time. At the kaolinite surface, Zn is incorporated into a mixed metal Zn-Al layered double hydroxide (LDH). At the goethite surface, Zn initially forms a monodentate inner-sphere adsorption complex, with typical Zn-Fe distances of 3.18 Å. However, with increasing reaction time, the major Zn sorption mechanism shifts to the formation of a zinc hydroxide surface precipitate, with characteristic Zn-Zn bond distances of 3.07 Å. At the goethite coated kaolinite surface, Zn initially binds to FeOH groups of the goethite coating. With increasing aging time however, the inclusion of Zn into a mixed Zn-Al LDH takes over as the dominant sorption mechanism. These results suggest that the

formation of a precipitate phase at the kaolinite surface is thermodynamically favored over adsorption to the goethite coating. The formation of a Zn LDH precipitate at the pristine kaolinite and goethite coated kaolinite surface at near neutral pH over extended aging times is an important attenuation mechanism of metal contaminants in the environment.

3.2 INTRODUCTION

The bioavailability and migration of trace metals in the environment is dictated by reactions taking place at soil solution-particle interfaces (Brown and Parks 2001; Stumm and Morgan 1996; Hochella 1990). Determining the kinetics and mechanisms of these interfacial reactions is of utmost importance to insure the implementation of sound remediation strategies, to predict metal stability in the soil over time, and to successfully model the fate of trace metals in soils.

The type and stability of metal sorption complexes formed at solution-particle interfaces depend on the solution conditions (pH and ionic strength) and the solid phase present. Phyllosilicates and metal-(oxy)hydroxides are among the most reactive mineral surfaces in the environment (Sparks 1995). Metal-(oxy)hydroxides, including aluminum oxides (i.e. gibbsite), iron oxides (i.e. ferrihydrite, goethite, hematite) and manganese oxides (i.e. lithiphiorite, birnessite) often occur in the environment as reactive surface coatings on other minerals. These coatings, often discrete particles in the nanosize range, are the result of weathering of primary minerals and subsequent

reprecipitation (Coston et al. 1995). Organic coatings (Nachtegaal and Sparks 2003; Zachara et al. 1995) and biofilms (Templeton et al. 2001) have been shown to reduce metal uptake by the mineral surfaces, but not to change the intrinsic metal uptake mechanism of the underlying mineral surface. Little is known on the effect of metal oxide coatings on the intrinsic sorption mechanisms of trace metals to clay mineral surfaces.

Among potentially toxic trace metals, zinc (Zn) is one of most widespread contaminants in the environment (Nriagu and Pacyna 1984). It accumulates in soils by atmospheric deposition originating from smelting operations and by agricultural applications of sewage sludge and agrochemicals (Alloway 1990; Manceau et al. 2000; Roberts et al. 2002). Zinc plays an essential role in cellular systems and enzymes (Fráusto da Silva and Williams 1991). A deficiency of Zn in animals and humans can lead to anorexia and growth depression (Fráusto da Silva and Williams 1991). Although Zn is relatively non-toxic, elevated levels of Zn are detrimental to the environment (Chaney 1993).

The partitioning of Zn to phyllosilicate minerals has been extensively studied (Brown and Parks 2001; Sparks 1995). In acidic to near neutral environments, Zn partitioning to phyllosilicate surfaces mainly occurs by electrostatic interactions, due to a net negative structural charge developed within the octahedral layers of phyllosilicates due to isomorphic substitutions, and by specific chemical binding to hydroxyl edge sites. At higher solute concentrations and pH > 6.5, Zn, similar to Ni

and Co, can be incorporated into stable precipitates, formed at the surfaces of phyllosilicate minerals (Ford and Sparks 2000, Scheidegger et al. 1997; Thompson et al. 1999; Ford et al. 1999). These surface precipitates form at solution conditions undersaturated with respect to homogeneous precipitation and the metal becomes increasingly stable over time (Ford et al. 1999; Scheckel et al. 2001). Depending on the type of phyllosilicate present, initially a mixed Me-Al layered double hydroxide or LDH forms, with the structural formula generally written as $[Me^{2+}_{1-x}Me^{3+}_{x}(OH)_2]^{x+} \cdot (x/n)\ A^{n-} \cdot mH_2O$. With time, the anionic species in the interlayer space of the LDH can be replaced by silica polymers transforming the LDH gradually into a more stable precursor Me-Al phyllosilicate (Ford et al. 1999).

Goethite (α-FeOOH) is the most common and thermodynamically stable Fe oxide in soils (Schwetmann et al. 1985) and often occurs as a coating on clay minerals (Boudeulle and Muller 1988). Zinc adsorption on goethite is independent of ionic strength, indicating that metals mainly partition to goethite by chemisorption (Trivedi and Axe 2001a). X-ray absorption fine structure (XAFS) spectroscopic studies, employed to delineate zinc sorption complexes formed at the goethite surface at pH 7, confirmed that inner sphere sorption complexes are formed (Trivedi and Axe 2001b; Schlegel et al. 1997).

Coughlin and Stone (1995) found an increasingly stable fraction of Co, Ni and Cu sorbed to goethite with aging effects. It was proposed that, similar to the formation of Me-Al LDH precipitates on clay mineral surfaces, microscale formation of metal

spinels, $(Me^{2+}, Fe^{2+})Fe^{3+}{}_2O_4$, at the goethite surface may have caused the net increase in sorption and the subsequent decrease in the ability to desorb partitioned metals.

In this chapter we report on the effect of crystalline iron oxide (goethite) coatings on the mechanisms of Zn sorption to kaolinite, an ideal 1:1 clay mineral. A heterogeneous suspension reaction was used to obtain a stable goethite coating at the kaolinite surface (Scheidegger et al. 1993). The advantage of using this method is that the resulting surface coating consists of crystallographically pure and well- characterized goethite in contrast to traditional coating methods, where iron oxide coated clay particles are synthesized by adding base to an acidic Fe (III) solution in the presence of the clay (Chao et al. 1964; Hendershot and Lavkulich 1983). The sorption complexes formed at the goethite coated kaolinite surface and the individual sorbents are delineated using XAFS spectroscopy and systematically studied as a function of pH (5 and 7), aging time and surface loading.

3.3 MATERIALS AND METHODS

3.3.1 Materials

The kaolinite used in this study was a well-crystallized Georgia kaolinite (Clay Mineral Society source clay, KGa-1). The kaolinite was treated for the possible presence of carbonates, organic matter and manganese/iron oxides using standard procedures (Jackson 1956). Carbonates and exchangeable divalent ions were removed

by reaction with a NaOAc buffer at pH 5 in a near boiling water bath. Organic matter was removed by treating the kaolinite with H_2O_2. Iron oxides were removed with a dithionite-citrate-bicarbonate mixture in a 80°C warm water bath. The resulting kaolinite was washed twice with 1 M NaCl, and twice with DI water. The <0.2 μm fraction was separated by centrifugation, dialyzed against milli-Q H_2O, and freeze-dried. The specific surface area of the resulting kaolinite was determined by a five point N_2 Brunauer-Emmett-Teller (BET) gas adsorption isotherm method and was 14.01 m^2g^{-1}.

A well defined goethite was synthesized according to the method outlined in Schwertmann et al. (1985) and modified by Peak et al. (1999). Initially, ferrihydrite was precipitated by adding 50 ml of a 1 M ferric nitrate solution to 450 ml of 1 M KOH. The suspension of amorphous hydrous ferric oxide was aged for 21 days at 25°C to obtain crystalline goethite. This suspension was washed via centrifugation, where the supernatant was replaced with DI water to remove residual KOH. The rinsed solid was re-suspended in 0.4 M HCl and shaken for 2h using a mechanical shaker (Peak et al. 1999). This treatment was used to remove any remaining ferrihydrite from the surface of the goethite. The acidified goethite suspension was then washed with milli-Q H_2O to remove HCl, dialyzed against milli-Q H_2O and freeze dried. The BET surface area of the goethite was 66.49 $m^2.g^{-1}$.

Coatings of the well-defined goethite on the kaolinite surface were prepared using the method of Scheidegger et al. (1993). Two separate batches were prepared which yielded different amounts of goethite coatings on the kaolinite surface. Essentially, 130 and 200 mg of goethite were mixed with 2.5 g of kaolinite in 200 mL of a pH = 7.5 and I = 0.01 M $NaNO_3$ solution. This suspension was shaken for 48 hours and re-suspended three times in a $NaNO_3$ solution at the pH and ionic strength of the reaction medium (pH 7, I = 0.1 M $NaNO_3$). The coated kaolinite particles were washed several times with the background solution and finally with DI water. The resulting solids were oven dried at 110°C. Four samples (100 mg each) of the coated kaolinite were dissolved in 2 ml HNO_3 (95%) and 1 ml HF (40%) to determine the extent of the goethite coating. Al and Fe concentrations in the clear solution were measured on a Finnigan ELEMENT 1 high resolution magnetic sector inductively coupled plasma mass spectrometer (HR-ICP-MS) at the National High Magnetic Field Laboratory (Tallahassee, FL). A simple mass balance indicated that 10.7 or 6.1 weight percent goethite was coated at the kaolinite surface by this method. The BET surface areas of the resulting goethite coated kaolinite were 22.01 $m^2.g^{-1}$ and 16.56 $m^2\ g^{-1}$ respectively. The extent of coating was also checked with scanning electron microscopy (SEM) using a Hitachi SEM S4700 of the Delaware Biotechnology Institute.

3.3.2 Zn adsorption isotherms

Adsorption isotherms were conducted at constant pH 7 and room temperature. In 250 mL polyethylene centrifuge bottles, 100 mL of a 0.1 $g.L^{-1}$ kaolinite, goethite or 10 wt% goethite coated kaolinite suspensions were equilibrated at pH 7 for 24 hours under constant agitation. Zinc was then added from an acidified 0.1 M $Zn(NO_3)_2$ solution, to achieve initial Zn concentrations ranging from 0.01-1 mM. The initial zinc concentrations were chosen below solution saturation conditions (Ford and Sparks 1999) and above instrument detection limits. A 0.05 M (MES) buffer was used to maintain a constant pH. This buffer does not interfere with metal sorption (Kandegedara and Rorabacher 1999). All experiments were performed in a glove box at a nitrogen atmosphere, to prevent the formation of Zn-carbonates and hydrozincite. After centrifugation, Zn concentrations in the supernatant were analyzed with flame atomic absorption spectrometry (AAS).

3.3.3 Preparation of Zn sorption samples for XAFS

Zinc sorption to kaolinite, goethite and a goethite-coated kaolinite were studied as a function of pH, surface loading and aging time. All sorption experiments were performed in a glove box at constant pH, using a 0.05 M MES buffer, and constant ionic strength (0.1 M $NaNO_3$). At pH 5, maximum loading samples were prepared by reacting 3 mM Zn with 10g $solid.L^{-1}$. At pH 7, the solid suspension density, reaction time and initial [Zn] were varied to achieve a range of loading levels (Table 3.1). To study the effect of reaction time at pH 7, another batch was prepared with a suspension

density of 10g solid.L^{-1} and an initial [Zn] of 1 mM. These suspensions were placed on a reciprocal shaker for 46 days. At day 4 and 46, samples were collected for EXAFS analysis. All Zn reacted solids were separated from suspension via vacuum filtration through a 0.2 μm filter to minimize the entrapment of aqueous Zn. The resulting wet pastes were immediately loaded into acrylic sample holders, which were sealed with 0.0005-in. Kapton polyamide tape (CHR Industries, type K-104) to avoid moisture loss during analysis. The supernatants were analyzed on flame AAS for Zn, to determine surface loading levels.

3.3.4 Preparation of Reference Compounds

A solvated $Zn^{2+}_{(aq)}$ reference was prepared by dissolving $Zn(NO_3)_2$ in DI water to obtain a total Zn concentration of 15 mM. The pH was adjusted to 5 to prevent any polymerization. A synthetic mixed Zn-Al layered double hydroxide (LDH) reference was prepared at pH 6.3 using the method of Taylor (1984). The final precipitate had a Zn:Al ratio of 1.7 based on total dissolution of the solid and measurement of dissolved Zn and Al by flame AAS (Ford and Sparks 1999).

3.3.5 XAFS data collection and analysis

X-ray absorption spectra were collected at beamline X-11A of the National Synchrotron Light Source (NSLS), Brookhaven National Laboratory, Upton NY. The electron storage ring operated at 2.8 GeV with an average beam current of 180 mA. The monochromator consisted of two parallel Si (111) crystals with an entrance slit of

0.5mm. Higher order harmonics were suppressed by detuning 30% from the maximum beam intensity. The monochromator position was calibrated by assigning the first inflection point on the K-edge of a zinc metal foil to 9659.0 eV. The spectra were collected in fluorescence mode using an Ar-filled Lytle detector. Two sheets of Al (when Fe was present in the system), a 6μm-Cu filter and soller slits were placed between the sample and the detector to reduce elastic scattering. The incoming beam was measured with a N_2-filled ion chamber. All spectra were collected at room temperature and at least three scans were collected per sample to improve the signal to noise ratio.

XAFS data reduction was performed using WinXAS 2.1 (Ressler 1998) following standard procedures (Nachtegaal and Sparks 2003, Eick and Fendorf 1998). The χ function was extracted from the raw data by fitting a linear function to the pre-edge region and a spline function to the post-edge region, and normalizing the edge jump to unity. The energy axis (eV) was converted to photoelectron wave vector units ($Å^{-1}$) by assigning the origin, E_o, to the first inflexion point of the absorption edge. The resulting $\chi(k)$ functions were k^3 weighted to compensate for dampening of the XAFS amplitude with increasing k and were Fourier-transformed to obtain pseudo radial structure functions (PRSFs). A Bessel window with a smoothing parameter of 4 was used to suppress artifacts due to the finite Fourier filtering range between $\Delta k \approx 1.5$-12.4 $Å^{-1}$ for the kaolinite samples, $\Delta k \approx 1.6$-10.9 $Å^{-1}$ for the goethite coated kaolinite

samples and $\Delta k \approx 1.7\text{-}11.0$ Å^{-1} for the goethite samples. The two major peaks below 3.6 Å in the Fourier transformed curves were isolated and backtransformed. A R range of ≈ 0.7-3.6 Å was used for the first two peaks of the kaolinite samples, a R range of ≈ 0.8-3.6 Å was used for the goethite coated kaolinite samples and a R range of ≈ 0.8-3.2 Å was employed for the goethite samples. These backtransformed peaks were fit in k space. Structural parameters were extracted with fits to the standard EXAFS equation. *Ab initio* Zn-O and Zn-Zn/Al scattering paths were generated using the FEFF 7.02 (FEFF project 1996) code from the refinement of the structure of lizardite where Zn or Al was substituted for Mg in octahedral positions (Mellini 1982). Zn-O and Zn-Zn/Fe scattering paths were generated from the refinement of Franklinite. Optimization of the parameters was performed with the E_o shifts constrained to be equal and the amplitude reduction factor, $(S_o)^2$, fixed at 0.85. The value for $(S_o)^2$ was obtained from fitting Zn_{aq} and fixing the Zn-O coordination number to 6. A good fit was determined on the basis of the minimum residual error.

3.4 RESULTS AND DISCUSSION

3.4.1 Adsorption Isotherms

The heterogeneous suspension reaction, used to coat crystalline goethite at the kaolinite surface, yielded goethite coatings of ~ 6 and ~10 wt%. SEM images of this goethite coated kaolinite, collected at a 400 fold magnification showed 0.5-1 μm large

hexagonal kaolinite platelets, with 0.2-0.5 μm needle or rod shaped goethite particles coated onto the kaolinite surface (Figure 3.1).

Typical Zn adsorption isotherms in suspensions of kaolinite, goethite, and 10 wt% goethite coated kaolinite, are presented in Figure 3.2. None of the isotherms display typical Langmuirian shape (Stumm and Morgan 1996), with the possible exception of the goethite coated kaolinite. Thus, site saturation could only be estimated. The goethite coated kaolinite reached site saturation at ~ 2 μmol Zn/m^2. Site saturation occurred at ~ 1 μmol Zn/m^2 for kaolinite and ~ 1.5 μmol Zn/m^2 goethite. The steep increase for the Zn kaolinite adsorption isotherm after C_f = 0.3 mM Zn, suggests that Zn was precipitating out of solution, despite solution conditions being undersaturated with respect to homogeneous precipitation of any Zn containing solid (Ford and Sparks 1999). This suggests that a surface induced precipitate was forming. There was no apparent Zn sorption on kaolinite or goethite below equilibrium concentrations of 0.1 M Zn. A more definitive finding on the Zn sorption mechanisms taking place on these three solids can be derived from EXAFS spectroscopic analyses. Samples for EXAFS analysis were prepared at different surface loadings, representing different regions of Figure 3.2.

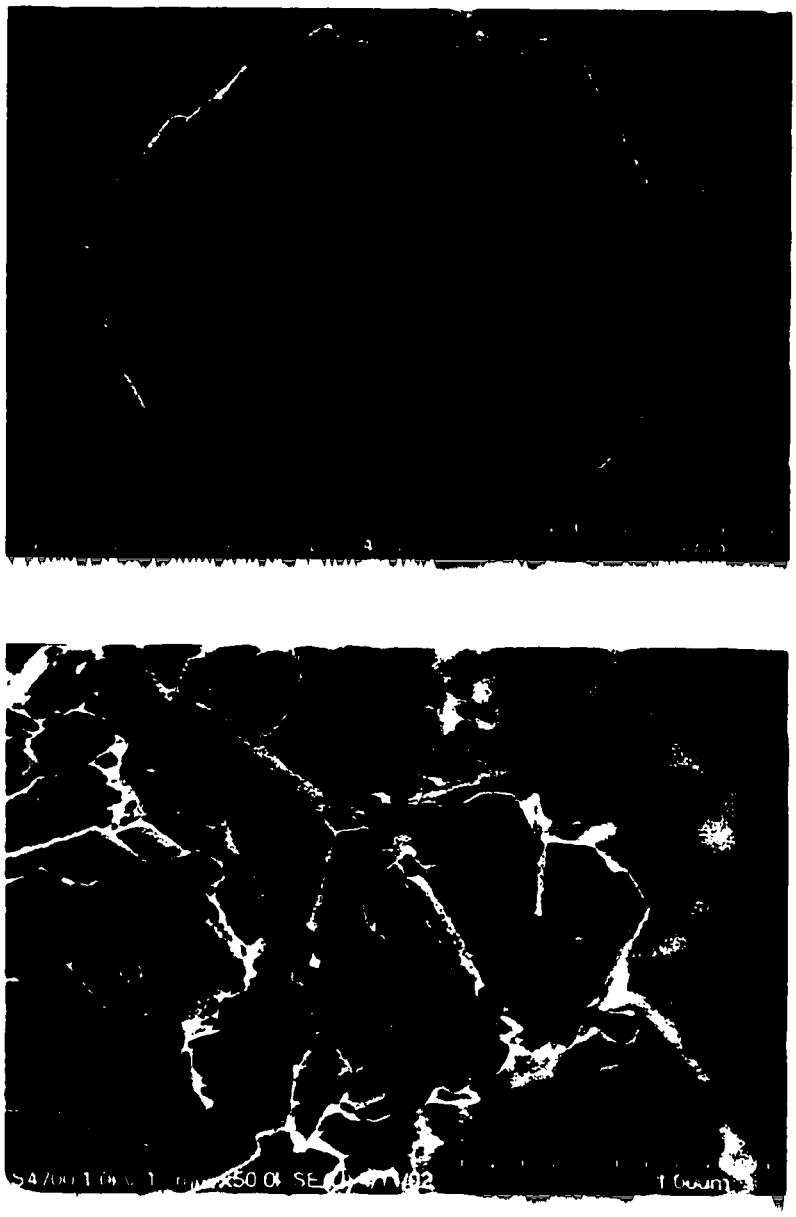

Figure 3.1: SEM photographs of the goethite coated kaolinite, taken at a 400 fold magnification. The hexagonal platelets are the kaolinite minerals and the needle shaped rods are goethite minerals.

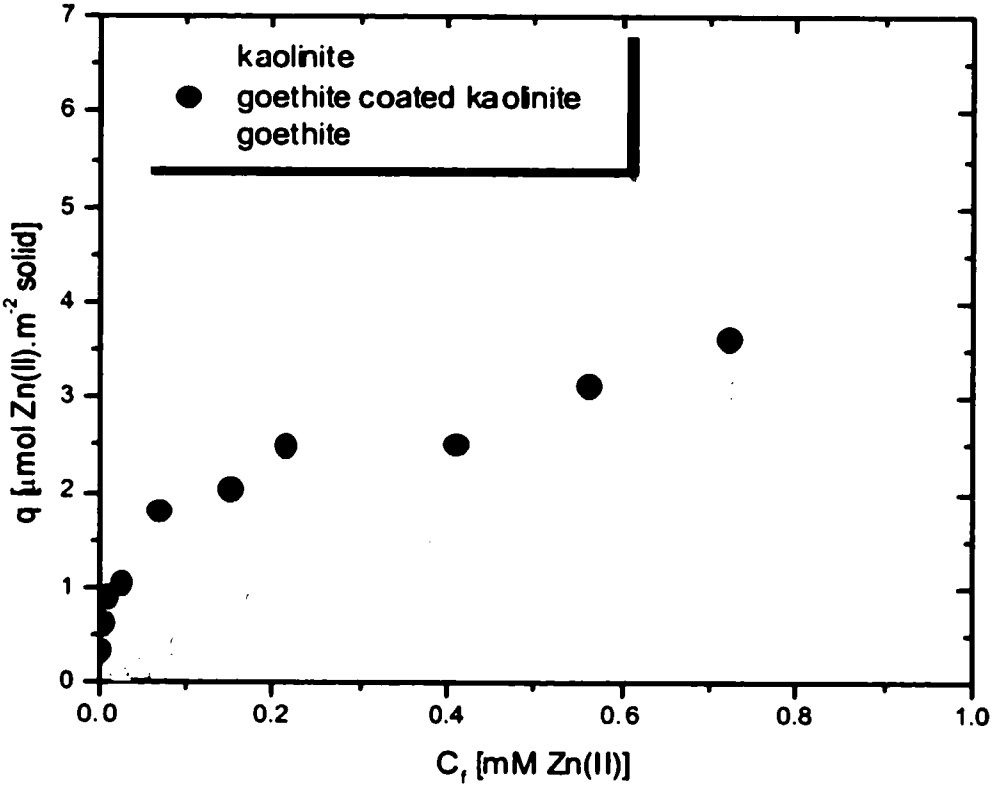

Figure 3.2: Zinc adsorption isotherms conducted on kaolinite, goethite and 10.7 wt% goethite-coated kaolinite. Experimental conditions: T (294K), pH =7.0, IS = 0.1 M $NaNO_3$, suspension density of 0.1 $g.L^{-1}$.

3.4.2 Zn sorption at pH 5

Figure 3.3a shows the raw k^3-weighted χ spectra of aqueous zinc, Zn/kaolinite, Zn/goethite and Zn/goethite coated kaolinite sorption samples, reacted with 3 mM Zn at pH 5 for 2 days and a mixed Zn-Al layered double hydroxide (Zn-Al LDH) reference. The spectrum for Zn^{2+}_{aq} has a single wave frequency, and its amplitude monotonically decreases with increasing k. This monotonic decrease with k is consistent with the presence of a single ordered coordination sphere. In contrast, the χ spectrum of the mixed Zn-Al LDH has several distinct frequencies, resulting from multiple scattering paths of higher atomic shells. Compared to the χ spectrum of aqueous zinc, the χ spectra of the Zn sorbed samples do have more structure and the phase of the wave frequency is shifted. This indicates that these spectra contain the signature of more than one atomic shell, probably due to the formation of bonds with the mineral surfaces. The lack of very distinct frequencies in the spectra, such as is present in the spectrum of the synthetic Zn-Al LDH, indicates that no Zn containing precipitates formed in the sorption samples. The raw χ spectra of the sorption samples, and especially of the Zn/goethite sorption sample, are very noisy. This is due to the fact that very little Zn could actually be sorbed onto the mineral surfaces at pH 5 (Table 3.1). The point of zero charge (pzc) of goethite is normally around 8 (Sparks 1995), which means that at pH 5 it is positively charged. This positive charge might repel the positively charged Zn ions away from the surface. The pzc of kaolinite lies

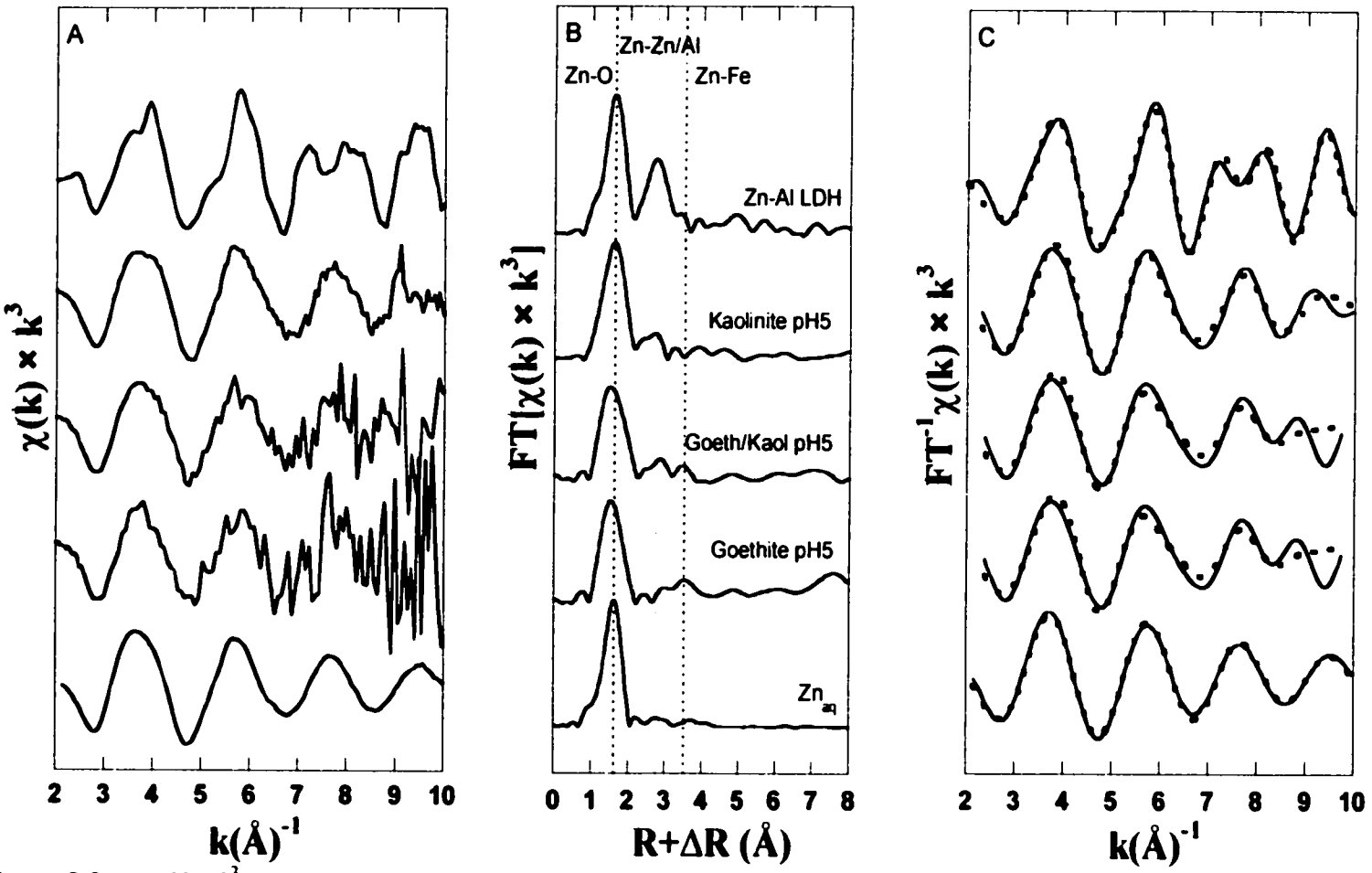

Figure 3.3: (A) The k^3-weighted $\chi(k)$ of the pH 5.0 Zn adsorption samples, aqueous Zn and the synthetic Zn-Al LDH reference compound, (B) the corresponding Fourier transforms (not corrected for phase shift) and (C) the fitted Inverse Fourier Transform of the two first shells of the Fourier transforms, with the solid lines representing the experimental data and the dotted lines the best fits.

	Time)	Γ(μmol /m²)	[C]ₜ	s:s (g/l)	Zn-O			Zn-Zn/Fe/Al				ΔE₀(eV)	χ²rcs%
					CN	R(Å)	σ²(Å)²	Atom	CN	R(Å)	σ²(Å)²		
References													
Zn^{2+} (aq)			15		6.0	2.07	0.009					-0.45	9.04
Zn-Al LDH					6.2	2.07	0.008	Zn	4.3	3.09	0.010	0.06	19.52
								Al	2.2	3.10	0.010		
pH 5.0													
Kaolinite		1.496	3	10.0	6.6	2.07	0.011	Al	1.4	3.09	0.010	0.46	21.30
Goethite		0.183	3	10.0	5.0	2.05	0.009	Fe	2.6	3.65	0.010	-0.15	31.33
Kaol-6Goeth		0.889	3	10.0	6.6	2.06	0.015	Al	1.8	3.14	0.010	0.68	31.96
pH 7.0 surface loading													
Kaolinite		2.818	1	5.3	6.3	2.05	0.013	Zn	3.6	3.13	0.010	0.64	12.62
								Al	0.9	3.19	0.010		
Kaolinite		2.171	1	8.0	5.2	2.03	0.010	Zn	4.9	3.10	0.011	-0.26	14.78
								Al	2.6	3.12	0.010		
Goethite		2.033	1	5.3	6.1	2.04	0.013	Fe	0.8	3.18	0.001	0.64	28.06
Goethite		1.217	1	8.0	4.9	2.01	0.010	Fe/Zn	1.5	3.06	0.013	-1.87	25.12
Kaol-6Goeth		2.070	1	5.3	6.7	2.04	0.014	Zn	2.0	3.15	0.012	1.71	10.67
Kaol-6Goeth		2.230	1	8.0	6.0	2.05	0.013	Zn/Fe	2.8	3.13	0.010	0.78	16.52
pH 7.0 reaction time													
Kaolinite	4	1.408	1	10.0	5.5	2.02	0.013	Zn	1.2	3.10	0.010	0.22	16.77
								Al	1.0	3.09	0.010		
Kaolinite	46	1.597	1	10.0	6.2	2.03	0.010	Zn	3.9	3.11	0.010	0.76	17.38
								Al	1.8	3.14	0.010		
Goethite	4	1.260	1	10.0	6.0	2.04	0.014	Fe	1.0	3.18	0.010	0.62	19.18
Goethite	46	1.496	1	10.0	5.8	2.06	0.011	Fe/Zn	1.2	3.07	0.010	0.57	15.89
Kaol-10Goeth	4	2.244	1	10.0	5.2	2.01	0.013	Fe	0.6	3.19	0.011	1.05	14.16
Kaol-10Goeth	46	2.190	1	10.0	5.7	2.02	0.012	Zn/Fe	1.5	3.11	0.010	0.35	20.46
								Al	0.9	3.11	0.010		

Table 3.1: Experimental and Structural Parameters for Zn Sorption and Reference Samples

Γ = Surface loading

$[Zn]_i$ = Initial Zn concentration

s:s = Solid: Solution ratio

CN = Coordination number ($\pm$ 30%)

R(Å) = Radial distance ($\pm$ 0.02 Å for the first shell and $\pm$ 0.05 Å for the second shell)

$\sigma^2(Å)^2$ = Debye-Waller factor

$\Delta E_0(eV)$ = Phase shift

$\chi^2_{res}\%$ = Fit error

† = 6.6 wt% goethite coating and 10.7 wt% goethite coating

around 5, therefore it is not repelling Zn ions and a much higher surface loading can be obtained.

Figure 3.3b shows the pseudo radial structure functions (PRSFs) obtained by Fourier transforming the raw χ spectra. The main peaks in the PRSF were backtransformed to k space (Figure 3.3c) and fit with calculated scattering paths (dashed lines). Structural parameters obtained from best fitting the backtransformed χ spectra are recorded in Table 3.1.

The PRSF of aqueous zinc, not corrected for phase shift, displays only one peak located at $R + \Delta R = 1.8$ Å, which was fitted with 6 oxygen atoms at 2.07 Å (Table 3.1). This coordination number and bond length is in good agreement with previous work (Munoz-Paez 1995) and with a sixfold coordination of Zn^{2+} by water (Hartmann et al. 1997). The first peak for the Zn/goethite and Zn/goethite coated kaolinite samples seems to be shifted to a lower radial distance, compared to Zn (aq), the Zn-Al LDH and the Zn/kaolinite sorption sample. Zn(II) is commonly found in both four-and sixfold coordination with oxygen atoms (Shriver and Atkins 1999). The Zn-O first-shell coordination number is well correlated with bond length, with Zn-O bond lengths of $\approx$ 1.96, Å typical of fourfold coordination, and Zn-O bond lengths of $\approx$ 2.08 Å typical of sixfold coordination (Waychunas et al. 2002). A shift of the first peak of the Zn/goethite and Zn/goethite coated kaolinite samples to shorter bond distances, suggest that these two sorption samples have a lower coordination number than the sixfold coordination found for aqueous zinc. However, fitting results only

indicated a slighter (within the reported fitting error) shorter bond length of 2.05 Å for Zn/goethite and 2.06 Å for goethite coated kaolinite. The coordination number of approximately 6 suggests that Zn is in an octahedral environment in all sorption samples.

All three sorption samples exhibit one or two smaller peaks at larger radial distances (Figure 3.3b). The second-shell feature in the Zn/kaolinite sample is best fit with ~ one Al atom at 3.09 Å, indicating that Zn is sorbed as an inner-sphere sorption complex to aluminol groups on the edge sites of the kaolinite. In a study on the sorption mechanisms of Zn to an acidic forest soil at pH 5.5, Voegelin et al. (2002) found significantly shorter Zn-Al bond distances of ~ 2.99 Å and attributed these to aluminol groups on edge surfaces of either phyllosilicates or amorphous Al hydroxides. In a study on the sorption mechanisms of Zn on aluminum powders, Trainor et al. (2000) found Zn-Al bond distances ranging from 2.95 to 2.99 Å, suggesting that the Zn-Al bond distances found by Voegelin et al. are indicative of Zn sorbed to Al hydroxides, rather then to phyllosilicates.

The second shell feature in the Zn/goethite sample is best fit with ~ two Fe atoms at 3.65 Å. However, the very low surface loading (0.183 μmol /m^2, Table 3.1) gave rise to a very noisy spectrum, which leads to a high uncertainty in the fit of the second shell feature. Similarly, Trivedi et al. (2001b) reported 2-3 Fe atoms at 3.54 Å for Zn sorption to goethite at pH 6.0 and attributed this to the formation of a not further defined inner sphere sorption complex. They also reported Zn in tetrahedral coordination with O, while in our system Zn is always in an octahedral coordination.

This might be caused by differences in crystallinity of the starting material. The PRSF for the Zn/goethite coated kaolinite sample displayed a second and a third shell. The second shell is at the same position as the second shell in the Zn/kaolinite spectrum and the third shell is at the same position as in the Zn/goethite spectrum (Figure 3.3b), suggesting that Zn sorption in a goethite coated kaolinite suspension is a combination of Zn sorption on both kaolinite and goethite surfaces. Again, the raw χ spectrum is noisy, due to the low (0.889 μmol /m^2) surface loading. The best fit, but with a high uncertainty, to the backtransformed χ spectrum indicated only two Al atoms at 3.14 Å, suggesting that a bidentate sorption complex is formed with the aluminol edge sites of the kaolinite.

3.4.3 Zn sorption at pH 7

The raw k^3 weighted χ spectra, their Fourier transforms and the fitted backtransformed k^3-weigthed spectra of the Zn sorption samples, prepared at pH 7, are shown in Figures 3.4 and 3.5. We prepared Zn sorption samples with increasing surface loadings, representing different regions in the Zn adsorption isotherms (Figure 3.2). Different surface loadings were achieved by varying the solid : solution ratio and the reaction time (Table 3.1). The higher surface loading samples are displayed in Figure 3.4. The raw χ spectra of the kaolinite samples and the goethite coated kaolinite samples look very similar and compare well with the χ spectrum of the synthetic Zn-Al LDH. The similarities in these spectra indicate that Zn containing precipitates,

similar in structure to the synthetic Zn-Al LDH, are formed at the kaolinite and the goethite coated kaolinite surfaces. The raw χ spectra of the Zn/goethite sorption samples are again noisy, although reasonable surface loadings were achieved. This may have been caused by the fact that the goethite surface is less well ordered. The χ spectra of the Zn/goethite sorption samples are distinctly different from the other Zn sorption samples and lack the high frequency patterns found in the other Zn sorption spectra. In fact, the wave frequency is very similar to the ones observed for the pH 5 Zn sorption samples, suggesting that at pH 7, Zn forms an inner sphere sorption complex with hydroxyl groups of goethite, rather then a precipitate phase.

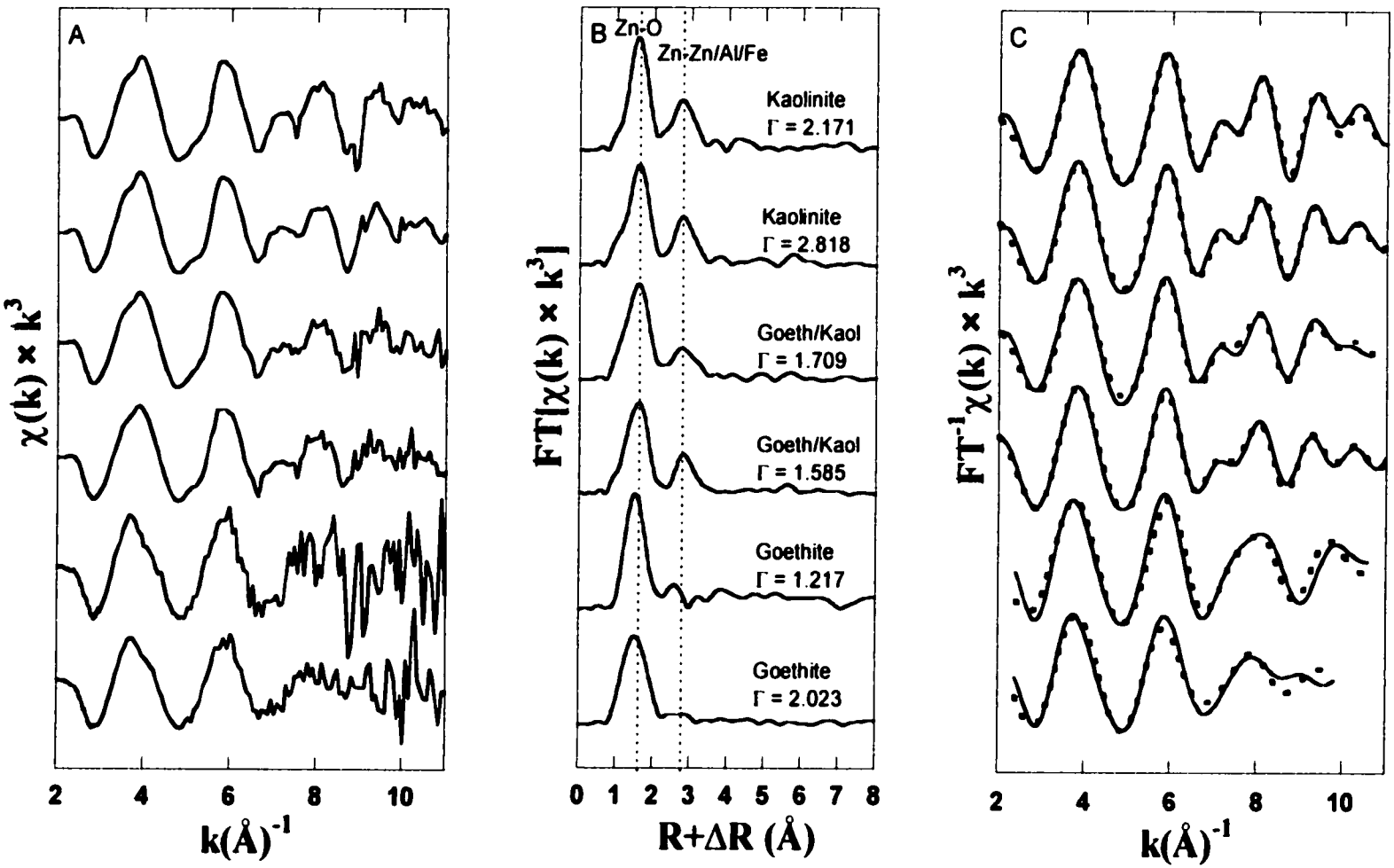

Figure 3.4: (A) The k^3-weighted $\chi(k)$ of the high surface loading, pH 7.0 Zn adsorption samples, (B) the corresponding Fourier transforms (not corrected for phase shift) and (C) the fitted Inverse Fourier Transform of the two first shells of the Fourier transforms, with the solid lines representing the experimental data and the dotted lines the best fits.

The PRSF of the pH 7, high surface loading samples all contain two dominant shells (Figure 3.4b). The first shell, at a radial distance of ~ 1.8 Å, was fit with ~ 6 oxygen atoms at 2.02-2.06 Å, which is indicative of octahedral coordination around the Zn atoms (Table 3.1). The second shell for the Zn sorbed kaolinite was fit with 3.6 Zn atoms at 3.13 Å, and 0.9 Al atoms at 3.19 Å for the 2.818 μmol /m^2 surface loading sample, and 4.9 Zn at 3.10 Å and 2.6 Al at 3.12 Å for the 2.171 μmol /m^2 sample (Table 3.1). These bond distances and coordination numbers are in agreement with bond distances found in a study of the Zn sorption mechanisms to pyrophyllite, a 2:1 clay mineral, at pH 7.5 (Ford and Sparks 2000). The only solids that can be formed in our system, sharing the same type of local structure are Zn-Al layered double hydroxide (Zn-Al LDH) and $Zn_3(OH)_4(NO_3)_2$, of which Zn-Al LDH is the most likely phase to form (Ford and Sparks 2000). In their study, Ford and Sparks (2000) observed the formation of a Zn-Al LDH phase at the pyrophyllite surface at every surface loading studied, with an increasing Zn-O bond length with increasing surface loading levels. They attributed this increasing Zn-O bond length to an increase of the Zn:Al ratio in the octahedral layer with increasing loading levels. The explanation lies in the atomic radii of the atoms. Since the Al atomic radius is smaller than that of Zn, the larger the Zn:Al ratio, the larger the Zn-O and Zn-Zn bond distances have to be to accommodate both Al and Zn in the solid structure. Our results suggest that the number of Al atoms incorporated into the octahedral layer of the Zn-Al LDH surface precipitate is determined by the equilibration time. The longer the metals are allowed to react with the clay mineral surface, the more Al becomes available by metal

promoted dissolution of the clay structure, which can then be incorporated into the precipitate. The finding that a Zn-Al LDH phase forms at the kaolinite surface at pH 7 is significant since this potential metal sequestering mechanism could lead to important contaminant attenuation in certain soil types.

Second shell fitting for the Zn/goethite sorbed samples revealed that Zn in the high surface loading sample is bound to 1 Fe atom at 3.18 Å. This result corresponds well with the findings of a study by Schlegel et al. (1997) to the Zn sorption complexes formed at the goethite surface. At pH 7 they found that Zn, in octahedral coordination, binds to 1 Fe atom at 3.00 Å and 1 Fe atom at 3.20 Å of the goethite surface, corresponding to an edge sharing sorption complex. Contrary to our study and the study by Schlegel et al., Trivedi et al. (2001b) found that at similar reaction conditions, Zn changed to tetragonal coordination upon binding to 2 Fe atoms at a radial distance of 3.51 Å. The different findings in these three studies may well be related to the crystallinity of the goethite minerals or to the sorption kinetics. In our study we carefully removed any non-crystalline iron oxide with HCl. When goethite is not washed carefully, the surface chemistry of the remaining solid may resemble that of a hydrous ferric oxide (Peak et al. 1999). Interestingly, in an extensive study on Zn sorption onto ferrihydrite, a hydrous ferric oxide, Waychunas et al. (2002) found a change in the Zn coordination environment to tetragonal coordination upon binding two Fe neighbors of the ferrihydrite at a radial distance of 3.44 Å. From a chemical point of view, Zn has a completely filled d shell, therefore it does not gain or lose any energy when it changes from octahedral to tetrahedral coordination (Shriver and

Atkins 1999). Zinc in the sodium nitrate background solution is in octahedral coordination. Therefore it is expected that Zn changes its coordination sphere upon sorption to octahedral goethite only when sorption requires structural rearrangement. Upon changing from an octahedral to a tetrahedral bonding environment, 2 water molecules come off and entropy is gained.

In the lower surface loading sample, Zn was bound to 1.5 Fe or Zn atoms at 3.07 Å. This bond distance is similar to the Zn-Zn distances found in our synthetic Zn-Al LDH and for the precipitate formed at the kaolinite surface. These results suggest that at lower surface loadings, Zn is included in a surface cluster (similar in structure to brucite), while at greater surface loading, Zn forms inner-sphere complexes with goethite. Alternatively, since the low loading sample was aged for 7 days, compared to 1 day for the high loading samples, one could conclude that initially all Zn sorbs to the goethite surface and over time is included into a surface precipitate, which is thermodynamically favored over the adsorption complex.

As inferred from the raw χ spectra, the Zn sorption complexes formed at the 6 wt % goethite coated kaolinite surface are very similar to the ones formed at the kaolinite surface. On both the high and the low loading sample in Figure 3.4, a surface precipitate formed: At the lower surface loading, a Zn-hydroxide formed, with 2 Zn atoms in the second shell; at the higher surface loading, a Zn-Al LDH formed with 2.8 Zn and 0.5 Al atoms in the second shell. The total number of atoms in the octahedral layer is lower than the total number of atoms in the octahedral layer of the precipitate

phases formed at the kaolinite surface, suggesting that the formation of a surface precipitate is retarded by the presence of a 6 wt % goethite coating.

3.4.4 Effect of aging time

Figure 3.5 shows the effects of aging time on the Zn sorption complex formed at pH 7 at the different solid surfaces. The initial surface loadings were chosen to be relatively low (Table 3.1 and Figure 3.5). An increase in surface loading at the goethite and kaolinite surface occurs with longer reaction times, and in the case of kaolinite corresponds with an increase in intensity of the second shell in the PRSF (Figure 3.5b). In the case of goethite, the second shell peak position shifts to lower radial distances with increasing reaction time (Figure 3.5b).

Fits to the first shell indicated that Zn sorbed on all three solids was octahedrally coordinated by 5.5-6.6 O atoms at a radial distance of 2.02-2.06 Å. After 4 days, Zn is bound at the kaolinite surface to one Zn atom at 3.10 Å and one Al atom at 3.09 Å. These Zn-Zn/Al distances are again indicative of the presence of a Zn-Al LDH. The low second shell coordination numbers indicate that instead of a fully developed precipitate, a smaller surface cluster may have formed. An increase in the number of atoms in the octahedral layer to 3.9 Zn atoms at 3.11 Å and 1.8 Al at 3.14 Å was recorded for the Zn sorption sample aged for 46 days. This explains the observed increase in intensity of the second shell in the PRSF, and is indicative of the growth of a surface precipitate over time. Comparing these results to the Zn adsorption isotherm (Figure 3.2) suggests that concurrent with site saturation (Γ = 1.0 μmol /m^2), small Zn-

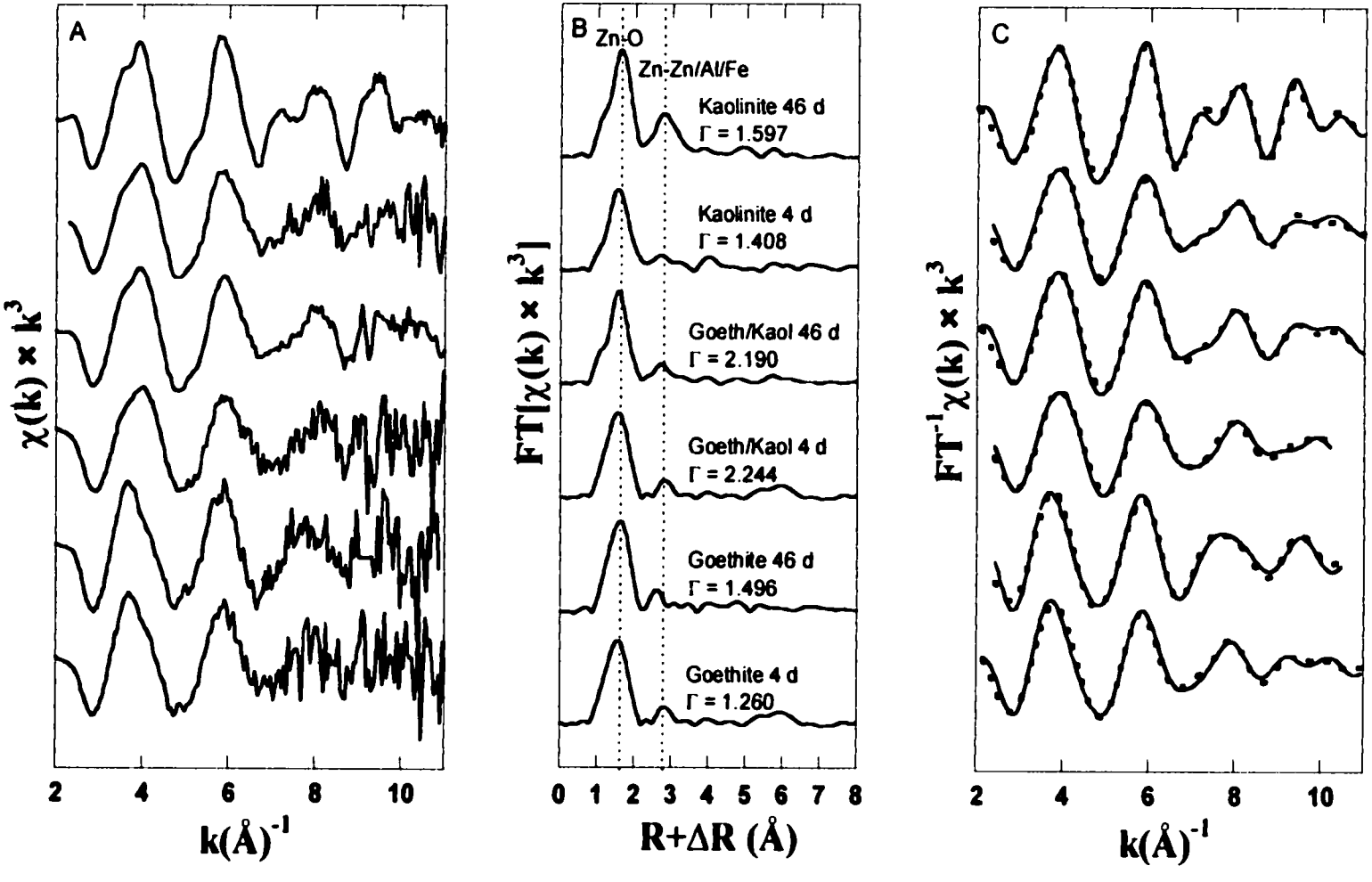

Figure 3.5: (A) The k^3-weighted $\chi(k)$ of the time series, pH 7.0 Zn adsorption samples, (B) the corresponding Fourier transforms (not corrected for phase shift) and (C) the fitted Inverse Fourier Transform of the two first shells of the Fourier transforms, with the solid lines representing the experimental data and the dotted lines the best fits.

Al surface clusters form at the kaolinite surface. With increasing reaction time, these small clusters develop into full three dimensional Zn-Al LDH surface precipitates.

The shift of the second shell feature in the PRSF of the Zn/goethite sorption sample with increasing reaction time to lower radial distances indicates a shift in the major sorption mechanism. The second shell of the 4 day reacted goethite spectrum was fit with one Zn-Fe neighbor at 3.18 Å, which is indicative of a monodentate inner sphere Zn sorption complex (see discussion above). After aging the Zn-reacted goethite suspensions for 46 days, a Zn-Zn/Fe coordination number of 1.2 was found, at a significantly shorter radial distance of 3.07 Å (Table 3.1). This bond length is characteristic of edge sharing Zn octahedra in some type of solid structure. Following the discussion above, only a Zn hydroxide precipitate, similar in structure to brucite, can be formed in our system that shares the same short range order. These results confirm the result obtained from the loading samples (Figure 3.4), in that Zn binds initially directly to the goethite surface, but over time is incorporated into a Zn hydroxide like surface cluster, suggesting that the incorporation of Zn into a Zn hydroxide phase is thermodynamically more favorable than the formation of adsorption complexes on goethite. Our adsorption studies were performed in a nitrogen atmosphere and at concentrations undersaturated with respect to homogeneous precipitation, which excludes the formation of any other solid phase that could potentially share the same short range order.

The spectroscopic results of this study provide a plausible explanation for other research (Coughlin and Stone 1995 and references therein) where an increasing stable

metal fraction, with respect to acidification, was observed at the goethite surface after aging the metal reacted goethite. Coughlin and Stone (1995) found a rapidly desorbing metal fraction and a slowly desorbing fraction of adsorbed metal upon acidification, with the slowly desorbed fraction increasing in significance with longer aging times for metals such Ni, Co and Cu, but not for Pb. The labile metal fraction is most likely the adsorbed metal fraction, whereas the stable metal fraction represents the metal fraction incorporated into a metal hydroxide. The ionic radius of Pb is too large to fit into the hydroxide structure, explaining why it does not show this biphasic desorption behavior. Since Fe^{2+} is not present in our system, this rules out the possible restructuring of the goethite surface into some type of spinel like structure.

Using the same initial solution conditions, much higher Zn surface loadings were achieved at the 10 wt% goethite coated kaolinite surface compared to the goethite or kaolinite alone. A similar trend was observed in the absorption isotherms (Figure 3.2), which suggests that the coated kaolinite complex has a much higher sorption capacity. Some release of Zn was observed after aging the Zn reacted goethite coated kaolinite for 46 days. This Zn release led to a lower surface loading and suggests a change in the major sorption mechanism. After aging the Zn reacted goethite coated kaolinite for 4 days, the best fits (Table 3.1) indicated that the main Zn sorption mechanism is the formation of a monodentate inner-sphere complex with goethite, with Zn bound to 0.6 Fe atoms at 3.19 Å. These results differ from the 6 wt% goethite coated kaolinite, where the formation of a Zn hydroxide surface precipitate

seemed to be the major sorption mechanism. The larger amount of goethite at the surface does determine the initial sorption behavior.

Similar to the effect of aging on the Zn sorption complex formed at the goethite surface, after aging the Zn sorption complex formed in the 10.7 wt% goethite-coated kaolinite suspension, a change in the major sorption mechanism takes place. After an incubation time of 46 days, Zn is bound to 1.5 Zn/Fe atoms at 3.11 Å and 0.9 Al atoms at 3.11 Å. This corresponds to the transition from an adsorption complex to the incorporation of Zn into a mixed Zn/Fe-Al LDH surface precipitate.

In conclusion both the extent of the iron oxide coating and the reaction time determines the final complex formed at the goethite coated kaolinite surface. With a goethite surface coating of 6 wt%, Zn immediately forms a Zn hydroxide precipitate, which with increasing reaction time resembles more a Zn-Al LDH. This suggests that Al becomes increasingly available over time. In 10.7 wt% goethite coated kaolinite suspensions, Zn first forms an inner-sphere sorption complex with the surface hydroxyl groups. This indicates that goethite has a higher affinity for Zn than the kaolinite clay mineral. Over time, the inclusion of Zn into a Zn-Al LDH precipitate becomes the dominant sorption mechanism. This suggests that the formation of a precipitate phase at the kaolinite surface is favored over adsorption on the goethite coating. More studies are needed to determine the effect of reaction kinetics on the sorption complexes formed.

3.5 SUMMARY AND CONCLUSIONS

EXAFS spectroscopic studies indicate that at pH 5, Zn forms inner-sphere sorption complexes with all solids in this study. A monodentate inner-sphere sorption complex is formed at the kaolinite surface, with Zn binding to Al-OH edge groups at a radial distance of 3.14 Å. Our results suggest that Zn forms a bidentate innersphere complex with hydroxyl groups at the goethite surface, with Zn-Fe distances of 3.65 Å. The PRSF of the Zn sorption complex formed at the goethite-coated kaolinite surface suggests that a combination of the sorption mechanisms of Zn to the individual sorbents, but only Zn bound to Al-OH edge groups of the kaolinite could be fitted.

The sorption complexes formed at pH 7 changes with surface loading levels and reaction time. At the kaolinite surface, Zn is incorporated into a mixed metal Zn-Al layered double hydroxide already at low loading levels. This surface precipitate phase increases in size with increasing aging time. At the goethite surface, Zn initially forms a monodentate inner-sphere sorption complex, with Zn binding to one Fe atom at 3.18 Å. With increasing reaction time however, the major Zn sorption mechanism changes to the formation of a zinc hydroxide surface precipitate.

Both the extent of the iron oxide coating and the reaction time determine Zn complex formation at the goethite-coated kaolinite surface at pH 7.0. With a surface coating of 6 wt% FeOOH, Zn is immediately incorporated into a Zn-Al LDH surface precipitate. In the presence of a 10 wt% goethite coating, the initial dominant sorption mechanism is the formation of an inner-sphere sorption complex of Zn with the surface hydroxyl groups of goethite. This indicates that at pH 7.0, goethite has a

higher affinity for Zn then the kaolinite clay mineral or the surface precipitate. With increasing aging time, the inclusion of Zn into a precipitate phase (similar in structure to brucite) takes over as the dominant sorption mechanism. This suggests that the formation of a precipitate phase at the kaolinite surface is thermodynamically favored over adsorption to the goethite coating.

3.6 REFERENCES

Alloway B.J. 1990. Heavy metals in soils. Blackie. London,

Boudeulle, M., and J.P. Muller. 1988. Structural characteristics of hematite and goethite and their relationships with kaolinite in a laterite from Cameroon -- a TEM study. *Bull. Mineral.* **111:** 149-166.

Brown, G.E., Jr. and G.A. Parks. 2001. Sorption of trace elements on mineral surfaces: Modern perspectives from spectroscopic studies, and comments on sorption in the marine environment. *Int. Geol. Rev.* **43:** 963-1073

Chaney, R.L. 1993. *In* Zinc in Soils and Plants. Robson, A.D. (Ed.) Kluwer Academic Publishers, the Netherlands.

Chao, T.T., M.E. Harward and S.C. Fang. 1964. Iron or aluminum coatings in relation to sulfate adsorption characteristics of soils. *Soil Sc. Soc. Proc.* **28:** 632-635.

Coston, J.A., C.C. Fuller and J.A. Davis. 1995. Pb2+ and Zn2+ adsorption by a natural aluminum-bearing and iron-bearing surface coating on an aquifer sand. *Geoch. Cosmochim. Acta* **59:** 3535-3547

Coughlin, B.R. and A.T. Stone. 1995. Nonreversible adsorption of divalent metal-ions (Mn-II, Co-II, Ni-II, Cu-II and Pb-II) onto goethite – effects of acidification, Fe-II addition, and picolinic-acid addition. *Environ. Sci. Technol.* **29:** 2445-2455.

Eick, M. J. and S. E. Fendorf. 1998. Reaction sequence of Nickel(II) with kaolinite: Mineral dissolution and surface complexation and precipitation. *Soil Sci. Soc. Am. J.* **62:** 1257-1267.

FEFF Project, 7,02 ed.: Department of Physics, University of Washington, Seattle, WA, 1996.

Ford, R.G., A.C. Scheinost, K.G. Scheckel and D.L. Sparks. 1999. The link between clay mineral weathering and the stabilization of Ni surface precipitates. *Environ. Sci. Technol.* **33:** 3140-3144.

Ford, R.G. and D.L. Sparks. 2000. The nature of Zn precipitates formed in the presence of pyrophyllite. *Environ. Sci. Technol.* **34:** 2479-2483.

Fráusto da Silva, J.J.R. and R.J.P. Williams. 1991. The biological chemistry of the elements. Oxford University Press Inc. New York.

Hartmann, M., T. Clark, and R.V. Eldik. Hydration and water exchange of zinc(II) ions. Application of density functional theory. 1997. *J. Am. Chem. Soc.* **119:** 7843-7850.

Hendershot, W.H. and L.M. Lavkulich. 1983. Effect of sesquioxide coatings on surface-charge of standard mineral and soil samples. *Soil Sc. Am. J.* **47:** 1252-1260.

Hochella, M.F. 1990. Atomic-structure, microtopography, composition, and reactivity of mineral surfaces. *In* Mineral-Water Interface Geochemistry. Hochella, M.F. and A.F. White Jr. (Eds.) Mineralogical Society of America: Washington. DC. Vol. **23:** 87-132.

Jackson, M.L. 1956. Soil chemical analysis-advanced course. University of Wisconsin. Madison. Wisconsin. Madison, WI.

Kandegedara, A. and D.B. Rorabacher. 1999. Noncomplexing tertiary amines as "better" buffers covering the range of pH 3-11. Temperature dependence of their acid dissociation constants *Anal. Chem.* **71:** 3140-3144.

Manceau, A., B. Lanson, M.L. Schlegel, J.C. Hargré, M. Musso, L. Eybert-Bérard, J.-L. Hazemann, D. Chateigner and G.M. Lamble. 2000. Quantitative Zn speciation in smelter-contaminated soils by EXAFS Spectroscopy. *Am. J. Sci.* **300:** 280-343.

Mellini, M. 1982. The crystal-structure of lizardite 1T - hydrogen-bonds and polytypism. *Am. Mineral.* **67:** 587-598.

Munoz-Paez, A., R.R. Pappalardo, and E. S. Marcos. (1995). Determination of the 2nd hydration shell of Cr^{3+} and Zn^{2+} in aqueous solutions by extended X-ray absorption fine structure. *J. Am. Chem. Soc.* **117:** 11710-11720.

Nachtegaal, M. and D.L. Sparks. 2003. Nickel sequestration in a kaolinite-humic acid complex *Environ. Sci. Technol.* **37:** 529-534.

Nriagu, J.O. and J.M. Pacyna. 1984 Quantitative assessment of worldwide contamination of air, water and soils by trace-metals. *Nature* **333:** 134-139.

Peak, J.D., R.G. Ford and D.L. Sparks1999. An in situ ATR-FTIR investigation of sulfate bonding mechanisms on goethite. *J. Colloid Interface Sci.* **218:** 289- 299.

Ressler, T. 1998. WinXAS: a program for X-ray absorption spectroscopy data analysis under MS-Windows. *J. Synchrotron Radiat.* **5:** 118-122.

Roberts, D.L., A.C. Scheinost, and D.L. Sparks. 2002. Zinc speciation in a smelter-contaminated soil profile using bulk and microspectroscopic techniques. *Environ. Sci. Technol.* **36:** 1742-1750.

Scheckel K.G., A.C. Scheinost, R.G. Ford and D.L. Sparks. 2000. Stability of layered Ni hydroxide surface precipitates - A dissolution kinetics study. *Geochim. Cosmochim. Acta* **64**: 2727-2735.

Scheidegger, A., M. Borkovec, and H. Sticher. 1993.Coating of silica sand with goethite: preparation and analytical identification. *Geoderma* **58:** 43-65.

Scheidegger A. M., G. M. Lamble and D. L. Sparks. 1997. Spectroscopic evidence for the formation of mixed-cation hydroxide phases upon metal sorption on clays and aluminum oxides. *J. Colloid Interface Sci.* **186:** 118-128.

Schlegel, M.L., M. Manceau, and L. Charlet. 1997. EXAFS study of Zn and ZnEDTA sorption at the goethite (alpha-FeOOH)/water interface. *J. Phys. IV Fr.* **7C-2:** 823-824.

Schwertmann, U., P. Cambier and E. Murad. 1985. Properties of goethites of varying crystallinity. *Clays Clay Miner.* **33:** 369-378.

Shriver, D.F., and P.W. Atkins. 1999. Inorganic Chemistry. W.H. Freeman and Company, New York, NY.

Sparks D.L. 1995. Environmental Soil Chemistry. Academic Press, Inc. London.

Stumm, W. and J.J. Morgan. 1996. Aquatic Chemistry. Wiley, New York.

Taylor, R.M. 1984. The rapid formation of crystalline double hydroxyl salts and other compound by controlled hydrolysis. *Clay Miner.* **19:** 591-603.

Templeton, A.S., T.P. Trainor, S.J. Traina, A.M. Spormann and G. E. Brown Jr.. 2001. Pb(II) distributions at biofilm-metal oxide interfaces. *P. Natl. Acad. Sci. USA* **244:** 11897-11902.

Thompson, H.A., G.A. Parks and G.E. Brown Jr. 1999. Dynamic interactions of dissolution, surface adsorption, and precipitation in an aging cobalt(II)-clay-water system. *Geochim. Cosmochim. Acta* **64:** 1767-1779.

Trainor, T.P., G.E. Brown Jr., and G.A. Parks 2000. Adsorption and precipitation of aqueous Zn(II) on alumina powders. *J. Colloid Interface Sci.* **231,** 359-372.

Trivedi, P., and L. Axe. 2001a. Ni and Zn sorption to amorphous versus crystalline iron oxides: Macroscopic studies. *J. Colloid Interface Sci.* **244:** 221-229.

Trivedi, P., L. Axe and T.A. Tyson. 2001b.An analysis of zinc sorption to amorphous versus crystalline iron oxides using XAS *J. Colloid Interface Sci.* **244:** 230- 238.

Voegelin, A., A.C. Scheinost, K. Bühlmann, K. Barmettler and R. Kretschmar. 2002. Slow formation and dissolution of Zn precipitates in soil - A combined column-transport and XAFS study. *Environ. Sci. Technol.* **36:** 3749-3754.

Waychunas, G.A., C.C. Fuller, and G.A. Davis. 2002. Surface complexation and precipitate geometry for aqueous Zn(II) sorption on ferrihydrite I: X-ray absorption extended fine structure spectroscopy analysis. *Geoch. Cosmochim. Acta* **66,** 1119-1137.

Zachara, J.M., C.T. Resch and S.C. Smith. 1994. Influence of humic substances on Co^{2+} sorption by a subsurface mineral separate and its mineralogic components. *Geochim. Cosmochim. Acta* **58:** 553-556.

Chapter 4

EFFECTS OF *IN SITU* REMEDIATION ON THE SPECIATION AND MOBILITY OF ZINC IN A SMELTER CONTAMINATED SOIL

4.1 ABSTRACT

We report results from an extensive study to the speciation and mobility of zinc in a smelter contaminated soil and in an *in situ* remediated area of this contaminated soil, 12 years after the application of beringite (a modified aluminosilicate) and compost. Special attention was placed on the role of neo-formed surface precipitates in controlling the Zn speciation and mobility under different environmental conditions. Twelve years after remediation, the pH of the treated and non-treated soil differed by 0.5 pH unit. Using state of the art electron and X-ray microscopies in combination with μ-focused extended X-ray absorption fine structure (EXAFS) spectroscopy, no significant differences in Zn speciation were found between samples of the treated and non-treated soil. Thirty percent of Zn was in smelter related minerals (mainly willemite), ten percent of Zn was chemisorbed to iron and manganese oxides and sixty percent of Zn was incorporated into newly formed surface precipitates, which resembled a mixed Zn-Al layered double hydroxide (LDH) in the non-treated soil samples and a Zn-phyllosilicate in the treated soil sample. Desorption experiments, using a stirred flow set-up with a pH 6.5 0.1 M $CaCl_2$ and a pH 4.0 HNO_3 solution were performed to determine the exchangeable fraction and the fraction which will be mobilized under more extreme weathering conditions

respectively. No differences were found in desorption behavior between the treated and non-treated soil. Using the pH 4.0 solution, 30-40% of Zn was desorbed after 80 chamber volumes and the reaction was not yet complete, indicating that Zn was not in a stable form. We concluded that the incorporation of Zn into stable surface precipitates leads to a significant natural attenuation of the exchangeable/bioavailable Zn fraction at near neutral pH conditions. The formation of surface precipitates did however not lead to a permanent sequestration of Zn from the soil solution.

4.2 INTRODUCTION

Elevated concentrations of non-ferrous metals (Zn, Cd, Pb, etc.) and their toxic effects to the local ecosystem have been frequently documented in surface soils near base metal smelters. This has lead in some cases to the complete destruction of the natural vegetation cover (Vangronsveld et al. 1996). In a 1983 survey of worldwide trace element emissions, the Zn flux into the atmosphere from Zn production was estimated at 50-70 % of the total atmospheric Zn flux (Nriagu 1988). Most Zn used in today's industries is extracted from the ore by a hydro-metallurgical process. However, the highly polluting pyrrometallurgical smelting process has been used for over two centuries (Wickham 1990).

In situ remediation (immobilization/inactivation) of these contaminated sites using soil amendments, modifying the physicochemical properties of the contaminating heavy metals, is a valuable alternative for more expensive and complicated civil-engineering techniques, e.g. excavation and landfilling of the

contaminated soil (Vangronsveld, 1996). Many additives have been screened for their potential to immobilize heavy metals in soils. Examples of these additives include lime (Sparks 1995), zeolites (Oste et al 2002), incinerator ashes (Vangronsveld et al 1995, 1996), red mud (Lombi et al 2003) and hydroxyapatite (Boisson et al 1999). Each of these additives has a different effect on the bioavailability of the metals, micronutrient availability, soil pH and microstructure (Lombi et al 2003, Oste et al 2002).

Regulatory acceptance of *in situ* immobilization as an effective reclamation method depends on the ability to predict the long–term stability of such remedial treatments. To realistically address the long term stability of the metals, one needs to probe Zn speciation changes as a result of the soil reclamation activities and determine if these changes in the speciation of Zn lead to a long-term sequestration of the metal.

Traditionally, metal speciation in soils has been determined using sequential extraction techniques (Tessier 1979), which is a relatively inexpensive method, and therefore widely applied. However, there are uncertainties related to the selectivity of the various extractants and to the changes in metal speciation caused by the chemical reagent used in each extraction step (Ostergren 1999, Webb 2000). Sequential extractions do not yield molecular information and may overlook the presence of minor phases that could control the metal bioavailability.

Synchrotron based X-ray absorption fine structure (XAFS) spectroscopy is a technique that can provide detailed chemical and structural information about a

specific absorbing element in situ with minor or no pretreatments, be it a major component of a solid phase (crystalline or amorphous), a trace component of the bulk phase, or a surface-associated component (Bertsch and Hunter 1998). XAFS spectroscopy has become the method of choice for probing the speciation of metal contaminants at the molecular level and its use has demonstrated the variable reactivity and speciation of Zn in model systems. One important conclusion of studies on the complexation mechanisms of Zn with aluminosilicates, is that Zn forms inner-sphere surface complexes with aluminosilicates at lower pH and is incorporated into a neo-formed surface precipitate under neutral to basic conditions (Ford and Sparks 2000; Trainor et al. 2002). The formation of Zn-containing surface precipitates may greatly reduce the bio-availability of Zn in contaminated soils when the pH is raised (Juillot et al. 2003).

One of the problems with using bulk XAFS to speciate Zn in heterogeneous systems, such as soils, is that it probes a volume of several cubic millimeters, thereby averaging over all the atoms of a certain Z in the system under study, regardless of their chemical state (Manceau et al 2003). The short range structural information extracted by multishell fitting is usually sufficient to determine the most predominant species in a sample. However, when Zn is present in multiple phases, the atomic shells from the different species overlap so that one cannot separate them out when there is a mixture (Manceau et al. 2003). With the advent of high-brilliance synchrotron radiation sources it is now possible to identify metal species in dilute samples with high spatial resolution, using μ-focused extended X-ray absorption fine structure

spectroscopy (EXAFS). When probing only a small area of a sample, typically several square micrometers, one can minimize the number of species contributing to the overall spectrum. By treating the μ-EXAFS spectra of the unknown sample as a whole, i.e. fitting linear combinations of reference spectra to the unknown spectra, one can than deconvolute up to three major species contributing to the overall spectrum. The success of such a fitting approach depends on the availability of all unknown species in the reference database. Even when a large database of reference spectra is available and a good fit is achieved, there is some doubt whether a unique solution is achieved (Wasserman 1999). By collecting a great number of spectra of the sample one can use principal component analysis (PCA) to determine how many independent components are needed to reproduce the complete dataset.

The objectives of this study were: 1) to evaluate impact of long term remediation with beringite, a modified aluminosilicate and compost on Zn speciation in smelter contaminated soils, 2) to relate speciation differences to Zn mobility and 3) to ascertain whether Zn-Al LDH or Zn-phyllosilicate phases occurred in the soils.

The two soil samples used in this study were collected from a highly contaminated site close to a former Zn smelter in Belgium, where several remediation strategies have been evaluated. Samples were collected from the bare non-treated area, and from an area 12 years after treatment with beringite (an aluminosilicate byproduct of coal burning) and compost, in combination with sowing of metal tolerant plants, had occurred. The soil properties and pH of these two soils are similar 12 yrs after *in*

situ remediation (Table 4.1); however the remediated area has a restored ecosystem, while the non-treated area remains an ecological desert.

We combined conventional soil chemistry techniques with state of the art electron microprobe analyses and μ-focused synchrotron based X-ray fluorescence (SXRF) and extended X-ray absorption fine structure (EXAFS) spectroscopy to speciate Zn in the both the treated and non-treated soil. Using a large set of selected zinc reference compounds, the Zn-bearing components in the soil were speciated by utilizing PCA to determine the minimum number and type of probable components and then quantified from the experimental EXAFS spectra using a least-squares fitting (LSF) procedure. To determine whether the speciation changes after remediation persist with time, desorption experiments, using a stirred-flow technique were conducted, using a 0.1 M $CaCl_2$ solution adjusted to the soil pH, and a pH 4 HNO_3 solution to simulate normal and more extreme weathering conditions. A stirred-flow set-up was used for the desorption experiments, to speed up the weathering reactions. The small sample chamber, relatively low solid: solution ratio and constant flow rate ensure that none of the desorption products will be re-adsorbed onto the soil. Our aim is to make a prognosis on the long-term Zn availability in the remediated and non remediated soils, based on our direct speciation assessment and the stirred-flow desorption experiments. A major goal is to evaluate the importance of Zn containing surface precipitates in the reduction of the (bio)available Zn fraction in the contaminated soils.

4.3 MATERIALS AND METHODS

4.3.1 Site Description and Sampling

Soil samples were collected from a zinc smelter contaminated area and a 3 ha remediated area. The sampling site is located 1 km east of the 'Lommel' smelter in the Maatheide Natural Reserve in northeastern Belgium. Due to the high concentrations of different non-ferrous metals in the soil, there was not vegetative cover over a 135 ha area. In 1990, 3 ha of this area were successfully revegetated by immobilizing in-situ toxic metals with a mineral additive and then growing metal tolerant plants (Vangronsveld 1994). The mineral additive used in this study was beringite (a modified aluminosilicate produced by burning coal refuse in a fluidized bed) together with compost. Samples were taken from the upper 20 cm of the bare contaminated area (called non-treated from here on) and from the upper 20 cm of the remediated site (called treated from here on), 12 yrs after the addition of beringite. The samples were dried at 80°C and sieved through a 2 mm sieve.

4.3.2 Methods

The pH of the treated and non-treated samples were determined by mixing a 0.01 M $CaCl_2$ solution with the soil in a 10:1 weight ratio, equilibrated for 2h and subsequently measuring the pH. Dry weight Pb, Zn, Cu, Cd, As, Ni, Co, Fe, Mn, P, S, Ba, Al, Ti and Zr concentrations and Pb isotope ratios were measured on a Finnigan ELEMENT 1 High Resolution magnetic sector Inductively Coupled Plasma Mass

Spectrometer (HR-ICP-MS) at the National High Magnetic Field Laboratory (Tallahassee, Fl). All sample handling was conducted in a class 100 clean lab and flow bench. 100 mg of soil was digested at 125°C for 16h, in an ultra pure acid mixture, consisting of: 3 ml HF (double distilled), 4 ml HNO_3 (double distilled) and 3 ml $HClO_4$ (SEASTAR Chemicals Inc.). Digests were dried at 175 C, taken up in 2 ml of 6N HNO_3 and diluted to 100 ml total volume in pre-cleaned HDPE bottles. For HR-ICP-MS analyses, samples were diluted 100-fold with 0.17 N HNO_3, such that the total dissolved solid (TDS) fraction was 10 ppm. Triplicate samples and procedural blanks were analyzed against a mixture of known standards (High Purity Standards). All samples, blanks and standards were spiked with Sc, In and Tl to track instrument drift and potential matrix effects. The precision for the triplicate samples was better than 10% for most elements.

For Pb isotope ratio measurements, an external fractionation correction was applied by alternatively measuring NBS981 and the samples in the 10ppm TDS sample dilution. Pb isotopes were measured in low resolution with an analogue detection mode. Reproducibility based on in-run replicates of NBS981 (n=5) was better than 0.05 % for all ratios.

4.3.3 Desorption Experiments

Desorption experiments were conducted using two different desorptive solutions: i) a 0.1 M calcium chloride solution, adjusted to the soil pH, and ii) a nitric acid solution, adjusted to pH 4. The experimental setup for the Zn desorption studies was similar to

that illustrated by Strawn and Sparks (2000). Briefly, a stirred-flow reaction chamber was connected to an HPLC pump at inlet and to a fraction collector at the outlet. The desorptive solution was pumped through the chamber at a flow rate of 0.8 mL min^{-1}. The chamber was covered with a 25 mm filter membrane of 0.2 μm pore size to separate the solid from the solution. The chamber volume of ca. 8 mL contained a suspension of 0.3 g of soil, which was stirred at 400 rpm with a magnetic stir bar. Effluent aliquots of 10 mL were sampled at the chamber outlet and analyzed for Zn by inductively coupled plasma optical emission spectrometry (ICP-OES). The data from the stirred-flow studies were plotted as a function of chamber volumes (CV), which were calculated by multiplying the flow rate and the time and dividing by the volume of the chamber (8 mL).

4.3.4 Electron Probe Microanalysis (EPMA)

Electron microprobe analysis was performed using a JEOL JXA-8600 microprobe (John Hopkins University) equipped with both wavelength-dispersive and energy-dispersive spectrometers (WDS and EDS). Two air dried subsamples of the treated and the non-treated samples were embedded in Scotchdale© Resin, mounted on pure quartz slides, polished to 30 μm thick thin sections, and carbon coated before microprobe analysis. Samples were scanned manually at magnifications of 85-300x using backscatter electron imaging to identify heavy metal rich particles. Particles of interest were identified by EDS screening. At selected, representative spots, several elements (Zn, Pb, Si, Al, S, Mn, Ca, Fe) were mapped.

4.3.5 Extended X-ray Absorption Fine Structure (EXAFS) Spectroscopy Analysis of References

Zn K-edge (9659 eV) EXAFS spectra of the treated and the non-treated soil samples and Zn reference compounds were collected at beamline X-11A at the National Synchrotron Light Source (NSLS), Upton, NY. The electron storage ring operated at 2.5 GeV yielding an electron beam of 300-100 mA. The double crystal Si(111) monochromator was detuned by reducing I_o by 30%. The beam energy was calibrated by assigning the first inflection on the K-absorption edge of a Zn metal foil to 9659 eV. All samples were mounted into Teflon sample holders, sealed with Kapton tape, and measured at room temperature in fluorescence mode using a 13-element solid state detector. Depending on the Zn concentration, multiple scans were collected until satisfactory signal-to-noise ratios were achieved.

A large library of natural and synthetic Zn minerals and Zn sorption samples was generated to aid in the spectral analysis. Franklinite ($ZnFe_2O_4$), willemite (Zn_2SiO_4), hydrozincite ($Zn_5(OH)_6(CO_3)_2$), zincite (ZnO) and smithsonite ($ZnCO_3$) were provided by the Museum of Natural History, Washington, DC. Sphalerite (ZnS) was obtained from Aldrich (99.9+% purity). A Zn-Al layered double hydroxide, a Zn-kerolite (provided by Dr Manceau) and an amorphous Zn hydroxide were synthesized following published methods (Ford and Sparks, 2000; Schlegel et al. 2001; Waychunas 2002). Sorption samples were prepared by reacting Zn with ferrihydrite (2-line, freshly precipitated) (Schwertmann and Cornell 1991), goethite (ferrihydrite

aged for 3 weeks and washed with 0.4 M HCl, 66 $m^2 g^{-1}$) low-surface area gibbsite (synthesized and aged 30 days, 90 $m^2 g^{-1}$), birnessite (45 $m^2 g^{-1}$) (McKenzie 1971), kaolinite (University of Missouri Source Clays Repository, Kga-1, cleaned, 14 $m^2 g^{-1}$), hydroxy-Al interlayered vermiculite (Al-verm) (University of Missouri Source Clays Repository, Sanford vermiculite, cleaned, 90 $m^2 g^{-1}$), and fulvic acid (Aldrich, 99% purity). All sorption samples were prepared in an N_2 atmosphere glovebox using ACS reagent grade chemicals and CO_2-free DDI H_2O. A 0.1 M $Zn(NO_3)_2$ stock solution was slowly added to suspensions of 10 g/L solids at an ionic strength of 0.1 M $NaNO_3$. The pH of the kaolinite suspension was adjusted to pH 7 to induce the formation of a mixed Zn-Al layered double hydroxide surface precipitate. (Nachtegaal and Sparks 2003b). Zn was sorbed to goethite and kaolinite at pH 7 and 5, respectively to create inner and outer sphere sorption complexes (Nachtegaal and Sparks 2003b). The spectra of the other sorption complexes were obtained from Dr Roberts and were prepared by adjusting the pH to 6.0 ± 0.3 and maintained during a 24 h reaction period (Roberts et al 2002). This resulted in Zn loadings of ca. 3.5μ-mol/m^2 for birnessite, 2.0 μ-mol/m^2 for fulvic acid, 0.5 μ-mol/m^2 for ferrihydrite, 1.2 μ-mol/m^2 for goethite and 1.5μ-mol/m^2 for the remaining sorbents. Solids were separated by centrifuging at 10 000 rpm for 10 min and stored in a refrigerator as wet pastes until EXAFS analyses.

XAFS data reduction of the reference minerals was performed using WinXAS 2.1 (Ressler, 1997) following standard procedures (Eick et al., 1998; Nachtegaal and

Sparks, 2003a). The χ function was extracted from the raw data by fitting a linear function to the pre-edge region and a spline function to the post-edge region, and normalizing the edge jump to unity. The energy axis (eV) was converted to photoelectron wave vector units ($Å^{-1}$) by assigning the origin, E_o, to the first inflexion point of the absorption edge. The resulting $\chi(k)$ functions were weighted with k^3 to compensate for the dampening of the XAFS amplitude with increasing k and were Fourier-transformed to obtain radial structure functions (RSF). A Bessel window with a smoothing parameter of 4 was used to suppress artifacts due to the finite Fourier filtering range between Δk = 1.5-12 $Å^{-1}$. The two major peaks below 3.5 $Å^{-1}$ in the Fourier transformed curves were isolated and back-transformed. The backtransformed peaks were individually fit in k space. *Ab initio* Zn-O, Zn-S, Zn-Fe, Zn-Mn, Zn-Al, Zn-C and Zn-Zn scattering paths were generated using the FEFF 7 code (Zabinsky et al. 1995) from the refinement of the structure of lizardite (Mellini 1982) where Zn, Fe or Mn was substituted for Mg in octahedral positions, and from the structures of franklinite, willemite, smithsonite and zincite. After each of the individual peaks in the Fourier transform spectra were backtransformed and fit, multishell fitting was done in k space over the entire k-range (Δk = 2.1-10.8) using the same parameters. The E_o shifts were constrained to be equal and the Debye Waller factors were constrained to be equal for the metals in the second shell when two metals were present in the second shell. The amplitude reduction factor, $(S_o)^2$, was fixed at 0.85.

The errors in the bond distances (R) were estimated to be accurate to R ± 0.02 Å and R ± 0.05 Å, for the first and second shells, respectively, and coordination numbers (CN) were accurate to N ± 20% and N ± 40% for the first and second shells, respectively (Roberts et al. 2002). Error estimates were determined by a comparison of XRD and EXAFS results for franklinite and sphalerite, in agreement with estimates previously published (O'Day et al., 1998; Scheidegger et al., 1997).

4.3.6 Micro- SXRF and μ-EXAFS Data Collection

Micro-focused synchrotron based X-ray fluorescence (μ-SXRF) and Zn-K-edge μ-EXAFS on two resin embedded thin sections of the treated and non-treated smelter soils were performed on beam line 10.3.2 of the Advanced Light Source (ALS), Lawrence Berkeley National Lab, Berkeley, CA. A pair of Si(111) channel-cut crystals were employed as monochromators, and the beam was focused down to approximately 2-5 μm using a set of grazing incidence, platinum-coated, elliptically bent, Kirkpatrick-Baez (K-B) focusing mirrors (MacDowell et al., 2001). Thin sections were placed at an angle of 45° to the incident beam. Fluorescence X-ray yield was measured at room temperature with a Ge solid-state detector positioned approximately 1-2 cm from the sample, depending on the Zn concentration in the sample. μ-SXRF maps were collected at 10 keV and with a 20 μm step size for large overview maps and a 5 μm step size for detailed maps. The fluorescence yield was normalized to I_0 and the dwell time. μ-EXAFS spectra were collected on selected

representative regions in the thin sections, based on elemental associations obtained from μ-SXRF mapping and optical images from the thin sections. The beam energy was calibrated with a Zn metal foil. The μ-EXAFS spectra were collected using the same settings as for the bulk-EXAFS spectra collected at NSLS. To assess systematic deviations in EXAFS data collection at the two different beamlines, selected reference samples were run at both beamlines. Independent of the beamline employed, μ-EXAFS and bulk-EXAFS spectra were highly reproducible.

4.3.7 Micro-EXAFS Analyses of Soil Thin Sections

The background corrected, k^3-weighted χ spectra of the non-treated and treated soil samples were analyzed using principal component analysis (PCA) (Malinoski, 1991; Ressler et al., 2000; Manceau et al., 2003) to determine the number of independent components contained in the set of spectra, followed by least-squares fitting of the spectra using linear combination of known Zn references. The number of primary components was evaluated using two criteria; the weight of each component, which is directly related to how much of the signal it represents and the indicator of each component, which reaches a minimum for the least significant component representing a real signal (Malinowski, 1991). The number of principal components found with PCA corresponds to the number of Zn species present in the set of spectra, provided no species has a constant fractional background (Manceau et al., 2003). The abstract principal components do not resemble real spectra. With a target

transformation the real references which might make up the abstract principal components can be identified. An objective way of determining whether the target transformed candidate really resembles the original reference spectrum is given by the SPOIL value (Manceau et al. 2003). SPOIL measures the degree to which replacing an abstract component with the reference would increase the fit error. This is a non-negative dimensionless number for which values of 1.5 are considered excellent, 1.5-3 are good, 3-4.5 are fair, 3.5-6 are poor and > 6 are unacceptable.

Linear combinations of the references identified by the target transformations as likely components were optimized to fit the k^3-weighted chi μ-EXAFS spectra, with only the fractions of each reference spectrum as an adjustable parameter. Fits were optimized by minimizing the normalized sum-square (NSS = $\Sigma[k^3\chi(k)_{exp} - k^3\chi(k)_{reconstr.}]^2 / \Sigma[k^3\chi(k)_{exp}]^2$) (Manceau et al., 2003). A component was only added to the fit if the NSS improved by 20% or more. The accuracy of the fitting approach is dependent on the data quality, range of fitting, and how well the standards represent the unknown sample.

4.4 RESULTS

4.4.1 Bulk Soil Characteristics

Twelve years after remediation of the zinc smelter soil, the pH of the treated site has more or less reverted to its original value of 6.4 (Table 4.1). The ecosystem is

flourishing at the treated soil site, while at the non-treated site no vegetative cover is present. Concentrations of elements and isotope ratios for $^{206}Pb/^{207}Pb$ and $^{208}Pb/^{206}Pb$ of the soils are reported in Table 4.1 as averages of triplicate analyses. Both the treated and non-treated soil samples have extremely elevated toxic metal concentrations. The difference between the two soils is not related to the berengite treatment, but more likely reflects the in situ variation in pollutant concentrations which ranges from ~2000-18550 mg/kg Zn at the smelter site (Vangronsveld 1996).

Pb isotope ratios between treated and non-treated samples are not significantly different. A comparison of the $^{206}Pb/^{207}Pb$ and $^{208}Pb/^{206}Pb$ ratios of the treated and non-treated soils with a historic Pb isotope record of atmospheric dust deposition at the site (Sonke et.al, 2002) indicates that the ratios of the treated and non-treated soils are similar to recent Pb deposition (1960-1990, $^{206}Pb/^{207}Pb$: 1.133 ± 0.001 and $^{208}Pb/^{206}Pb$: 2.129 ± 0.002). This period reflects the last 15 years (1960-1974) of maximal production and pollution before the smelter was dismantled.

	Non-Treated pH=6.4 (ppm)	Treated pH=6.7 (ppm)
Fe	47880	21159
Al	18619	23264
Ti	1533	1765
Zr	170	175
Ba	513	368
Mn	1122	573
P	357	819
S	2351	1881
Zn	**20476**	**13144**
Pb	2996	1297
Cu	2132	762
As	312	115
Ni	348	165
Co	41	25
Cd	31	51
Hg	737	779
Ce	24	29
Nd	9.2	11.3
Eu	0.6	0.6
U	1.8	1.7
Pb206/Pb207	1.1326	1.1321
	0.0007	0.0007
Pb208/Pb206	2.1296	2.1298
	0.0014	0.0019

Table 4.1. Concentrations and Pb isotope ratios for non-treated and treated soils from the Maatheide smelter site.

4.4.2 Electron Microprobe Analysis

Backscattered electron images (BSE) and selected elemental distributions collected by electron-microprobe analysis are shown in Figure 4.1a and b for the non-treated soil and Figure 4.1 c-d for the treated soil. EDS scanning of grains in the thin sections of both soils indicated that about 80 % of the particles present are quartz grains. Zn concentrations in the soil thin sections were on the percent level, indicating the potential toxicity of Zn in the non-treated as well as the treated soil. In the non-treated soil, Zn is mainly found in franklinite ($ZnFe_2O_4$) (Figure 4.1b) and pyrite

Figure 4.1a Backscatter electron images (large maps) and elemental distribution maps (small map) of selected particles in the non-treated soil samples.

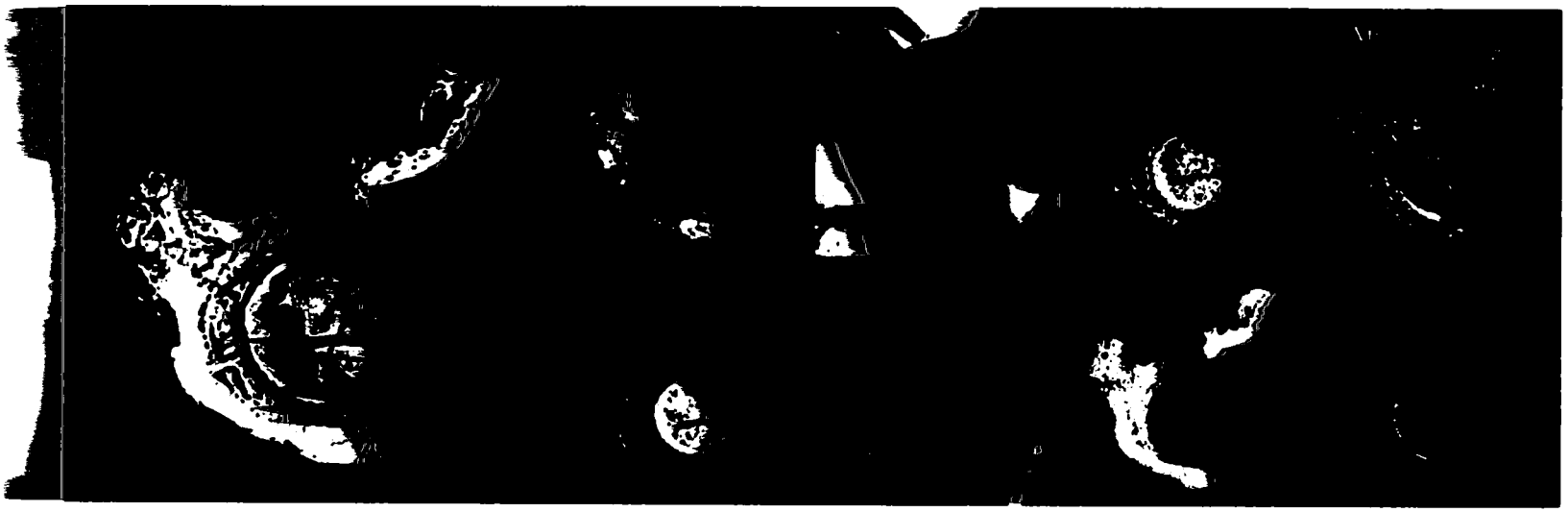

Figure 4.1b Backscatter electron images (large maps) and elemental distribution maps (small map) of selected particles in the non-treated soil samples.

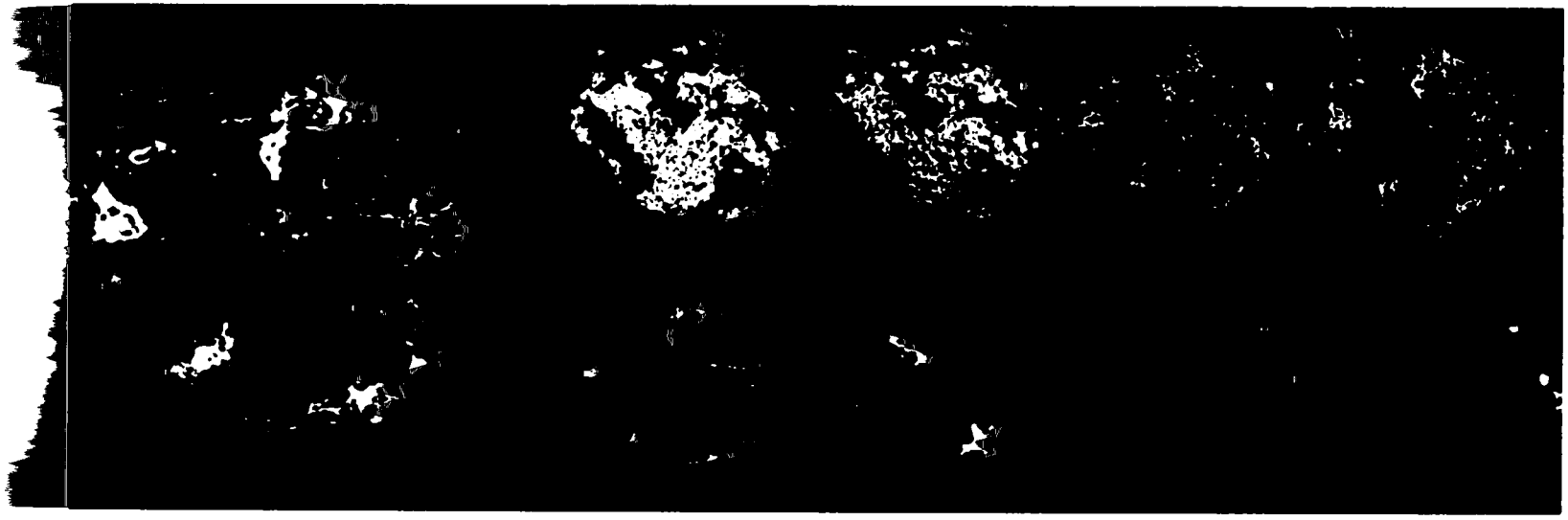

Figure 4.1c Backscatter electron images (large maps) and elemental distribution maps (small map) of selected particles in the treated soil samples.

Figure 4.1d Backscatter electron images (large maps) and elemental distribution maps (small map) of selected particles in the treated soil samples.

($(Zn,Fe)S_2$) (Figure 4.1a) phases, with minor traces of Cu, Ni and Pb incorporated in these phases. The iron oxide phases found in these soils varied in oxidation state, often within the same mineral.

In the treated soil we found the same Zn rich, slag related 'primary' minerals (franklinite and pyrite), which are mainly deposited on the soil by fall-out from the zinc smelter. However, in the treated soil, Zn was also associated with Si and Al in some isolated cases (Figures 4.1c and d). The shape of these Zn-Si associations (Figure 4.1c) is almost perfectly hexagonal, suggesting that it is a newly formed clay mineral. The hexagonal particles were found in a matrix of iron sulfide (Figure 4.1c), which suggest this is a weathered pyrite mineral. Upon remediation, the basic solution (pH 7.3-7.9 at the time of remediation, Vangronsveld et al. (1996)) containing Si (quartz will start to dissolve at this basic pH), comes into contact with the pyrite, where the localized pH could be very low. Consequently, Si minerals precipitate with Zn to form the observed, secondary minerals. We also found strong associations of Al with Zn (Figure 4.1d), probably as a result of Zn binding to clay minerals. Note that the detection limit of the microprobe for Zn is ~ 0.5 wt%, therefore the electron microprobe can only probe the zinc hotspots, i.e. the main Zn mineral associations. Lower Zn concentrations, i.e. Zn readsorbed to a mineral phase will not be detected, although this Zn fraction can play a very important role in the overall Zn speciation (Roberts et al. 2002). With μ-EXAFS and μ-SXRF the lower Zn levels can be probed, however, information on associations with soil particles can not be obtained.

4.4.3 EXAFS Analysis of Reference Spectra

To aid in the data analysis, we collected a large database of Zn reference spectra that could represent the various forms of Zn present in the smelter contaminated soil samples. The raw chi, k^3 weighted EXAFS spectra for the reference mineral and sorption samples are presented in Figure 4.2 as solid lines and the best fit as dotted lines. Fit results for these reference samples, using nonlinear, least-squares fitting of individual coordination shells, are presented in Table 4.2. The spectra were fit with theoretical scattering paths, calculated using FEFF 7. Only single scattering paths were included in the fit, leading to better fits for the sorption samples than the Zn mineral standards.

The mineral standards chosen, franklinite, willemite and sphalerite, are refractory products of the smelting process (Sobanska et al. 1999) and introduced into the environment by fall-out from the neighboring Zn smelter. Sphalerite is also the main ore mineral going into the smelting process. Under basic pH conditions, hydrozincite and smithsonite could possibly be formed

Reference spectra for the different surface precipitates that could potentially be formed in the Zn contaminated soils are shown in Figure 4.2b. Ford et al (1999) suggested the transformation of a transition metal surfaces precipitate from a hydroxide, to a mixed transition metal-Al layered double hydroxide (Me-Al LDH), to a neo-formed transition metal phyllosilicate upon aging. All possible intermediates

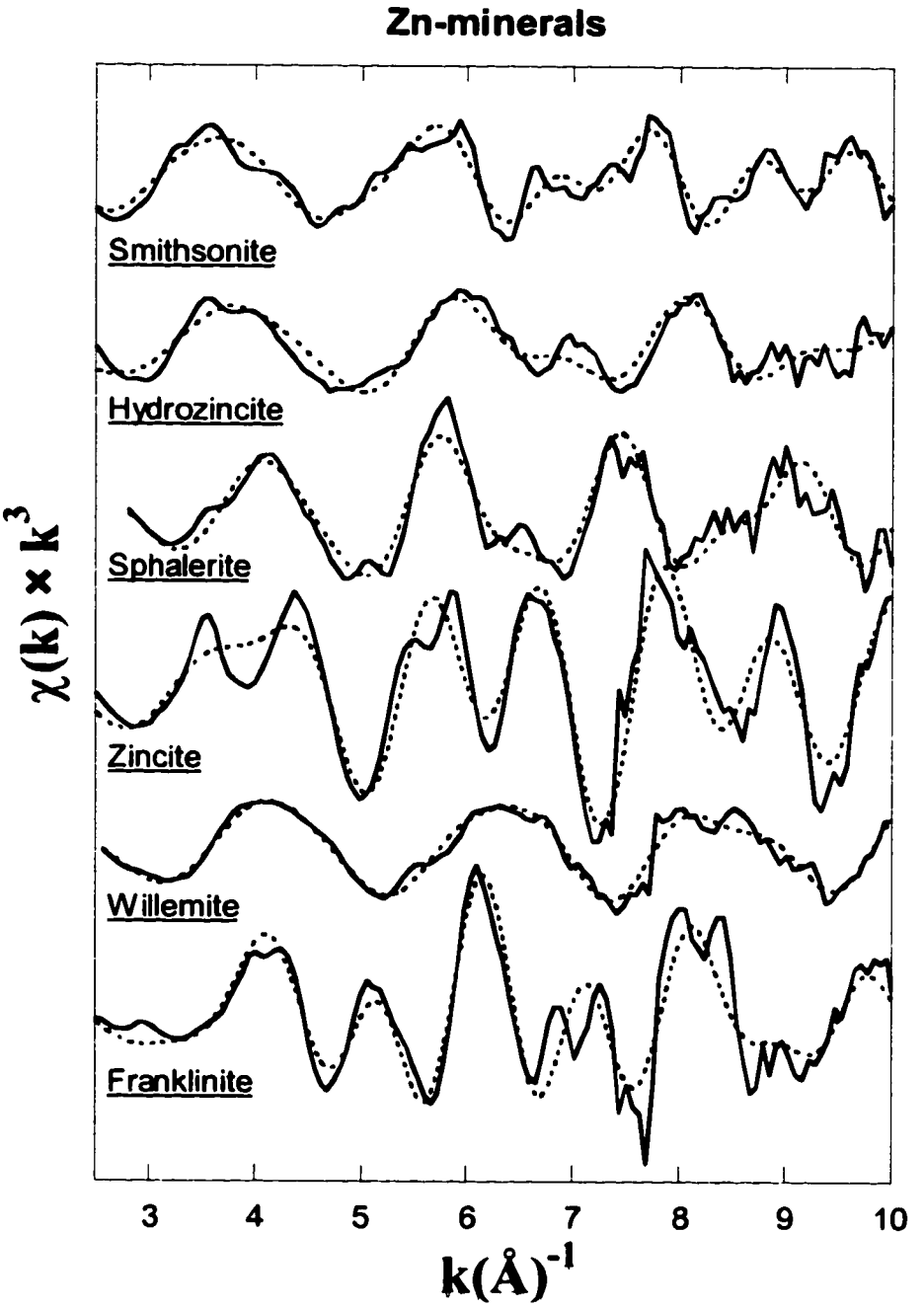

Figure 4.2a Zn-K_α k^3 weighted χ of reference Zn-phases of natural mineral samples. The solid lines indicate the raw data and the dotted lines indicate the best fits.

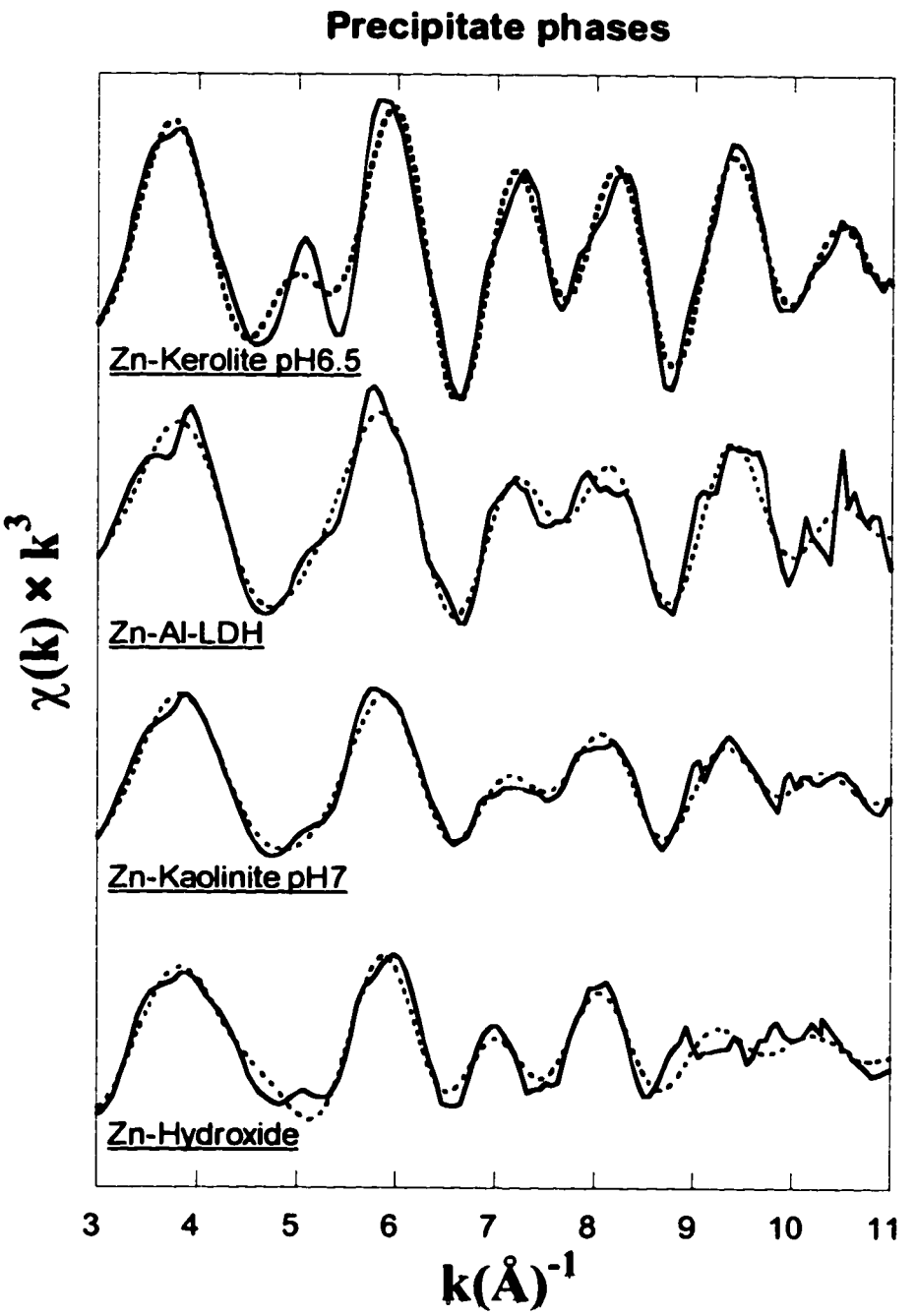

Figure 4.2b Zn-K_α k^3 weighted χ of reference Zn-phases of surface precipitates. The solid lines indicate the raw data and the dotted lines indicate the best fits.

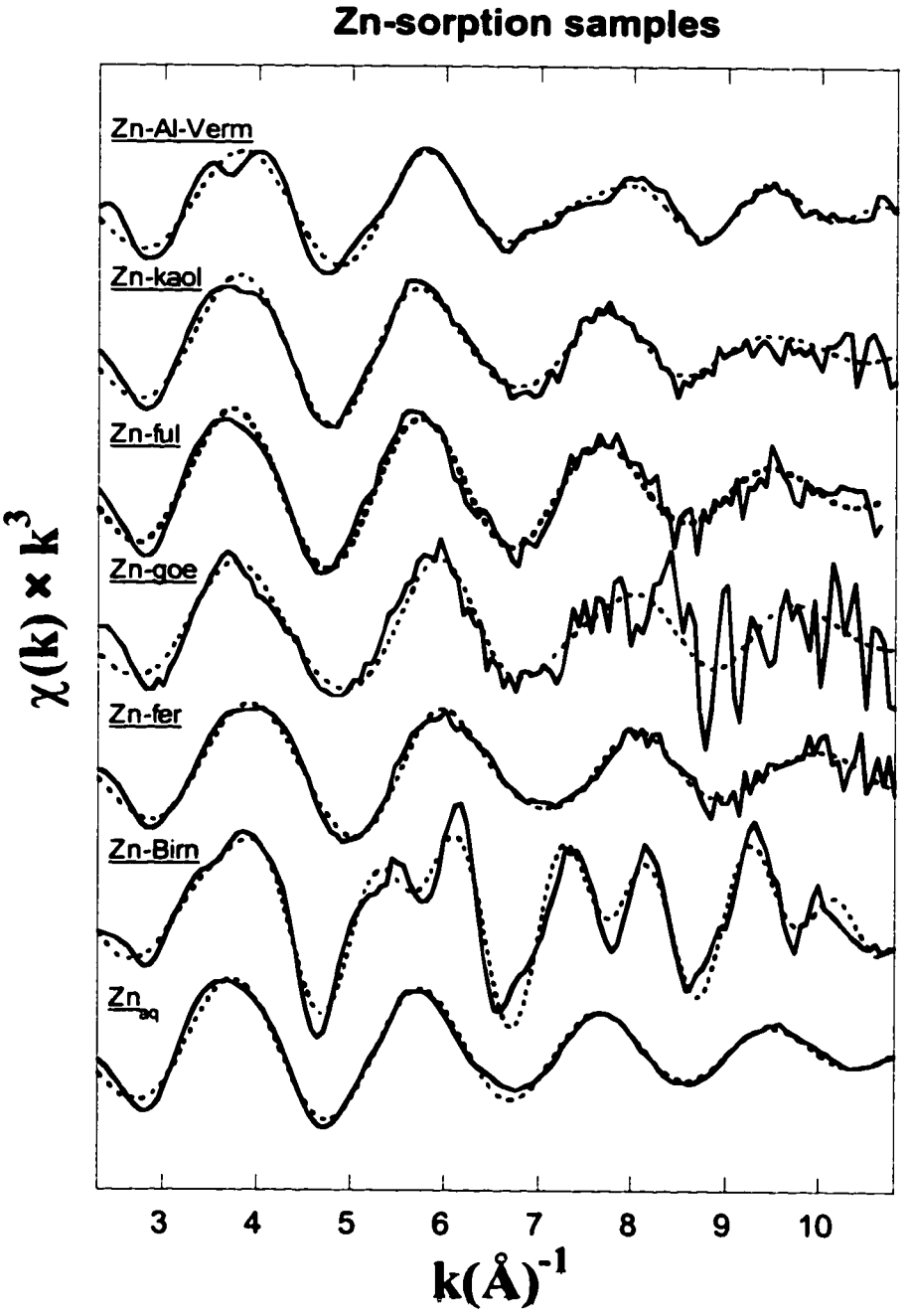

Figure 4.2c Zn-K_α k^3 weighted χ of reference Zn-phases of sorption samples. The solid lines indicate the raw data and the dotted lines indicate the best fits.

	First shell				Second shell					
	Atom	CN	R(Å)	$\sigma^2(Å)^2$	Atom	CN	R(Å)	$\sigma^2(Å)^2$	ΔE_0(eV)	% r
Minerals										
Franklinite	O	4.1	1.98	0.003	Zn	9.7	3.47	0.004	3.00	21.0
					Fe	13.2	3.60	0.004		
Willemite	O	3.6	1.94	0.003	Si	1.5	3.18	0.007	1.91	8.9
					Zn	2.1	3.20	0.007		
Zincite	O	3.9	1.96	0.003	Zn	22.8	3.22	0.014	-2.39	21.8
Sphalerite	S	4.3	2.34	0.007	Zn	18.0	3.83	0.020	3.11	27.0
Hydrozincite	O	3.4	1.98	0.005	Zn	3.0	3.12	0.010	-4.25	21.7
Smithsonite	O	6.0	2.10	0.010	C	3.8	3.28	0.007	2.97	22.6
					Zn	3.8	3.65	0.007		
Precipitates										
Zn-Kaolinite pH 7	O	6.0	2.05	0.011	Zn	3.7	3.13	0.010	0.75	14.1
					Al	1.0	3.17	0.010		
Zn-Al-LDH	O	6.2	2.06	0.008	Zn	4.3	3.09	0.010	0.06	14.0
					Al	2.2	3.10	0.010		
Zn-Kerolite	O	6.2	2.06	0.009	Zn	8.7	3.10	0.011	0.10	6.35
					Si	6.4	3.23	0.011		
Zn-Hydroxide	O	1.9	2.02	0.013	Zn	2.3	3.15	0.016	1.15	30.1
Zn-reacted										
Zn_{aq}	O	6.0	2.07	0.009						
Zn-Birnessite	O	5.6	2.06	0.006	Mn	7.0	3.50	0.008	0.15	16.6
Zn-Ferrihydrite	O	4.8	1.99	0.008	Fe	1.0	3.15	0.011	-0.16	14.1
Zn-Goethite	O	6.0	2.04	0.006	Fe	1.0	3.18	0.014	0.62	27.0
Zn-Fulvic acid	O	6.6	2.07	0.009					-0.20	16.0
Zn-Kaolinite pH5	O	6.4	2.06	0.011	Al	1.3	3.09	0.010	0.46	16.1
Zn-Al-Vermiculite	O	5.2	2.05	0.010	Al	0.7	2.98	0.002	0.75	13.7

CN = Coordination Number (± 20% (O'Day *et al* 1994))
R = Inter-atomic distance (± 0.02Å for first shell and ± 0.05Å for the second and third shell (O'Day *et al* 1994))
$\sigma^2(Å^2)$ = Debye Waller factor
ΔE_0 = Phase shift
% r = Residual error

Table 4.2 Best-fit XAFS parameters for reference mineral and sorption samples derived from XAFS analysis.

were included in our reference database. A Zn-Al LDH was synthesized in the lab and contained approximately 4 Zn and two Al atoms in the octahedral layers (Table 4.2). A Zn-Al LDH was also synthesized at the surface of a kaolinite clay mineral. This Zn-Al LDH was a bit more amorphous, with larger Zn-Zn (3.13 Å vs 3.09 Å) and Zn-Al (3.17 Å vs 3.10 Å) bond distances than the synthetic Zn-Al LDH. A proxy for a neoformed Zn containing phyllosilicate, Zn-kerolite, was obtained from Dr. Alain Manceau (Schlegel et al 2001). EXAFS data fitting allowed 8 Zn atoms to be fit in the octahedral layer, and 6 Si atoms in the tetrahedral layer, which is more than the maximum number of Zn and Si which could be fitted in these layers. The bond distances found, were very comparable to the bond distances found by Schlegel et al (Schlegel 2001), who fixed the coordination number of Si and Zn in the octahedral shells.

The raw and fitted chi spectra for the Zn sorption samples are shown in Figure 4.2c. The chi spectrum for aqueous zinc has a sinusoidal shape, which slowly extinguishes with higher k values, indicating that except for O in the first shell nothing else is present. Zinc formed a monodentate inner-sphere complex with ferrihydrite (1 Fe at 3.15 Å). It has ~ 4 O atoms in the first coordination shell at approximately 1.99 Å, which is indicative of tetrahedrally coordinated zinc (Waychunas et al. 2002). On goethite a bidentate inner-sphere complex is formed, with Zn bound to approximately 2 Fe atoms at 3.18 Å. Zinc formed an inner sphere monodentate sorption complex with the aluminol edge groups of kaolinite at pH 5, with zinc binding to 1 Al atom at approximately 3.09 Å. When sorbed to the aluminum hydroxyl interlayer of a 2:1

smectite, zinc forms also a monodentate inner-sphere sorption complex, but with a notable shorter bond distance (2.98 Å) compared to sorption onto aluminol edge sites of the clay mineral.

4.4.4 Synchrotron Based X-Ray Microprobe Analysis of Soil Thin Sections

The μ-SXRF maps of the treated soil are shown in Figures 4.3b and 4.4b and the μ-SXRF maps of the non-treated soil in Figures 4.5b and 4.6b. The maps are shown as a RGB tricolor map. In these images R (red) represents the distribution of iron, G (green) the distribution of Cu and B (blue) the distribution of zinc. The color values of each pixel are proportional to the amounts of the three elements. If the amount of all three elements is the same, then R=G=B, which will give a gray scale image. The overall brightness of a region is related to the sum of the concentrations and the hue is related to the difference (Manceau et al 2003).

Zn, Cu, Fe, Mn, Ni, Ti, Co, Ca and K were the elements simultaneously mapped in this study. At the energy at which the SXRF maps were collected, only relatively heavy elements can be probed. Therefore, the spatial relation of Zn with Fe and Mn bearing minerals was detected, but its relation to silicate minerals not. In general, the μ-SXRF maps show that Zn is heterogeneously distributed throughout the treated and non treated samples. In both the treated and non-treated samples, zinc was found correlated with Fe (e.g. Figure 4.4b, region 5 or Figure 4.6b, region 3), correlated with Mn (data not shown), in diffuse spots (e.g. Figure 4.6b, region 2) or in concentrated regions just by itself (e.g. Figure 4.5b, region 2). In some regions Zn was

found concentrated at the rims of particles, while Cu was concentrated in the interior (Figure 4.6b, region 1) or as a mixed Cu, Zn, Fe band (e.g. Figure 4.3b, region 4). Specific information on the chemistry and local bonding environment of Zn in the SXRF maps was obtained from μ-focused EXAFS spectroscopy.

4.4.5 Micro-EXAFS Analysis of Soil Thin Sections

Of selected spots (indicated with numbers on the μ-SXRF maps), μ-EXAFS spectra were collected. Principal component analysis (PCA) was performed on the whole set of μ-EXAFS spectra collected from the treated soil (17 in total, Figures 4.3a-4.4a) and the complete spectra set of the non-treated soil (12 spectra in total Figures 4.5a-4.6a) to determine the number of independent components contained in the set of spectra. This approach is useful for the analysis of natural samples containing multiple forms of the same metal, because the number and nature of these forms cannot be assumed a priori (Issaure et al., 2002). PCA indicated that three principal components are needed to reproduce the data set of the treated soil and four to reproduce the data set of the non-treated soil. All μ-EXAFS spectra could be reproduced very well with these 3 or 4 principal components (normalized sum square (NSS) between 0.080 and 0.165 for the treated soil and 0.037 and 0.126 for the non-treated soil, data not shown).

SPOIL factors indicate how well a Zn reference spectrum matches to the principal components. The SPOIL factors for the different references in our database, calculated using the first 3 principal components from the treated and the first four

Reference	Treated	Non-Treated
Chalcophanite	X	X
Franklinite	3.43	2.68
Hydrozincite	3.68	3.01
Willemite	1.69	2.18
Zn-Al LDH	2.03	*1.16*
Zn-Al-Vermicullite	3.05	1.94
Zn-Birnessite	3.70	3.08
Smithsonite	10.02	8.78
Zn-Ferrihydrite	3.66	3.23
Zn-Fulvic Acid	5.83	4.46
Zn-Goethite	6.26	4.88
Zn-Kaolinite pH5	6.01	4.60
Zn-Kaolinite pH7	2.28	1.57
Zn-Kerolite	*1.21*	1.58
Zn-Nitrate	6.65	5.94
Zincite	6.47	9.10
ZnOH	4.28	3.38
Sphalerite	2.81	2.01

Table 4.3: SPOIL factors for the reference spectra constructed from principal components. SPOIL factors < 1.5 indicate an excellent fit, 1.5-3 a good fit, values of 3-4.5 a fair and of 4.5-6 a poor fit and factors > 6.0 are unacceptable.

from the non-treated soils are collected in Table 4.3. The best spectral match to the principal components of the treated soil were obtained for; Zn- kerolite, willemite, Zn-Al LDH, Zn-sorbed kaolinite pH 7, sphalerite, zinc-sorbed hydroxyl Al interlayered vermiculite, franklinite and Zn-sorbed ferrihydrite. The best spectral match for the non treated soil was obtained with; Zn-Al LDH, Zn-sorbed kaolinite pH 7, Zn-kerolite, zinc-sorbed hydroxyl Al interlayered vermiculite, sphalerite, willemite, franklinite and Zn-sorbed birnessite.

Willemite, sphalerite and franklinite are mainly produced during the smelting process and subsequently distributed over the soil by fall-out. An excellent spectral fit (SPOIL < 1.4) was obtained with Zn-kerolite in the treated soil, which was used as a proxy for zinc incorporated in a neo-formed phyllosilicate surface precipitate. An excellent fit for the non-treated soil was obtained with Zn-Al LDH which was used as a proxy for zinc included into mixed Zn-Al layered double hydroxide surface precipitate. This suggests that zinc containing surface precipitates make up the main zinc component in both the treated and non-treated soil.

The proportion of each Zn reference species in the various μ-EXAFS spectra, identified by target transformation of the principal components, was determined by linear combination fitting (LCF). The maximum number of reference spectra going into the LCF was not allowed to exceed the number of principal components identified by PCA and only the Zn references positively identified by the target transformation were included into the fit. The solid lines in Figures 4.4-4.8a are the raw chi spectra

and the dotted lines are the best fits to the raw data. The normalized sum square (NSS) listed with each spectrum, indicates how well the linear combination of the Zn reference spectra fitted the μ-EXAFS spectra.

Two thin sections of both the treated and non-treated soil were extensively studied with μ-SXRF and μ-EXAFS. Four regions in thin section 1 of the treated soil were studied in more detail (Figure 4.3a-b). Region 1 contained a large zinc rich particle, which was identified primarily as willemite, a slag related Zn mineral. Besides the contribution of willemite to the overall spectrum, Zn incorporated in $Zn(OH)_2$ and Zn-sorbed birnessite were also identified in spot 1. In spot 2, Willemite, Zn-sorbed birnessite and a Zn-Al LDH (proxy for a surface precipitate) are the main components. In region 2 we found evidence for the neo-formation of a Zn containing phyllosilicate (Zn-kerolite was used as a proxy for this potential surface precipitate). Besides the incorporation of Zn into a neo-formed phyllosilicate, in spot 1 spectral contributions of Zn incorporated in willemite were detected, and in spot 2 both contributions of willemite and Zn sorbed onto ferrihydrite were resolved. A more diffuse zinc area (spot 3) could be fitted solely by a Zn-Al LDH, precipitated on the surface of kaolinite, a 1:1 clay mineral. Willemite gave the best fit for spot 4, but clearly did not fit the first oscillation well (NSS of 0.401). The Zn reference database was not complete enough to positively identify this Zn-species. The elemental associations obtained from μ-XRF mapping did not resolve what this particle might be. Region 4 contains sphalerite (spot 2) in the middle, in combination with some Zn

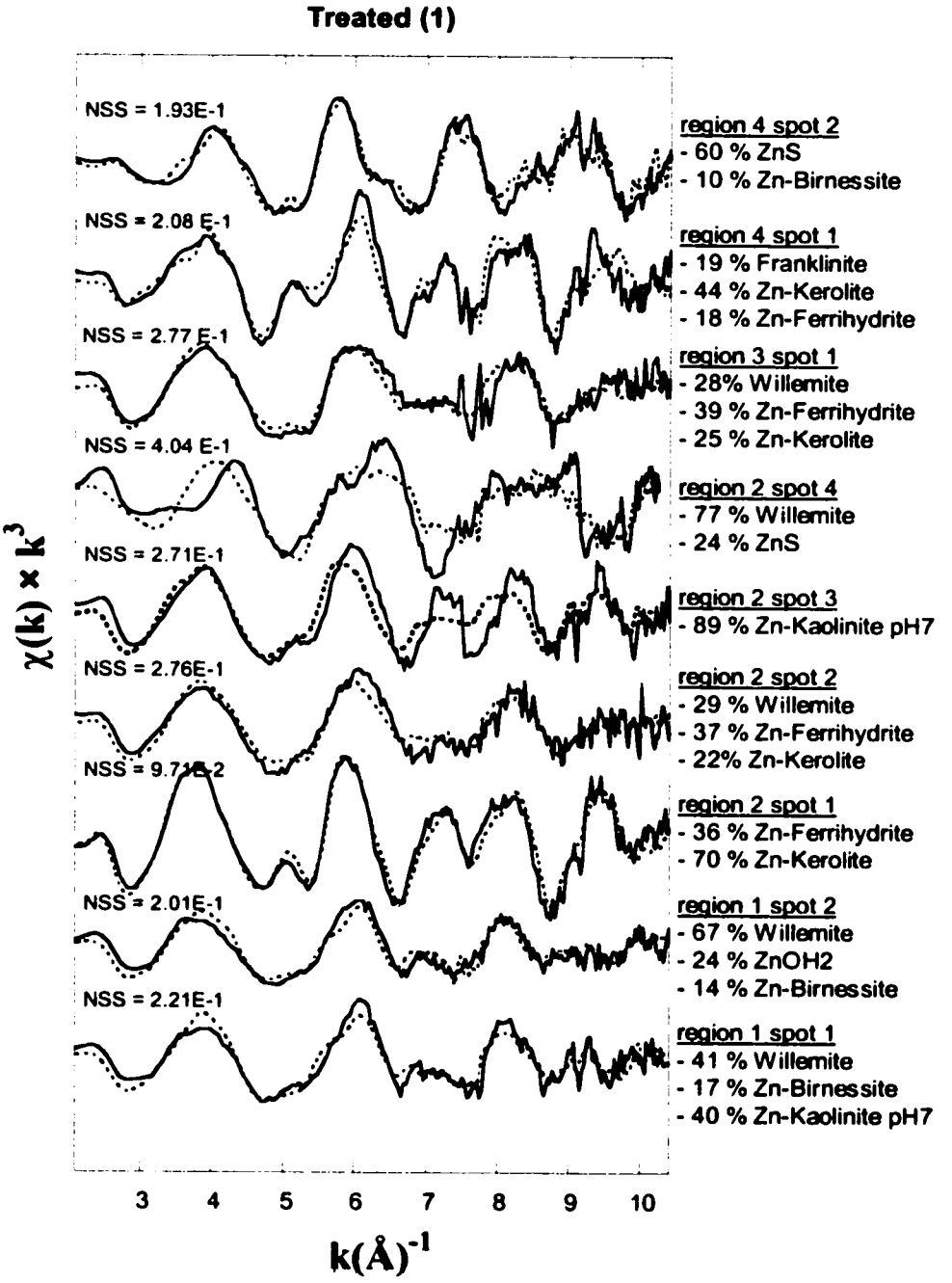

Figure 4.3a μ-EXAFS spectra from selected spots on thin section 1 from the treated soil. The solid line indicates the raw chi data and the dotted line indicates the best fits obtained with a linear fitting approach.

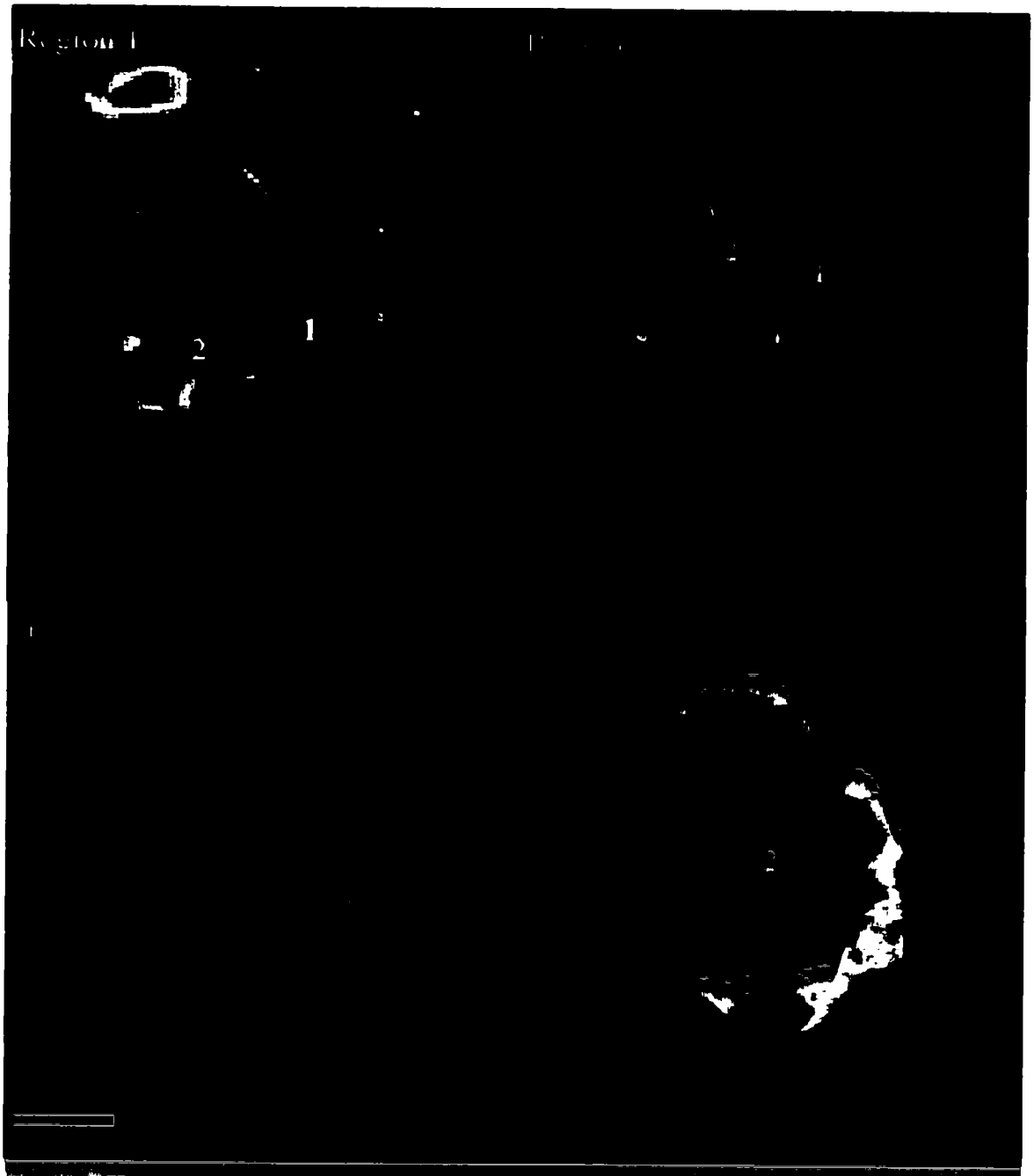

Figure 4.3 μ-SXRF tricolor maps for the treated soil samples of thin section 1. The numbers indicate the spots where μ-EXAFS spectra were collected. Red is indicative of the distribution of iron, green of copper and blue of zinc.

sorbed onto birnessite. The Zn-rich circular rim consists of a weathered franklinite (spot 1) where Zn after weathering of franklinite is partly sorbed to ferrihydrite and incorporated into a Zn-phyllosilicate surface precipitate (Zn-kerolite).

The second thin section of the treated soil (Figure 4.4a-b) shows a similar combination of Zn species. Region 1 contains the remains of a large sphalerite mineral (spot 1). The fit of the spectrum with our reference sphalerite (ZnS) did not resolve some of the fine structure. The elemental distributions in Figure 4.4b show that besides Zn also Cu and Fe are concentrated in this area. The presence of other metals in the sulfide could potentially add more structure to the chi spectrum. This mineral is therefore probably a mixed (Zn,Fe,Cu)S remaining from the smelting process. In the interior of this sphalerite mineral (spot 2) we found a mix of sphalerite, willemite and Zn-Al LDH. This mixture indicates that the primary zinc minerals, sphalerite and willemite, started to weather and the zinc released was being incorporated into a Zn-Al LDH precipitate formed at the surface of surrounding clay minerals. About 45 % of the spectrum of a large Zn particle in region 4 is contributed by our Zn-sorbed kaolinite and 64 % is contributed by Zn sorbed to the hydroxy-Al interlayers of vermiculite. We suggest this is a hydroxy-Al interlayered vermiculite, to which Zn is both sorbed to the hydroxyl-Al interlayer and included into a Zn-Al LDH formed at the surface of this clay mineral. Region 5 consists of willemite particles and different percentages of Zn sorbed ferrihydrite.

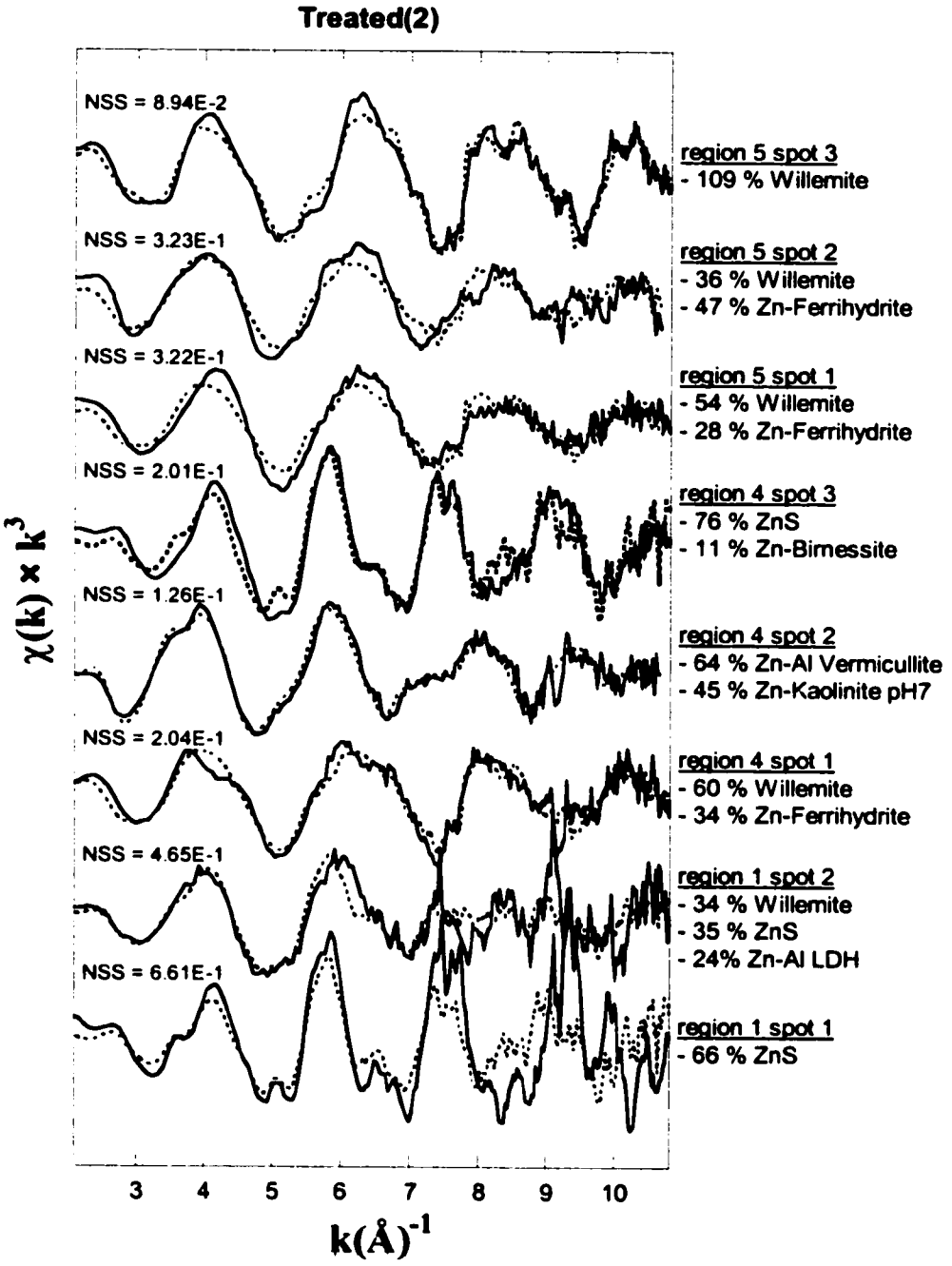

Figure 4.4a μ-EXAFS spectra from selected spots on thin section 2 from the treated soil. The solid line indicates the raw chi data and the dotted line indicates the best fits obtained with a linear fitting approach.

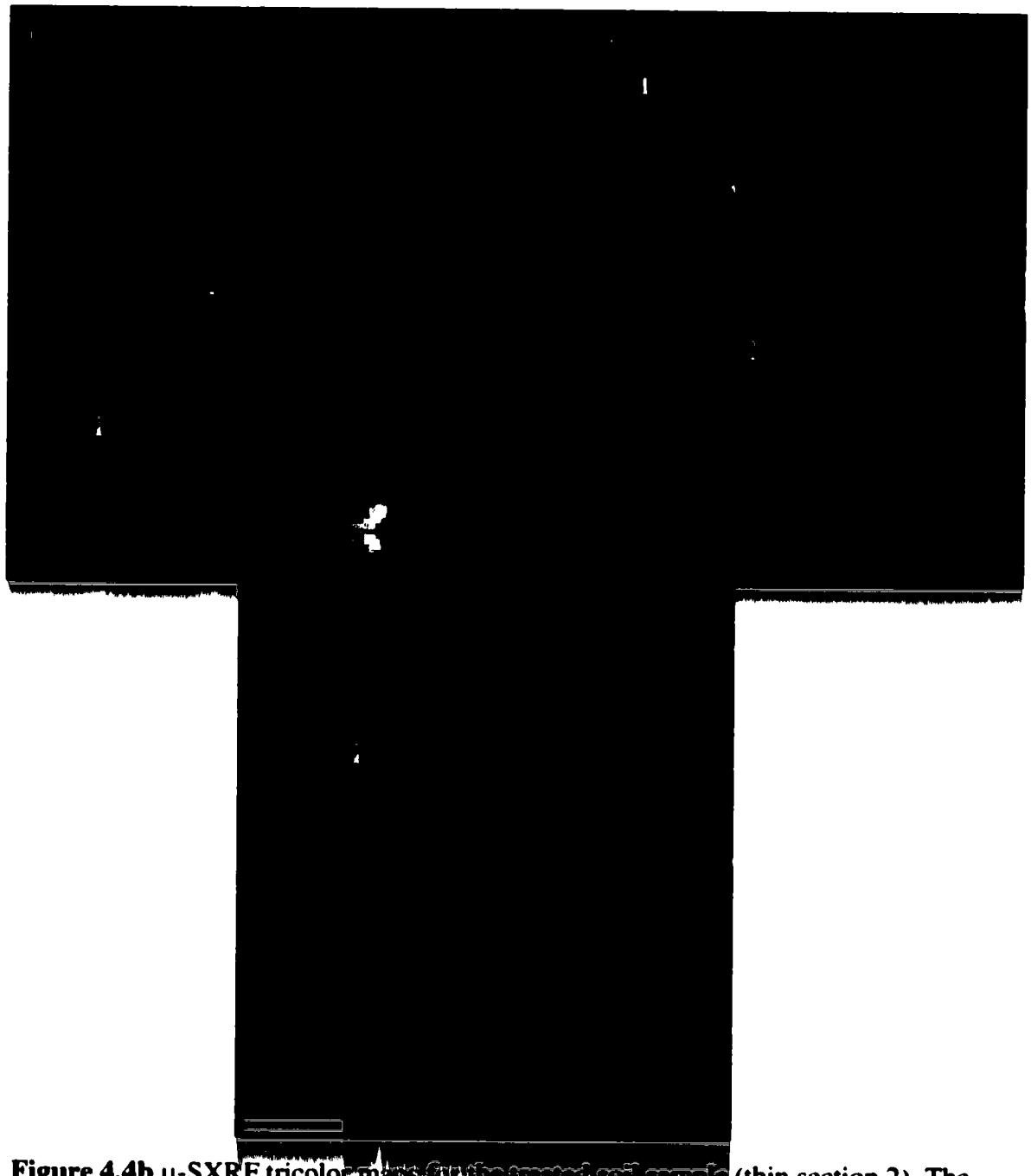

Figure 4.4b μ-SXRF tricolor maps for the treated soil sample (thin section 2). The numbers indicate the spots where μ-EXAFS spectra were collected. Red is indicative of the distribution of iron, green of copper and blue of zinc.

Two regions of the first thin section of the non-treated soil were studied in more detail (Figure 4.5a-b). Region 1 contains willemite, and some Zn sorbed to ferrihydrite, indicating that willemite started to weather and was sorbed to the surrounding ferrihydrite (spot 1). In region 2 we found a Zn phase which we could not identify with our reference database (spot 3). The chi spectrum is highly structured, suggesting that this is a primary Zn mineral and not a Zn sorption sample. Spot 1 is a mixture of sphalerite and zinc incorporated into a Zn-Al LDH, again suggesting that the primary sphalerite is partly weathered and the released Zn incorporated into a Zn containing precipitate, formed at the surface of surrounding clay minerals. Spot 2 is a mixture of 17% willemite, 70% zinc sorbed to the Al hydroxyl interlayer of a 2:1 clay mineral and 18% of Zn incorporated into a neo-formed surface phyllosilicate. Spot 4 of region 2 is a mixture of willemite and zinc sorbed to ferrihydrite.

The second thin section of the non-treated soil (Figure 4.6a-b) contained a mixture of willemite and Zn sorbed ferrihydrite in region 1. In region 2, spot 1 is a mixture of willemite and sphalerite and spot 2 is a sphalerite particle. Spot 3 is a mixture of willemite and a Zn-Al layered double hydroxide, suggesting that dissolution of willemite was followed by incorporation of Zn into a Zn precipitate at the surface of an aluminosilicate instead of sorbed onto ferrihydrite. Region 3 shows Zn sorbed to a hydroxy-Al interlayered vermiculite and also incorporated into a Zn-Al LDH at the surface of this clay mineral. In region 4 we found a Zn-Al LDH formed on a clay mineral surface, concentrated on the rims of a large iron rich particle.

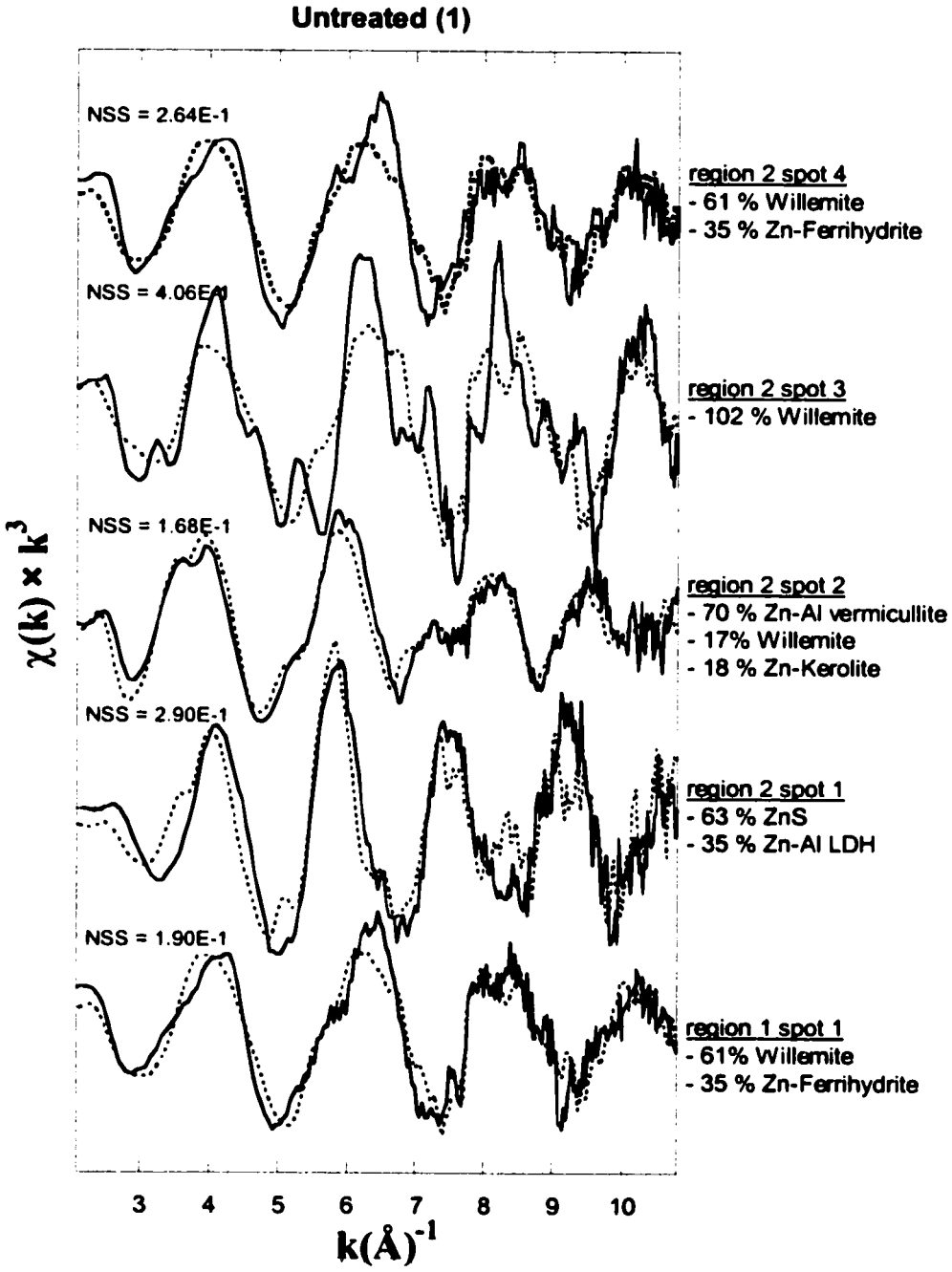

Figure 4.5a μ-EXAFS spectra from selected spots on thin section 1 from the non-treated soil. The solid line indicates the raw chi data and the dotted line indicates the best fits obtained with a linear fitting approach.

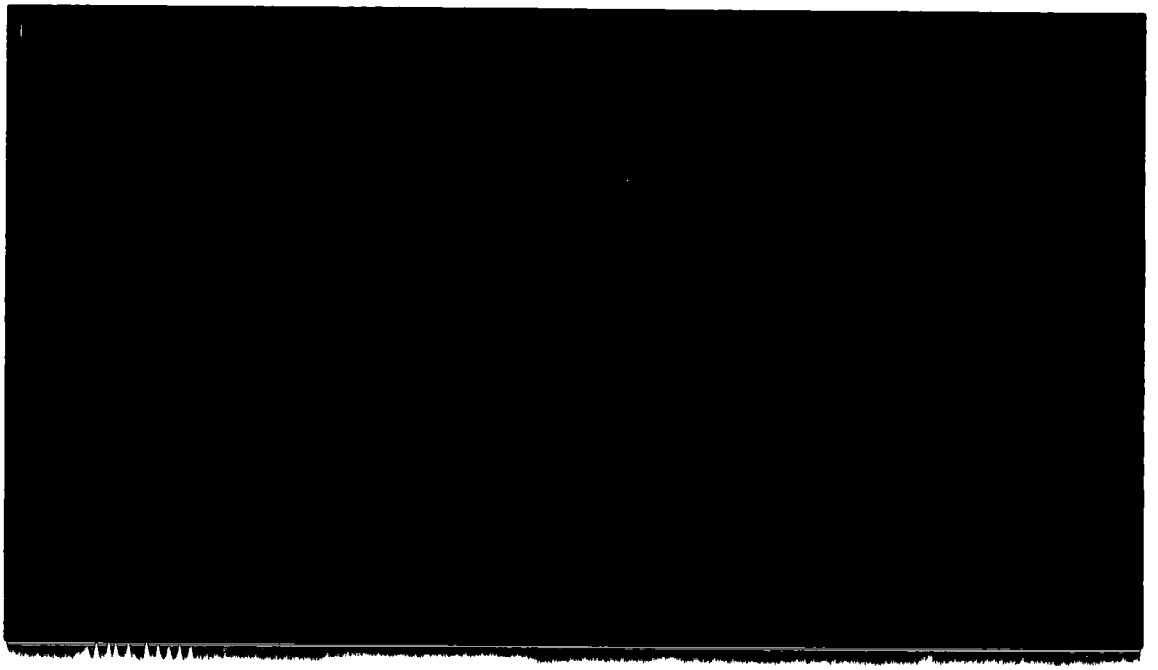

Figure 4.5b μ-SXRF tricolor maps for the non-treated soil sample (thin section 1). The numbers indicate the spots where μ-EXAFS spectra were collected. Red is indicative of the distribution of iron, green of copper and blue of zinc.

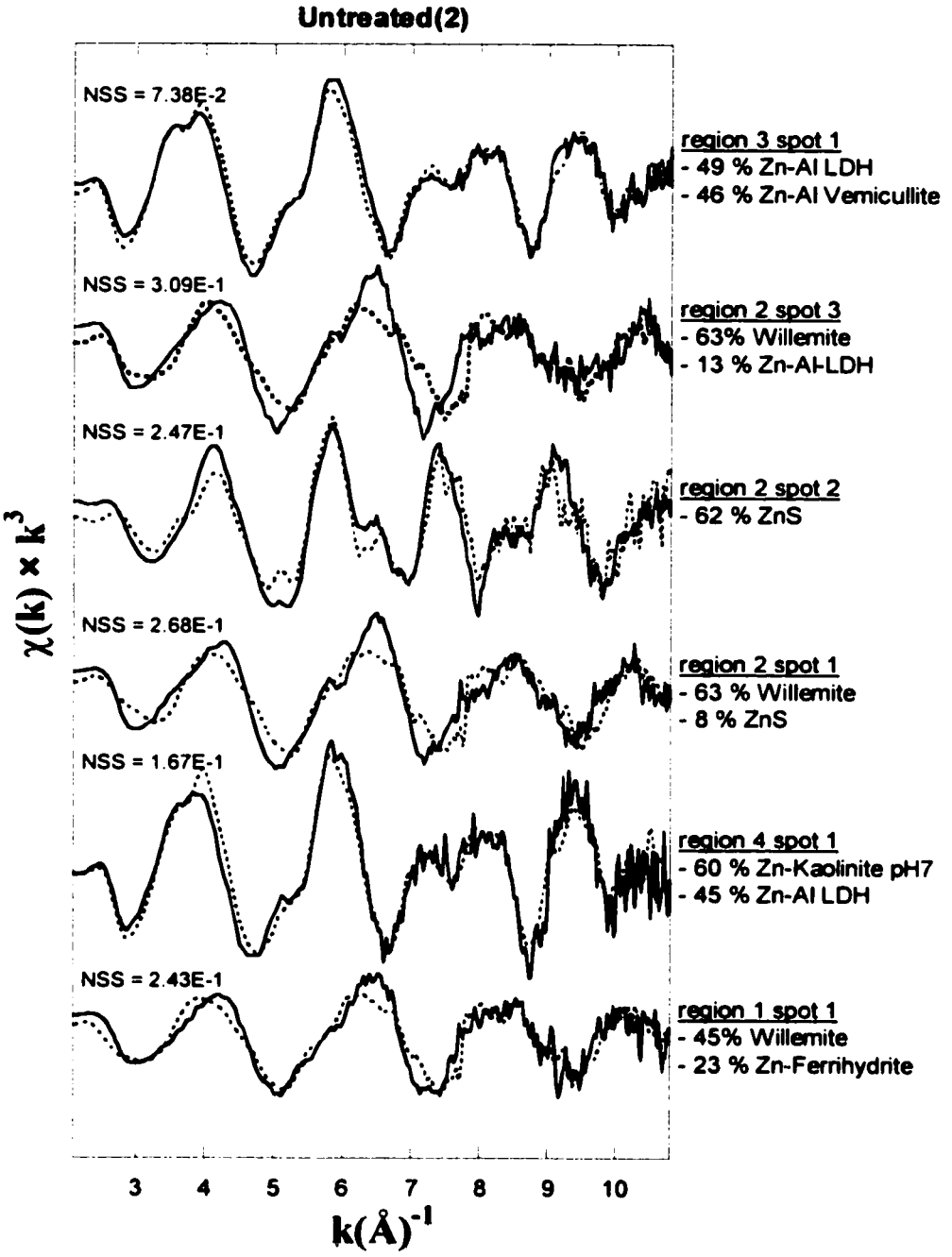

Figure 4.6a μ-EXAFS spectra from selected spots on thin section 2 from the non-treated soil. The solid line indicates the raw chi data and the dotted line indicates the best fits obtained with a linear fitting approach.

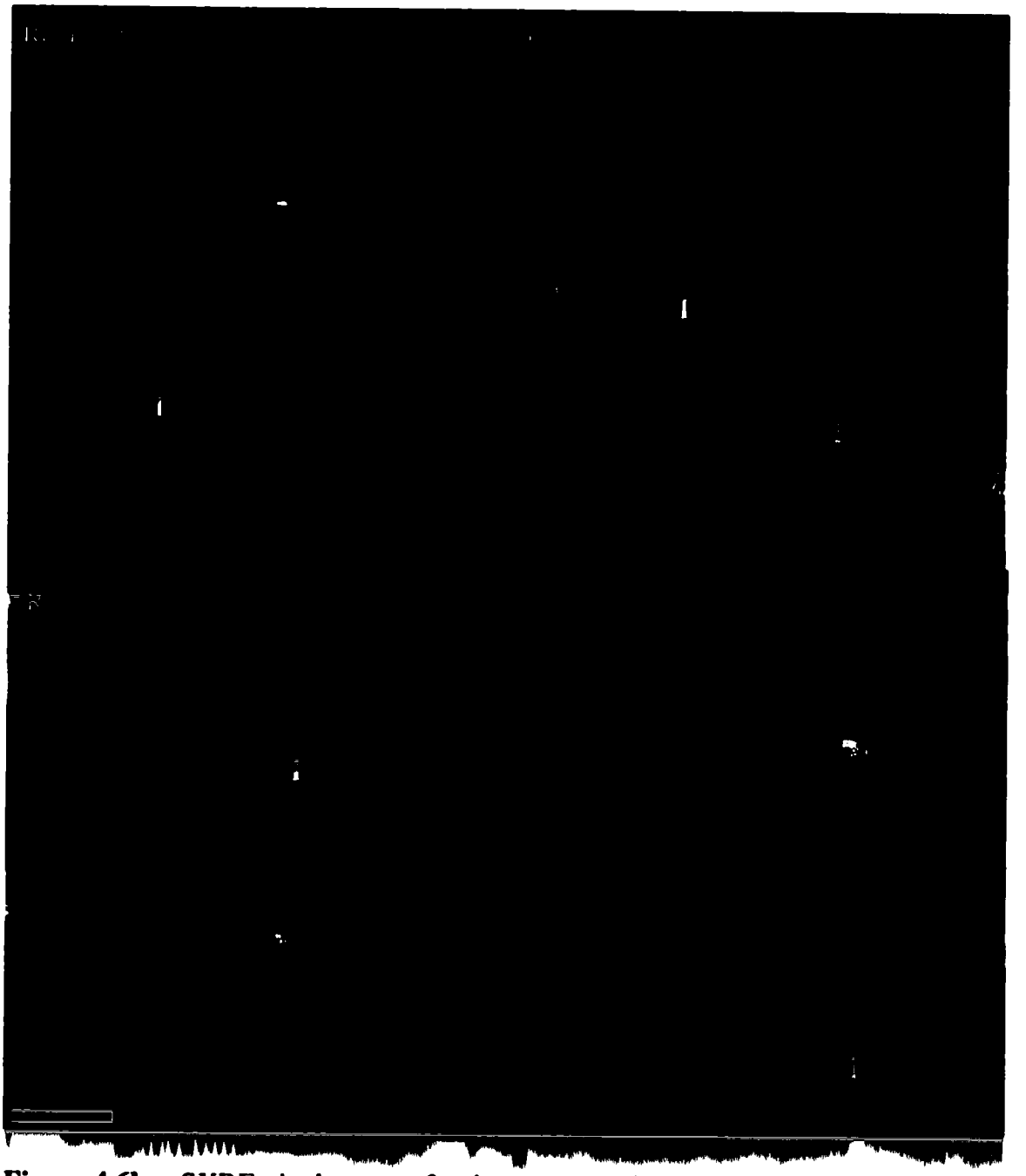

Figure 4.6b μ-SXRF tricolor maps for the non-treated soil sample (thin section 2).

In summary, the Zn-speciation from selected spots in the two thin sections of both the treated and non-treated soils did not differ much. Both soil samples contain a significant quantity of slag, fall-out, Zn-minerals; i.e. sphalerite (which most likely contains other metals such as Fe and Cu), willemite, and to a lesser extent franklinite and an unidentified mineral, which are evenly distributed throughout the soil. A study by Manceau et al. (2000) to samples from the same geographic area, positively identified hemimorphite ($Zn_4Si_2O_7(OH)_2$) as the other Zn-bearing mineral phase. We found significant evidence for the weathering of these primary minerals. Zinc is often adsorbed to ferrihydrite, an iron hydroxide mineral, and birnessite, a manganese oxide. We also found evidence for Zn-sorption onto clay minerals (either the hydroxyl-Al interlayers of 2:1 clay minerals or to edge site aluminol groups of clay minerals). Additionally, we found significant evidence for the incorporation of Zn into surface precipitates, resembling Zn-Al LDH and a neo- formed Zn phyllosilicate (Zn-kerolite).

4.4.6 Bulk EXAFS Analysis

Bulk EXAFS spectra of both the treated and non-treated soils were collected to quantify the major phases which contribute to the overall spectrum and are shown in Figure 4.7. The chi spectra were linearly fit by combinations of reference spectra, and with allowing the energy shifts to vary. With this approach, the major phases which contribute to the overall spectrum can be estimated. The treated and non-treated both have a similar fraction of willemite (~ 25 percent), that represents the main slag

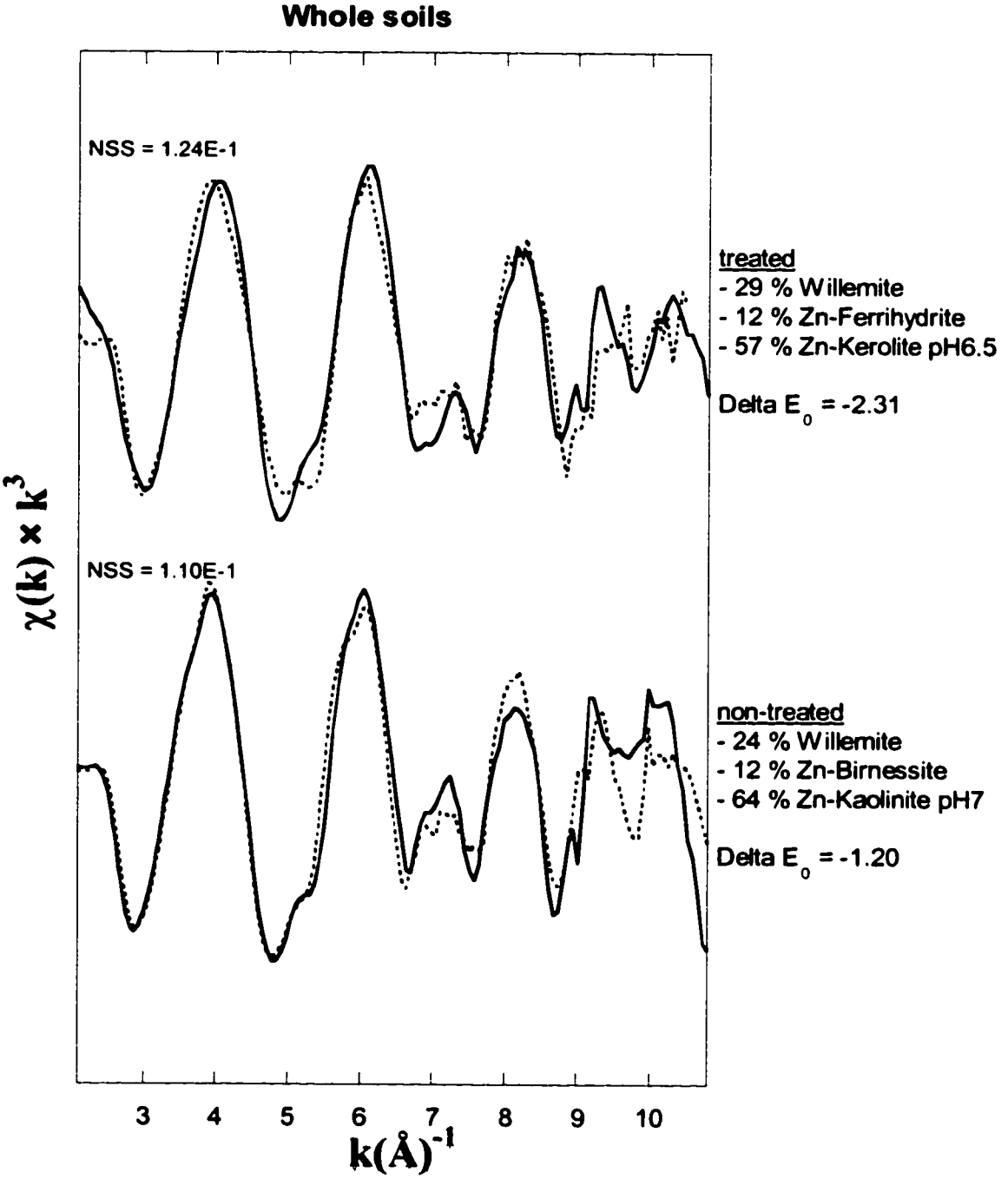

Figure 4.7: EXAFS spectra of the complete treated and the non-treated soil. The solid lines indicate the raw chi data and the dotted line indicates the best fits obtained with a linear fitting approach.

related phase (primarily fall-out mineral). Other slag related minerals such as sphalerite (ZnS) and franklinite, which we detected with μ-EXAFS could not be identified in the whole soil and were most likely contributing less than 10 % to the overall spectrum. A significant (~10%) zinc fraction formed inner sphere complexes with ferrihydrite and birnessite, which were used as proxies for the iron and manganese oxy(hydroxide) minerals. In the non-treated soil Zn-sorbed birnessite gave a slightly better fit, in the treated soil Zn-sorbed ferrihydrite. However, both could be fit almost equally well. The largest zinc fraction (~60%) is incorporated into neo-formed surface precipitates. In the non-treated soil the precipitate formed resembled Zn-Al LDH, whereas in the treated soil it resembled Zn-kerolite.

4.4.7 Stirred-flow Desorption Experiments

The results of the stirred-flow desorption experiments are collected in Figure 4.8. To compare the desorption behavior of both soils, the overall zinc concentration in the treated soil is almost half that of the non-treated soil (Table 4.1), the amount of zinc desorbed is normalized to the total soil Zn concentrations and plotted as a function of chamber volumes. The 0.1 M $CaCl_2$ solution caused a significant amount of zinc desorption in the first few chamber volumes from both soils. Less zinc came off in the first few chamber volumes with the low ionic strength pH 4 solution, suggesting that the first fraction desorbed may be electrostatically held (outer-sphere bound) Zn. After the initial fast desorption in the first 10 chamber volumes, zinc desorption tails off.

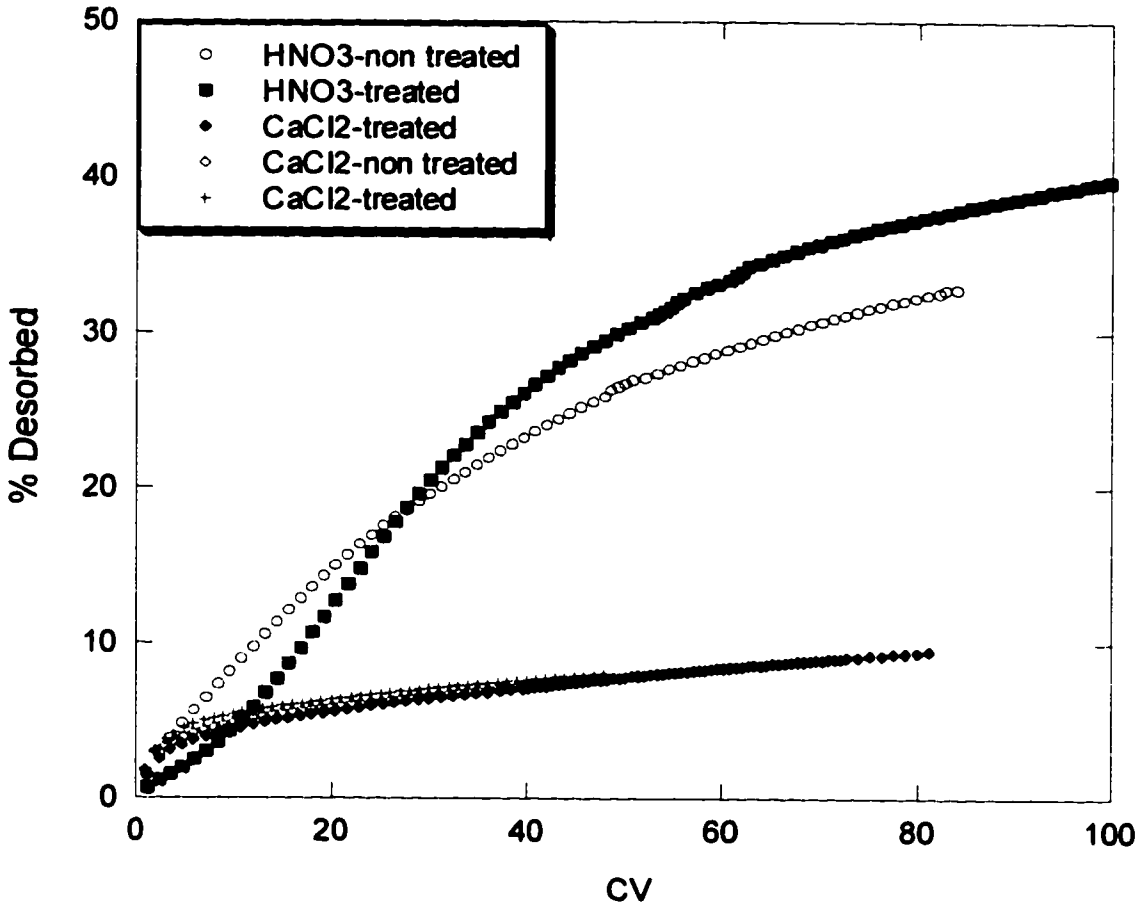

Figure 4.8: Percentage Zn desorbed from the treated and treated zinc smelter soils using a 0.1 M $CaCl_2$ solution adjusted to the soil pH and a pH 4 HNO_3 solution.

The pH 4 solution, which was chosen to simulate acid rainfall conditions, was able to desorb a significant amount of zinc from both the treated and non-treated soil, up to 35 percent after 80-100 chamber volumes. In the first 10 chamber volumes, Zn is more stable in the treated soil with respect to the pH 4 solution. But over the entire reaction range, Zn desorption from the treated soil is not significantly different than that from the non-treated soil. These results suggest that Zn is as stable in the treated as in the non-treated soil.

4.5 DISCUSSION

4.5.1 Zinc speciation

Several slag related zinc mineral phases, i.e. willemite, sphalerite and to a lesser extent franklinite and hemimorphite, were identified in the treated and non-treated soils by quantitative electron microprobe analysis, bulk and μ-focused EXAFS spectroscopy. These minerals have been deposited on the soil mainly by fall out downwind from the chimney stack of the smelter. Sphalerite (ZnS) minerals are remnants of the raw ore that by-passed the pyrometallurgical smelting process due to incomplete oxidation of ZnS (up to 20%), generating ZnS containing slags (Issaure et al 2002). Willemite (Zn_2SiO_4) is a high-temperature anhydrous silicate that originates from the smelting process. Hemimorphite ($Zn_4Si_2O_7(OH)_2$) and Franklinite ($ZnFe_2O_4$) are also formed in the smelting process and were occasionally found in both the treated and the non-treated soils. Linear combination fitting (LCF) of the EXAFS spectra of the treated

and non-treated bulk soils, indicated that of those four smelter minerals Willemite is the most prominent. These 'primary' smelter minerals only make up 30 % of the total Zn fraction in the soil. A significant percentage of the zinc (70 % according to LCF of the bulk soils EXAFS spectra) is distributed into secondary zinc phases. These results suggest that the primary slag related minerals, some already deposited on the soil more than a century ago, have been significantly weathered over time. Sphalerite (ZnS) in particular may have oxidized and dissolved in the oxygenated soil environment.

Both LCF fitting of the bulk soils and the detailed analyses of the soil thin sections with μ-focused EXAFS spectroscopy indicated that upon weathering a significant amount of Zn forms an inner-sphere complex with iron and manganese oxides and the Al hydroxyl interlayer of 2:1 clay minerals. The largest fraction of the weathered Zn fraction (60%) is incorporated into neo-formed precipitates. These precipitates are very similar in structure to our reference phases, a Zn-Al layered double hydroxide and a Zn-kerolite, which is a Zn-phyllosilicate (Figure 4.2b). In the non-treated soil the precipitate phase formed is more that of a layered double hydroxide (Zn-Al LDH), whereas the precipitate formed in the treated soil resembled more that of a Zn-phyllosilicate. Ford et al. (1999) monitored structural changes in a nickel surface precipitate (which is very similar to that of Zn precipitates (Ford and Sparks, 2000)), formed at the pyrophillite (an ideal 2:1 clay mineral) surface as a function of aging time. It was found that initially a Ni-hydroxide phase formed at the mineral surface, well below super saturation conditions in solution. Or in the presence

of Al, Al co-precipitation with Ni is thermodynamically was preferred; in which case a so-called Ni-Al layered double hydroxide (LDH) is formed. This Ni-Al LDH is more resistant to weathering than Ni-hydroxide (Scheckel et al. 2000).

The initial surface precipitation reaction may be explained by the combination of several processes (Yamaguchi et al., 2001). First, the electric field of the mineral surface attracts Ni ions through adsorption, leading to a local supersaturation of Ni at the mineral-water interface. Second, the solid phase may act as a nucleation center for polyhydroxy species and catalyze the precipitation process (McBride, 1994). Third, the physical properties of water molecules adsorbed at the mineral surface are different from those of free water (Sposito, 1989), potentially causing a lower solubility of metal hydroxides at the mineral-water interface.

Further stabilization of the precipitate can occur by diffusion of Si polymers ($(H_xSiO_4)^{x-4}$) in the interlayer space of the LDH, thereby replacing the anions. Polymerization and condensation of the interlayer Si polymers slowly transforms the LDH into a precursor Me-Al phyllosilicate, which might further develop into a tri-octahedral clay. Stabilization also occurs in precipitates formed on Al-free substrates. This stabilization was contributed to Ostwald ripening (Ford 1999).

The difference in the type of precipitate formed in the treated and non-treated soil suggests that in the treated soil, where the local pH varied between 7.3 and 7.9 at the time of the treatment (Vangronsveld 1994), more silica was available for the formation of a Zn-phyllosilicate or the transformation of a Zn-Al LDH into a Zn-

phyllosilicate. The higher pH of the soil solution at the time of remediation may have enhanced this process.

Our findings correlate with a study by Manceau et al. (2000) on Zn-contaminated smelter soils from the same geographic area. Manceau et al. used both conventional XRD and LCF of EXAFS spectra of bulk soils to speciate Zn in these soils (pH around 6.5), and distinguished willemite and hemimorphite as the primary polluting Zn minerals. Upon weathering, Zn was predominately incorporated in neo-formed Zn-containing phyllosilicates and to a lesser extent bound to Mn and Fe (hydr)oxides. Roberts et al. (2002) studied the Zn speciation in smelter contaminated soils at a significantly lower pH (~5). They found that at this pH, Zn was mostly bound to Al-groups of the clay minerals and to a lesser extent to Fe and Mn (hydr)oxides. No indication on the formation of zinc containing surface precipitates was found, suggesting that the formation of surface precipitates only takes place at near neutral pHs.

4.5.2 Long term zinc availability

It is important to monitor Zn release under changing environmental conditions, e.g. acidification of the soil, before making any predictions on long term zinc mobility. If in-situ remediation materials exert their effect through changes in soil pH only, then reacidification of the soil will cause metal bioavailability to return to its original toxic level. If remediation materials raise soil pH and sorb metals strongly, then

reacidification of soil will raise metal bioavailability but at a reduced level compared to the original soil, depending on the soil and amendment buffer capacity and the rate of change in amendment K_d with pH. If remediation materials promote fixation of metals in nonlabile pools (such as stable mineral phases) in the soil, then the availability will depend on solid-solution equilibrium kinetics or the solubility product of the solid phase formed, and is presumably more enduring (Hamon et al. 2002).

The striking similarities in zinc speciation suggests that both the treated and non-treated soil should show similar desorption behavior, with zinc being a little bit more stable in the treated than in the non-treated soil due to the presence of a presumably more stable surface precipitate (phyllosilicate vs LDH). To determine the stability of the sorption complex under different environmental conditions, desorption experiments, using a stirred-flow technique were conducted, using a 0.1 M $CaCl_2$ solution adjusted to the soil pH to desorb the exchangeable metal fraction, and a pH 4 HNO_3 solution to simulate normal and more extreme weathering conditions (Figure 8).

No significant differences in desorption behavior between the treated and non-treated soils were found using either desorption agent. About 10 wt% of the total Zn fraction was desorbed from the treated and non-treated soil samples using the $CaCl_2$ solution. The initial higher Zn concentration in the non-treated soil samples thus leads automatically to a Zn concentration in the exchangeable fraction and therefore a higher Zn toxicity in the non-treated soil. Using the pH 4.0 solution 30-40% of Zn was desorbed from the treated and non-treated soils. The slope of the desorption curves

suggest that Zn desorption did not reach its maximum yet after 80 chamber volumes, indicating that with prolonged desorption experiments even more Zn might come off. Zn is clearly not in a stable form with respect to a more extreme desorption agent.

4.6 CONCLUSIONS

This study shows that the *in situ* remediation method applied 12 yrs ago, addition of beringite and compost, did not lead to a long-term fixation of Zn in the smelter contaminated soil. No significant differences in speciation between the treated and non-treated soils was found, which lead to similar stabilities with respect to desorption. Neo-formed Zn containing surface precipitates, whether a Zn-Al LDH or a Zn-phyllosilicate, made up 60 % of the total Zn fraction in these smelter contaminated soils. Only with state of the art techniques such as EXAFS spectroscopy can these amorphous mineral phases be distinguished in soils. Surface precipitates are therefore very important at near neutral pH in highly contaminated soils and should be considered when modeling Zn speciation. The incorporation of Zn into stable surface precipitates could lead to a significant natural attenuation of the exchangeable/bioavailable Zn fraction under these conditions. The formation of surface precipitates does however not lead to a permanent sequestration of Zn from the soil solution. When the pH of the soil was lowered, i.e. when the buffer capacity of the additives is diminished, Zn was released from the precipitates, indicating that the precipitates are not thermodynamically stable at lower pH.

The surface precipitates in this soil provided a unique possibility to study its long term Zn sequestration possibilities, in that the natural pH of the soil is near neutral and high Zn concentrations have been present for at least a century. The fact that the precipitates are not stable when we lowered the pH indicates that no significant stabilization of surface precipitates takes place in natural soils and that these surface precipitates are only important at higher pHs.

4.7 REFERENCES

Bertsch, P.M. and D.B. Hunter. 1998. Elucidating fundamental mechanisms in soil and environmental chemistry: The role of advanced analytical spectroscopic, and microscopic methods. *In* P.M. Huang , D.L. Sparks and S.A. Boyd (eds.) Future of soil chemistry. Soil. Sci. Soc. AM., Madison, WI.

Boisson J., A. Ruttens, M. Mench and J. Vangronsveld. 1999. Evaluation of hydroxyapatite as a metal immobilizing soil additive for the remediation of polluted soils. Part 1. Influence of hydroxyapatite on metal exchangeability in soil, plant growth and plant metal accumulation. *Envion. Pol.* **104:** 225-233.

Eick M. J. and S.E. Fendorf. 1998. Reaction sequence of Nickel(II) with kaolinite: Mineral dissolution and surface complexation and precipitation *Soil Sci. Soc. Am. J.* **62:** 1257-1267.

Ford R.G., A.C. Scheinost, K.G. Scheckel and D.L. Sparks. 1999. The link between clay mineral weathering and the stabilization of Ni surface precipitates. *Environ. Sci. Technol.* **33:** 3140-3144.

Ford R.G. and D.L. Sparks. 2000. The nature of Zn precipitates formed in the presence of pyrophyllite. *Environ. Sci. Technol.* **34:** 2479-2483.

Hamon, R.E., M.J. McLaughlin, and G. Cozens. 2002. Mechanisms of attenuation of metal availability in in situ remediation treatments. *Environ. Sci. Technol.* **36:** 3991-3996.

Issaure, M.-P., A. Laboudigue, A. Manceau, G. Sarret, C. Tiffreau, P. Trocellier, G. Lamble, J.-L. Hazemann, and D. Chateigner. 2002. Quantitative Zn speciation in a contaminated dredged sediment by μ-PIXE, μ-SXRF, EXAFS spectroscopy and principal component analysis. *Geochim. Cosmochim. Acta* **66:** 1549-1567.

Juillot F., G. Morin, P. Ildefonse, T.P. Trainor, M. Benedetti, L. Galoisy, G. Calas, and G.E. Brown Jr. 2003. Occurrence of Zn/Al hydrotalcite in smelter-impacted soils from northern France: Evidence from EXAFS spectroscopy and chemical extractions. *Am. Miner.* **88:** 509-526.

Lombi E., R.E. Hamon, S.P. McGrath, M.J. McLaughlin. 2003. Lability of Cd, Cu, and Zn in polluted soils treated with lime, beringite, and red mud and

identification of a non-labile colloidal fraction of metals using isotopic techniques. *Environ. Sci. Technol.* **37:** 979-984.

MacDowell A.A., R. Celestre, C.H. Chang, G.M. Lamble, H.A. Padmore and J.R. Patel. 1998. Progress towards sub-micron hard X-ray imaging using elliptically bent mirrors: *in* McNulty, I. Editor, X-ray microfocusing: applications and techniques, 137-144.

Malinowski E.R. 1991. Factor Analysis in Chemistry. John Wiley, New York.

Manceau, A., B. Lanson, M. Schlegel, J.D. Hargé, M. Musso, L. Eybert-Bérard, J.L. Hazemann, D. Chateinger, and G.M. lamble. 2000 Quantitative Zn speciation in smelter-contaminated soils by EXAFS spectroscopy. *Am. J. Sci.* **300:** 289- 343.

Manceau A., M.A. Marcus, N. Tamura. 2003. Quantitative speciation of heavy metals in soils and sediments by synchrotron X-ray techniques. *In* NC Sturchio, P Fenter, SR Sutton, ML Rivers (eds). Applications of Synchrotron Radiation in Low-Temperature Geochemistry and Environmental Science. Reviews in Mineralogy. Mineralogical Society of America, Washington, D.C.

McBride M.B. 1994. Environmental Chemistry of Soils. Oxford University Press, New York.

McKenzie, R.M. 1971. The synthesis of birnessite, cryptomelane, and some other oxides and hydroxide surfaces. *Z. Pflanzenernahr. Bodenk.* **150:** 99-102.

Mellini, M. 1982. The crystal structure of Lizardite 1T-Hudrogen-Bonds and polytypism. *Am. Mineral.* **67:** 587-598.

Nachtegaal, M. and D.L. Sparks 2003. Nickel sequestration in a kaolinite-humic acid complex. *Environ. Sci. Technol.* **37:** 529-534.

Nachtegaal, M. and D.L. Sparks. 2003b. Effect of iron oxide coatings on zinc sorption mechanisms at the mineral/water interface. *Submitted.*

Nriagu J.O., and J.M. Pacyna. 1988. Quantitative assessment of worldwide contamination of air, water and soils by trace metals. *Nature* **333:** 134-139

O'Day P.A., S.A. Carroll and G.A. Waychunas. 1998. Rock-water interactions controlling zinc, cadmium, and lead concentrations in surface waters and

sediments, US Tri-Sate Mining District. 1: Molecular identification using X-ray absorption spectroscopy. *Environ. Sci. Technol.* **32:** 943-955.

Oste L.A., T.M. Lexmond and W.H. Van Riemsdijk. 2002. Metal immobilization in soils using synthetic zeolites. *Environ Quality.* **31:** 813-821.

Ostergren J.D., G.E. Brown Jr., G.A. Parks and T.N. Tingle. 1999. Quantitative speciation of lead in selected mine tailings from Leadville, CO. *Environ. Sci. Technol.* **33:** 1627-1636.

Ressler T. 1997. WinXAS: A new software package not only for the analysis of energy-dispersive XAS data. *J. Physique IV* **7:** C2-269.

Ressler T., J. Wong, J. Roos and I.L. Smith. 2002. Quantitative speciation of Mn-bearing particulates emitted from autos burning (mythylcyclopentadienyl) manganese tricarbonyl-added gasolines using XANES spectroscopy. *Environ. Sci. Technol.* **34:** 950-958.

Roberts, D.R., A.C. Scheinost and D.L. Sparks. 2002. Zinc speciation in a smelter-contaminated soil profile using bulk and microspectroscopic techniques. *Environ. Sci. Technol.* **36:** 1742-1750.

Scheckel K.G., A.C. Scheinost, R.G. Ford and D.L. Sparks. 2000. Stability of layered Ni hydroxide surface precipitates - A dissolution kinetics study. *Geochim. Cosmochim. Acta* **64:** 2727-2735.

Scheidegger A. M., G.M. Lamble and D.L. Sparks. 1997. Spectroscopic evidence for the formation of mixed-cation hydroxide phases upon metal sorption on clays and aluminum oxides. *J. Colloid Interface Sci.* **186:** 118-128.

Schlegel, M.L., A. Manceau and L. Charlet. 1997. EXAFS study of Zn and ZnEDTA sorption at the goethite (α-FeOOH)/water interface. *J. Phys. IV* **7:** 823-824.

Schlegel, M.L., A. Manceau, L. Charlet and J.L. Hazemann. 2001. Adsorption mechanisms of Zn on hectorite as a function of time, pH, and ionic strength. *Am. J. Sci.* **301:** 798-830.

Sobanska S., N. Ricq, A. Laboudigue, R. Guillermo, C. Bremard, J. Laureyns, J.C. Merlin and J.P. Wignacourt. 1999. Microchemical investigations of dust emitted by a lead smelter. *Environ. Sci. Technol.* **33:** 1334-1339.

Sonke J.E., J.A. Hoogewerff, S.R. van der Laan and J. Vangronsveld. 2002. A chemical and mineralogical reconstruction of Zn-smelter emissions in the Kempen region (Belgium), based on organic pool sediment cores. *Sci. Tot. Environ.* **292:** 101-119.

Sparks D.L. 1995. Environmental Soil Chemistry. Academic Press, Inc. London.

Sposito G. 1994. Chemical equilibria and kinetics in soils. Oxford University Press, New York.

Strawn, D.G. and D.L. Sparks. 2000. Effects of soil organic matter on the kinetics and mechanisms of Pb(II) sorption and desorption in soil. *Soil Sci. Soc. Am. J.* **64:** 144-156.

Schwertmann U., and R.M. Cornell R.M. 1991. Iron oxides in the laboratory: preparation and characterization. Weinheim, New York.

Tessier A., P.G.C. Campbell, M. Bisson. 1979. Sequential extraction procedure for the speciation of particulate trace metals. *Analytical Chemistry* **51:** 844-851.

Trainor T.P., G.E. Brown Jr. G.A. and Parks 2000. Adsorption and precipitation of aqueous Zn(II) on alumina powders. *J. Colloid Interface Sci.* **231:** 359-372.

Vangronsveld J., F. Van Assche and H. Clijsters. 1995. Reclamation of a bare industrial area contaminated by non-ferrous metals: *in situ* metal immobilization and fixation. *Environ. Pol.* **87:** 51-59.

Vangronsveld, J., J.V. Colpaert and K.K. Van Tichelen. 1996. Reclamation of a bare industrial area contaminated by non-ferrous metals: physico-chemical and biological evaluation of the durability of soil treatment and revegetation. *Environ Pol.* **94:** 131-140.

Wasserman S.R., P.G. Allen, D.K. Shuh, J.J. Bucher and N.M. Edelstein. 1999. EXAFS and principal component analysis: A new shell game. *J. Synchrotron Rad.* **6:** 284-286.

Waychunas, G.A., C.C. Fuller and J.A. Davis. 2002. Surface complexation and precipitate geometry for aqueous Zn(II) sorption on ferrihydrite I: X-ray absorption extended fine structure spectroscopy analysis. *Geoch. Cosmochimica Acta* **66:** 1119-1137.

Webb, S. M., G.G. Leppard and J.F. Gaillard. 2000. Zinc speciation in a contaminated aquatic environment: characterization of environmental particles by analytical electron microscopy. *Environ. Sci. Technol.* **34:** 1926-1933.

Wickham G.A. 1990. Zinc industry in the 1990s. *In* Lead-Zinc '90, eds. T.S. Mackey and R.D. Prengaman. The Minerals, Metals and Materials Society, Warrendale, PA, 13-21.

Yamaguchi N.U., A.C. Scheinost and D.L. Sparks. 2001. Surface-induced nickel hydroxide precipitation in the presence of citrate and salicylate. *Soil Sci. Soc. Am. J.* **65:** 729-736.

Zabinsky S.I., J.J. Rehr, A. Ankudinov, R.C. Albers and M.J. Eller. 1995. Multiple-scattering calculations of X-ray absorption spectra. *Phys. Rev.* **B52:** 2995-3009.

Chapter 5

C 1s-NEXAFS SPECTROSCOPIC AND SPECTROMICROSCOPIC STUDIES OF HUMIC ACIDS AND THEIR INTERACTIONS WITH METALS

5.1 ABSTRACT

The macroscopic structure and the distribution of functional groups within humic substances determine their reactivity towards metals and minerals. Up to now no technique was available to study both these properties *in situ* and with a high spatial and chemical resolution. In this study, a novel combination of X-ray spectromicroscopy and C1s near edge X-ray absorption spectroscopy (C1s-NEXAFS) was applied to study the chemistry and micro-heterogeneity of a humic acid (HA) in the solution phase. In particular, the effect of pH (4 and 7) and metal complexation (0.5 mM solutions of Al(III), Pb(II), Cr(III), Mn(II) and Fe(III) with 0.1 $g.L^{-1}$ of HA, at pH 5 and I=0.1 M $NaNO_3$) on the chemistry of the carbon functional groups of the HA was studied by extracting NEXAFS spectra from image stacks. In the NEXAFS spectra, the C 1s(C=O) $\rightarrow 1\pi^*_{C=O}$ transitions of the carboxyl functional groups proved to be sensitive to changes in pH and the presence of different metals. Upon the formation of ionic bonds (Al(III), no changes in peak position were observed. Upon formation of covalent bonds (Pb(II), Cr(III) and Mn(II)) a 0.2 eV shift of the carboxyl peak position to the left was observed, indicating (depending on the direction of the shift) a partial donation or subtraction of electron density from the HA carboxyl group to the metals. Upon reaction with Mn(II) a 0.7 eV shift to lower eV of the carboxyl

peak position was observed, corresponding to a partial oxidation of Mn(II) to Mn(III) by the carboxyl group. The micro-heterogeneity of a HA particle in the solution was revealed using novel multivariate statistical analysis of the image stack, where principal component analysis and cluster analysis were combined to group the statistical variation within the image stacks. Cluster analysis or pattern recognition of the HA image stacks revealed a concentration of hydrophilic carboxyl groups at the rims of the HA particle and hydrophobic, aromatic groups in the interior. These results show the great possibilities of X-ray microscopy, combined with NEXAFS spectroscopy, to study the chemistry and macromolecular structure of humic substances *in situ*.

5.2 INTRODUCTION

Humic substances (HS), defined as a series of relatively high-molecular-weight, brown- to black- colored substances formed by secondary synthesis reactions (Stevenson, 1994), play an important role in the retention and mobility of metals in the environment. HS, or alternatively soil organic matter (SOM) or biopolymers make up 0.5-5 wt% in mineral soils and nearly 100 wt% in organic soils (Sparks, 1995). Contrary to inorganic and small organic constituents of soils, the chemistry of these biopolymers and their role in different environmental processes is not well understood. The behavior of HS in the environment is dictated by both their functional group content, and their macromolecular structure (Schnitzer, 2000). These two properties

have been studied independently with a range of spectroscopic and microscopic techniques (Myneni, 2003). Nuclear magnetic resonance (NMR) spectroscopy has become the technique to semi-quantitatively study the functional group chemistry of HS (e.g. Mao et al., 2002). And atomic force microscopy (AFM) is the technique to study the macromolecular structure of HS under different solution conditions (e.g. Plaschke et al., 2002). However, functional group chemistry and macromolecular structure together define the reactivity of HS in the environment. Investigating only the functional group chemistry does not reflect the chemical heterogeneities that exist in these large biopolymers. Moreover, the presence of paramagnetic metals, such as Fe in the samples leads to line broadening of the NMR spectra. Thus HS can only be studied after extraction from the soil environment, using often harsh chemical treatments.

Similar to NMR spectroscopy, carbon near edge X-ray absorption structure (C-NEXAFS) spectroscopy has capability to semi-quantitatively determine the main carbon containing functional groups of HS (Scheinost et al., 2001). In contrast to solid state magic angle spinning (MAS) NMR, samples can be studied in their natural state, without using chemical extractions, which might be selective or change the chemistry of the HS. C-NEXAFS spectroscopy has been applied to study the bonding environment of C in complex macromolecules, such as polymers (Urquhart et al., 1999; Schöll et al 2003), amino acids (Boese et al., 1997; Kaznacheyev et al., 2002), coal (Cody et al., 1995 and 1998) and humic acid (Rothe et al., 2000; Scheinost et al. 2001). In C-NEXAFS spectroscopy, soft X-rays ($\lambda \approx 40$ Å) are used to promote

carbon core level (1s) electrons into various bound and virtual excited states consisting, largely, of anti-bonding molecular orbitals. Local variations in electron density surrounding the photoexcited cores impart differences in the energy gaps between the core and excited states leading to relatively well resolved spectra of absorption bands corresponding to carbon in different organic functional groups. Thus, the C-NEXAFS inner-shell spectrum reveals the manifold of excited states available for the photoexcited electrons. These excited states are well described by the lowest unoccupied or partially occupied molecular orbitals (LUMOs) of organic functional groups (Stohr, 1992).

With soft X-ray spectromicroscopy, the distribution of carbon in different chemical environments can be imaged *in situ*, i.e. in the water window, where C (C K edge 284 eV) does strongly absorb the X-ray energy, but thin layers of water (O K edge is 537 eV) are transparent to the X-ray energy. By tuning the X-ray energy to that of the carbon functional group of interest, the adsorption contrast will reveal the spatial distribution of carbon in that specific binding environment. The current resolution of the X-ray microscope is 50 nm, which is in between that of the visible light microscope and the electron microscope and which is the resolution needed to study the macromolecular structure of these biopolymers. Using soft X-ray spectromicroscopy, Myneni et al. (1999) examined the morphology of humic substances and their associations with mineral oxides and silicates as a function of pH and ionic strength. It was found that humic substances exhibit a range of structures in solution, with humic substances forming coiled up structures at lower pH and chain

like aggregates at higher pH. X-ray spectromicroscopic studies also revealed that complexing cations and the presence of mineral surfaces can also strongly influence the aggregate structure (Plaschke et al., 2002; Rothe et al 2001).

By collecting a stack of images with small energy steps in between each image ($\Delta eV = 0.05$ eV), spatial and chemical information are recorded simultaneously. Each pixel in the image stack contains a complete NEXAFS spectrum (Jacobsen et al., 2000). By rastering the X-ray beam over the sample to collect each image, radiation damage is kept to a minimum, compared to the collection of point spectra, where the sample is exposed to the X-ray beam for a prolonged time (Jacobsen et al., 2000). Despite the obvious benefits of such an approach, only a few studies exist which combined NEXAFS spectroscopy with spectromicroscopy to study HS in their natural state and their interactions with metals. In a preliminary study Rothe et al. (2000) characterized the main carbon chemistry of a humic acid (HA) interacting with montmorillonite. In a follow up study, Plaschke et al. (2002) studied the influence of Eu(III) on the agglomeration of humic acid and reported a segregation of the humic substances in dense and diffuse zones upon the introduction of Eu(III) which corresponds to a different local carbon chemistry.

In this study we report the spatial and chemical heterogeneity of humic substances isolated from a peat bog soil, using the unique combination of C-NEXAFS spectroscopy and spectromicroscopy. Spectroscopically significant differences in the specimen image stack datasets were identified using multivariate statistical analysis

methods. Principal component analysis was used to determine the most significant variations in the dataset, without prior knowledge of their chemistry. The corresponding eigenspectra cannot be interpreted in a straightforward manner, since they do not necessarily correspond to a unique chemical component, but more to successive differences in spectra (Jacobsen et al., 2002). Cluster analysis was then used to seek the natural grouping of the dataset.

Metal interactions with the isolated humic acid were studied in a similar fashion, but with emphasis on changes in the NEXAFS spectra (peak position and intensity) upon metal reaction. The electronic structure of a large organic molecule can in principle be described as the electronic transitions of simple diatomic molecules. This building block approach holds true when the orbital composition and energy states of an atom of interest are modified primarily by the energy states of its first neighbors (Stohr 1992). In this case no shifts in the spectra should be expected upon metal reaction, since interactions of the metals with carbon goes through oxygen atoms. This means that humic substances can be studied *in situ* using NEXAFS spectroscopy, since metals will not affect the overall spectrum. However, not only do the interactions of diatomic molecules and their respective orbitals contribute to the overall spectrum. The complete local coordination around the atom of interest and the nature of the hybridized orbitals of this atomic group should be considered (Schöll et al., Myneni, 2003).

5.3 EXPERIMENTAL SECTION

5.3.1 Materials

The humic acid used in this study was extracted from the first 20 cm of an unpolluted bog soil in the White Mountain National Park, New Hampshire. The isolation procedure and characterization are described elsewhere (Davies et al. 1997). Essentially the soil was pre-treated with mild solvents (a benzene-methanol mixture) to remove any lipids and proteins from the sample. After pre-extraction the humic substances were extracted with aqueous base. The supernatant was brought to pH 1.0 with concentrated HCl. The remaining HA gel was washed with 1.0 M HCl to remove any remaining metals and mineral fraction, washed with DI water and freeze-dried. The ash content of this HA is 0.25 wt%. From the freeze dried HA and the HA gel, 2 g L^{-1} HA stock solutions were prepared in DI water and adjusted to pH 5.0 using 0.1 M NaOH.

5.3.2 Sample preparation

To study the effect of pH on the HA NEXAFS spectra, pH 4 and pH 7 solutions of 0.1 $g.L^{-1}$ HA were prepared by diluting the stock solution with DI water and adjusting the pH with 0.05 M NaOH or 0.05 M HNO_3 as needed. These solutions were put on a reciprocal shaker for 24h.

Metal complexation by the HA was studied by reacting 0.5 mM metal from a metal stock solution with 0.1 $g.L^{-1}$ HA of the HA stock solution, at pH 5.0 and an

ionic strength of 0.1 M $NaNO_3$. One molar Al(III), Pb(II), Cr(III), Fe(III) and Mn(II) stock solutions were prepared by dissolving the corresponding metal nitrate salts in degassed DI water. The pH was adjusted with 0.1 M NaOH or 0.1 M HNO_3. These solutions were put on a reciprocal shaker for 24h.

Samples for scanning transmission x-ray microscopy were prepared by placing a 200 µL droplet of each solution in between two Si_3N_4 windows, which were tightly screwed together in a so-called wet cell until Newton interference fringes were observed, which indicated a uniform film thickness of ~ 60 nm (Neuhauser, 2000).

5.3.3 STXM

X-ray image stacks and C 1s NEXAFS spectra were acquired with the scanning transmission X-ray microscope (STXM) located at beamline X1A at the National Synchrotron Light Source at Brookhaven National Laboratory, Upton NY (Jacobsen et al., 1991). The electron storage ring operated at 2.8 GeV with an average beam current of 180 mA. Monochromator slits resulting in an energy resolution of ~ 100-140 meV were utilized. Focusing of the monochromatic X-ray beam was accomplished with a Fresnell phase-zone plate objective and an order sorting aperture yielding a spatial resolution of 55 nm. The energy of the spherical grating monochromator was calibrated by setting the 2^{nd}-strongest absorption band of carbon dioxide at 290.74 eV (Ma et al., 1991; Hitchcock and Mancini, 1994), resulting in an energy resolution of 0.15 eV fwhm.

Image stacks of the HA and the metal reacted HA solutions in the wet-cell were collected between 280 and 312 eV, with energy steps of 0.05 eV between 284 and 292 eV and energy sets of 0.3 eV in the other regions. The image stacks were aligned to correct for the mechanical shift of the sample stage out of the focus spot (Jacobsen et al., 2000). Spectra of selected sample regions were extracted by vertical projections of the corresponding zones, using Beer's law: $\mu^*d = \text{Ln}(I_o/I)$ and by selecting the I_0 in a carbon free region and by averaging I over the pixels of interests.

The image stack datasets were analyzed using multistatistical analysis methods following the approach of Jacobsen et al. (2002). Principal component analysis was performed to serve as a prefilter for cluster analysis. These principal components or eigenvalues, describe the energies where unique variations appear in the data. Cluster analysis, using the spectra at each pixel in the image stack as target spectra for the principal components was then used to seek the natural groupings of the data.

5.4 RESULTS AND DISCUSSION

5.4.1 Effect of pH on the HA NEXAFS spectrum

Figure 5.1 shows the spectra of the HA, collected in a wet cell at pH 4 and pH 7. The dotted lines represent the experimental data and the solid lines indicate the best fits and the residual. The spectra were deconvoluted using an arctangent function for the ionisation step at 290 eV, four Gaussian functions for the π^* and σ^* transitions below the ionisation energy, and two Gaussian functions for the σ^* transitions

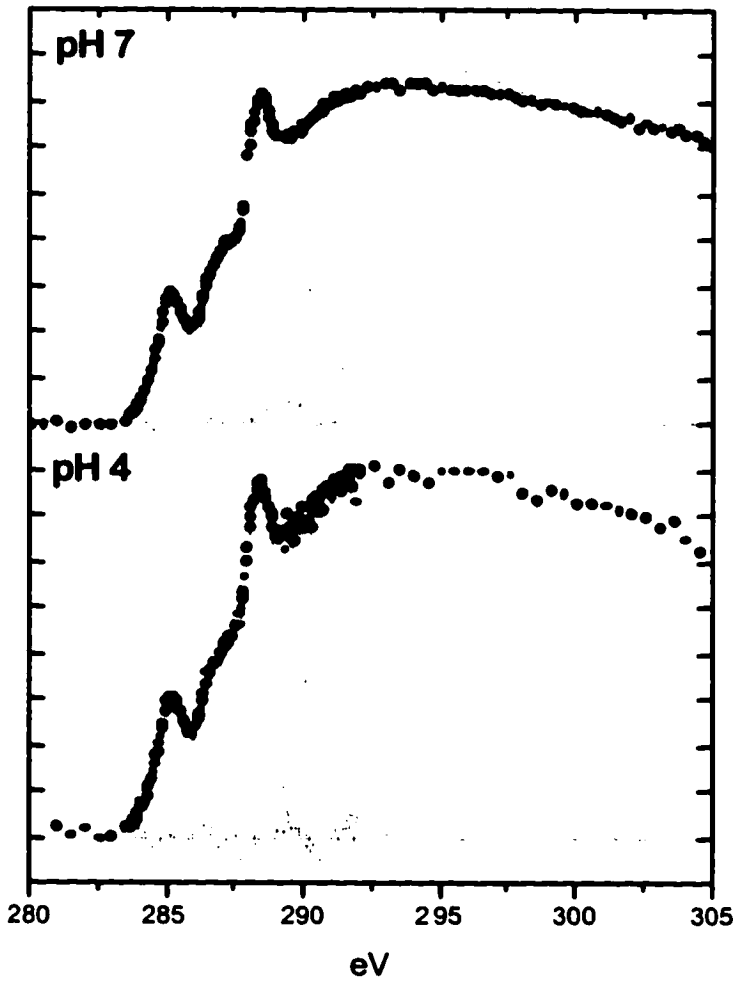

Figure 5.1 C1s NEXAFS spectra of HA at pH 4 and pH 7. The experimental data are indicated with the dots and the best fit and residual with the solid lines. The dashed lines are 6 Gaussians and an arctangent step function for the IP used for fitting the experimental NEXAFS spectra.

above the ionisation energy (Stohr, 1992). The assignment of the electronic transitions and their values derived from deconvoluting the NEXAFS spectra are collected in Table 5.1. Peak assignment is based on a literature study of published NEXAFS and electron energy loss spectroscopy (EELS, a similar technique) values for small organic molecules with known electronic transitions (Scheinost et al., 2001) and extensive calculations on electronic transitions in polymers (Urquhart et al., 1999). The first peak at ~285 eV is characteristic of the C 1s(C-H) $\rightarrow 1\pi^*_{C=C}$ transition of the aromatic groups (the core level is indicated parenthetically before the arrow, while the nature of the upper level of a given transition is indicated as the final subscript). The shoulder at 286.3 eV is assigned to the C 1s(C-OH) $\rightarrow 1\pi^*_{C=C}$ transition of OH groups attached to the phenyl ring. The position of this π transitions has been shown to shift depending on its chemical environment (Urquhart et al., 1999).The sharp peak at ~288.3 eV is characteristic of the C 1s(C=O) $\rightarrow 1\pi^*_{C=O}$ transition of the carboxyl functional groups. Ab initio calculations and experimental studies of carboxyl groups in different chemical environments have shown that this transition is very sensitive to different bonding environments (Urquhart and Ade, 2002). The broad peak at ~ 289 eV is assigned to C 1s $\rightarrow$ C-H transitions of both π^* and σ^* character of the carbon backbone (CH_3/CH_2) of the HA (Urquhart et al., 1999). Unfortunately, this peak also

	$\pi^*_{C=C}$ (aromatics	$\pi^*_{C=C}$ (phenyl)	$\pi^*_{C=O}$ (carboxyl)	π^*/σ^*_{C-H} (CH_2/CH_3)	σ^*_{C-C}	σ^*_{C-O}
pH						
HA-pH 4	284.8	286.3	288.0	289.0	294.6	301.0
HA-pH 7	284.8	286.3	288.2	288.8	294.7	301.5
p-elements						
HA-pH 5	284.8	286.4	288.0	289.0	294.6	301.0
Al(III)	284.9	286.5	288.1	289.2	294.7	301.0
Pb(II)	284.8	286.3	288.2	288.8	294.7	301.5
d-elements						
HA-pH 5	285.2	287.0	288.5	289.6	294.0	301.0
Cr(III)	285.2	287.0	288.3	289.0	293.4	299.6
Mn(II)	284.9	287.0	287.8	289.0	293.8	299.6
Fe(III)	285.2	286.8	288.3	289.0	293.4	300.1

Table 5.1 Energies (eV) of C1s $\rightarrow \pi^*$ and σ^* transitions of HA, studied as a function of pH and reacted with selected p and d elements. Energies were determined from deconvoluting the experimental spectra. Assignments indicate the final orbital.

overlaps with the C 1s $\rightarrow \sigma^*_{O\text{-}H}$ transitions of C in alcoholic groups, which are present in minor quantities in humic substances. The broad Gaussian above the ionisation step at ~ 294 eV is assigned to C 1s $\rightarrow \sigma^*_{C\text{-}C}$ transitions of the aromatic and aliphatic functional groups and the broad Gaussian at ~ 301 eV to the C 1s $\rightarrow \sigma^*_{C\text{-}O}$ transitions of the phenolic and acidic functional groups. The spectra were reasonably well fitted with these six Gaussians and the arctangent step functions (Figures 5.1, 5.2 and 5.3). The position of the aliphatic groups (CH_2/CH_3) was not very well resolved, since it is overlapping with the alcoholic groups. However in better resolved (gas phase) NEXAFS and EELS spectra C 1s $\rightarrow \sigma^*_{C\text{-}H}$ transitions and Rydberg transitions are also observed around 287 eV for the aliphatic groups (Scheinost et al., 2001), but an extra Gaussian in this region was not needed to obtain a better fit.

The carboxylic groups of the humic acid deprotonate between pH 3-5, whereas the phenolic groups deprotonate between pH 8-10. (Sparks, 1995) The other functional groups present in our HA C1s-NEXAFS spectrum are not affected by a change in pH. Therefore, we only expected small changes in the carboxylic functional groups upon changing the pH of the HA containing solution from 4 to 7, due to a slight change in the local bonding environment of the carboxylic functional groups. No notable differences in peak intensities were observed in Figure 5.1, between the HA spectrum recorded at pH 4 and at pH 7. The spectra were fitted with the Gaussian peak widths fixed for both spectra. Small differences in the peak positions of the C 1s(C=O) $\rightarrow$ $1\pi^*_{C=O}$ and the C 1s $\rightarrow \sigma^*_{C\text{-}H}$ transitions, which are superimposed in the spectrum,

were observed with changing pH. The carboxylic group shifted 0.2 eV to the right and the aliphatic peak positions 0.2 eV to the left. This shift of the carboxyl group peak position is caused by a change in the local environment upon protonation.

5.4.2 p-element reacted HA

The effect of metal complexation, using two environmentally important p-elements, Al(III) and Pb(II), on the NEXAFS spectra is shown in Figure 5.2. All spectra in each figure are collected in the same run. Small differences in energy between different data collection periods exist (Table 5.1), due to changes in the monochromator motor software and thickness changes in the Si_3N_4 windows. But spectra within each run (each figure) are collected under the same conditions and are therefore comparable. The spectral quality is a little lower than for the HA-pH samples, but it is obvious that few differences exist between the HA and the Pb(II) and Al(III) reacted HA spectra.

The HA used in this run was the HA gel, obtained before freeze drying the HA. The properties of the gel are thought to be different compared to the properties of the freeze dried HA, which is compacted upon freeze-drying (Ghabbour et al., 1998). These physical differences should not translate into differences in the HA chemistry. The second peak, which is a shoulder in the freeze dried HA (Figures 5.1 and 5.3), corresponding to the C 1s(C-R) $\rightarrow 1\pi^*_{C=C}$ transition of phenol groups, seems to be more pronounced in the spectrum of the HA gel. However, this is mainly due to the

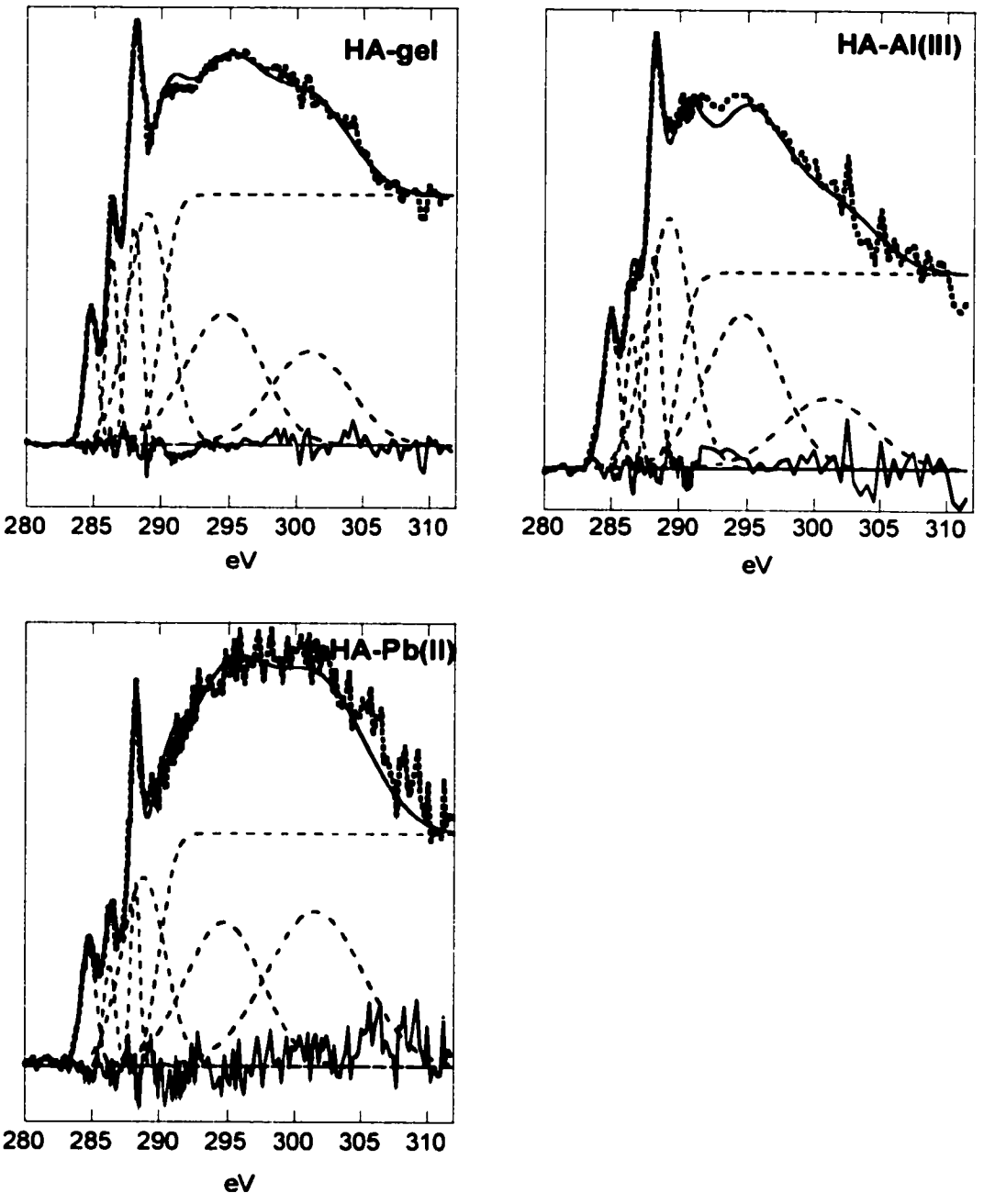

Figure 5.3 C1s NEXAFS spectra of HA reacted with Al(III) and Pb(II) respectively, at pH 5, I = 0.1 M $NaNO_3$ and t = 24h. The experimental data are indicated with the dots and the best fit and residual with the solid lines.

increase in intensity of the broad fourth peak, corresponding to the C 1s → C-H transitions of both π^* and σ^* character of the carbon backbone (CH_3/CH_2) in the HA gel. There are two possible explanations for this observed larger intensity of the aliphatic peak. First, the isolation used to extract the HA from the peat bog soil might have resulted in a slightly different composition of the HA at the time the HA gel was extracted compared to when the freeze dried HA was extracted from the soil. But more likely, the C-H Rydberg and σ^* transitions occurring around 287 (not identified in our HA) and 289 eV are less pronounced in dense solid structures than less dense structure. (Schöll et al. 2003). Although the difference in density between the gel and the solid phase is not that obvious, the HA gel consists of 98 % water (Ghabbour et al., 1998) and is thus less dense than the freeze dried HA.

The objective of reacting the Al(III) and Pb(II) with the HA, was to see if any information on group specific metal binding affinity could be derived from the NEXAFS spectra. Strictly speaking, only the nearest neighbours around carbon contribute to the NEXAFS spectra, if the building block principle holds true (Schöll et al., 2003; Stohr, 1992). The assumption that the character of the bonding and antibonding orbitals in single molecules are the most fundamental aspect, while intermolecular interactions and matrix effects are negligible only partly holds true for large organic molecules (Schöll et al., 2003; Urquhart et al. 2002). The carboxylic group is especially sensitive to changes in the local bonding environment (Urquhart et al. 2002) and therefore we focus our attention on changes in intensity and position of this group. Upon reaction with Al(III) no changes in peak position or intensity were

observed compared to the HA spectrum, indicating that Al mainly interacts with the carbon containing functional groups of the HA mainly through ionic interactions. Upon reaction with Pb(II) small shifts in the carboxyl and aliphatic peak positions were observed, which are similar to the ones observed when changing the solution pH from 4 to 7 (Figure 5.1), i.e. a 0.2 eV shift of the C 1s(C=O) $\rightarrow 1\pi^*_{C=O}$ transition position to the right and a 0.2 eV shift of the C 1s $\rightarrow \sigma^*_{C-H}$ transitions to the left. This indicates that, similar to the protonation of the deprotonated functional carboxylic groups, upon reaction with Pb(II) some sharing of electron density of the COO^- group and Pb(II) takes place. The bond formed is more of a covalent character than the ionic bonds formed with Al(III). This is not surprising, since Pb is much larger and therefore its outermost electrons are easily excited compared to those of Al(III). The shift to the right indicates that more energy is needed to excite an electron from the C core level into the $1\pi^*$ orbital, which corresponds to some subtraction of electron density from Pb(II). These results correspond well with the principle of hard and soft acids and bases (HSAB) (Pearson, 1963; Buffle and Stumm, 1994). Hard cations, such as alkali, alkaline earth metals, Al^{3+} and Fe^{3+} interact via electrostatic, ionic reactions, while soft cations, such as Pb^{2+}, Cu^+, Zn^{2+} and Cd^{2+} react to form covalent bonds. Metals such as Mn^{2+}, Fe^{2+}, Co^{2+}, Ni^{2+} and Cu^{2+} form complexes of intermediate strength. The degree of hardness can be determined from the term Z^2/r, where Z and r are the charge and radius of the cation, respectively.

5.4.3 d-element reacted HA

Upon reaction with Cr(III), Mn(II) and Fe(III), larger differences in the NEXAFS spectra were expected, since these d-elements can potentially donate or subtract electron density to and from the carboxylic functional groups, depending on the electron configuration in the d shell. Cr(III) has an electron configuration with 3 electrons in the t_{2g} level (Shriver and Atkins, 1999). Mn(II) and Fe(III) have a similar electron configurations, both are d5 metals, therefore similar C1s NEXAFS spectra were expected for the Mn(II) and Fe(III) reacted HA. The spectra of the Cr(III), Fe(III) and Mn(II) reacted HA are shown in Figure 5.3 and the corresponding peak positions are in Table 5.1.

Upon reaction with Cr(III) a small shift of 0.2 eV to the left of the C 1s(C=O) $\rightarrow 1\pi^*_{C=O}$ transistions and a shift of 0.6 eV to the left of the C 1s $\rightarrow \sigma^*_{C-H}$ transitions were observed. Similar to the Pb(II) reacted HA, the shift of the carboxylic group position to the left can be explained by considering donation of electron density of the Cr(III) metal to the carboxylic groups. This shift to the left indicates that less energy is needed to excite an electron from the C core shell into the antibonding molecular orbital, which corresponds to an increase in electron density in the antibonding molecular orbital. Upon reaction with Mn(II) a large shift, 0.7 eV to the left, of the C 1s(C=O) $\rightarrow 1\pi^*_{C=O}$ transitions was observed. Again, this shift to the left suggests the donation of electron density from Mn(II) to the carboxylic group. The large shift of almost 0.7 eV indicates that Mn(II) is partly oxidized to Mn(III) by the carboxylic groups of the HA. We expected similar results for Fe(III), based upon similar electron

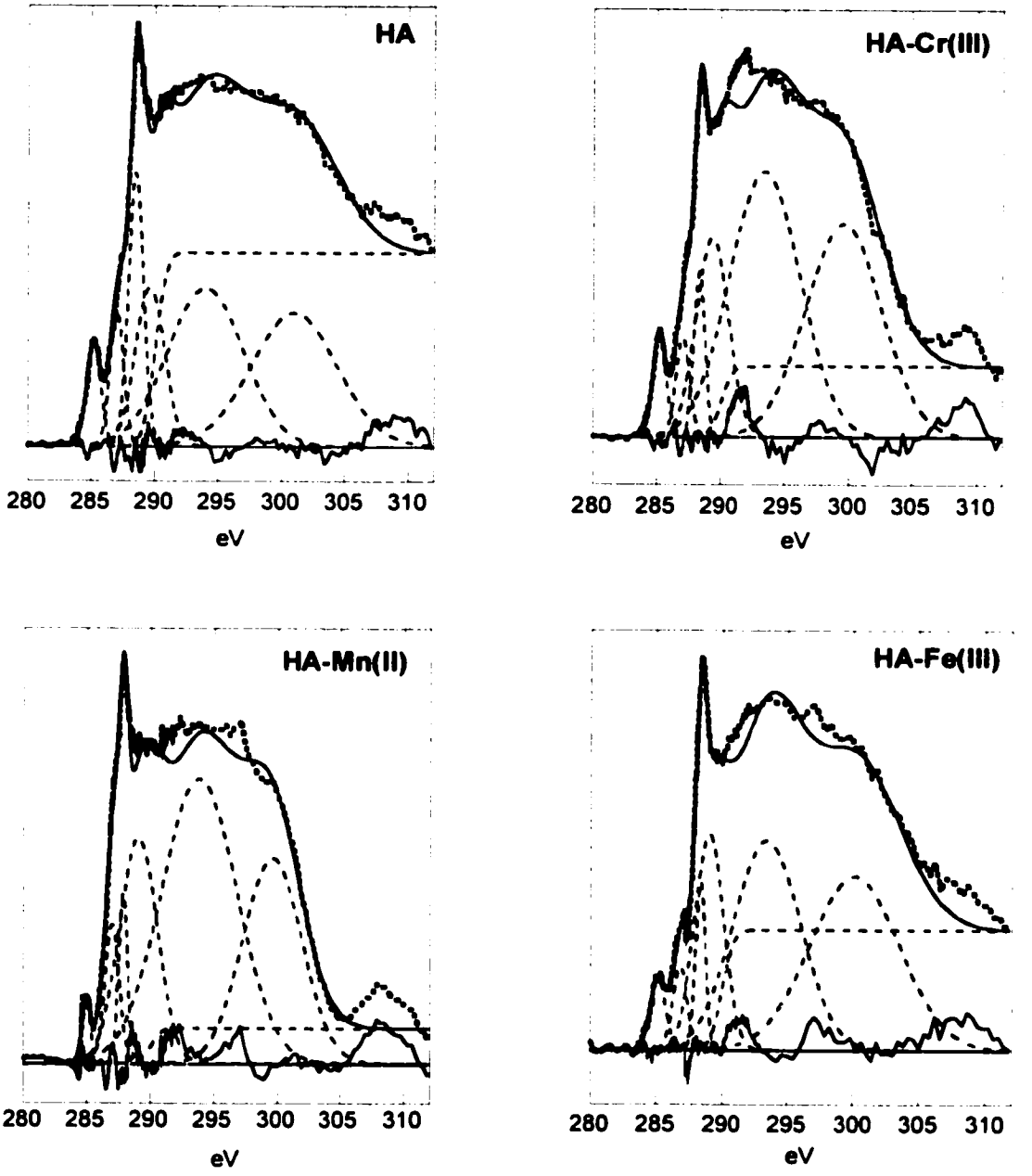

Figure 5.3 C1s NEXAFS spectra of HA reacted with Cr(III). Mn(II) and Fe(III) respectively, at pH 5, I = 0.1 M $NaNO_3$ and t = 24h. The experimental data are indicated with the dots line and the best fit and residual with the solid lines.

configurations of the d-shell. However, upon reaction with HA, only a small shift of 0.2 eV to the left of the C 1s(C=O) $\rightarrow 1\pi^*_{C=O}$ transitions to the left was observed.

Overall I conclude that in the presence of a hard cation, such as Al(III) no changes occur in the HA spectrum. The interactions of Al(III) with the carboxylic groups of the HA are mainly ionic. In the presence of Pb(II), Cr(III) and Fe(III), a covalent bond is formed, in the process of which part of the electron density of the carboxylic group is donated to the metals in the case of Pb(II) and subtracted in the case of Cr(III) and Fe(III). Upon reaction with Mn(II), a large shift of electron density Mn(II) to the carboxylic groups was observed, corresponding to a partial oxidation of Mn(II) to Mn(III).

5.4.4 Spatial distributions of functional groups in solution

In the preceding sections, the C-NEXAFS spectra shown were extracted from the image stack by averaging the spectrum over the complete HA particle. As we will show in this section, spatial heterogeneities exist within the HA particles itself. Principle component analysis (PCA) was used on the HA image stack used in the d-element reacted HA (Figure 5.3) to determine the number of mathematical components needed to reproduce the dataset. Since the corresponding eigenvalues of the PCA did not resemble chemical species and target transformations, fitting a reference spectrum with know spectral features with the eigenvalues, were unsuccessful, cluster analysis was used to group the data where unique variations

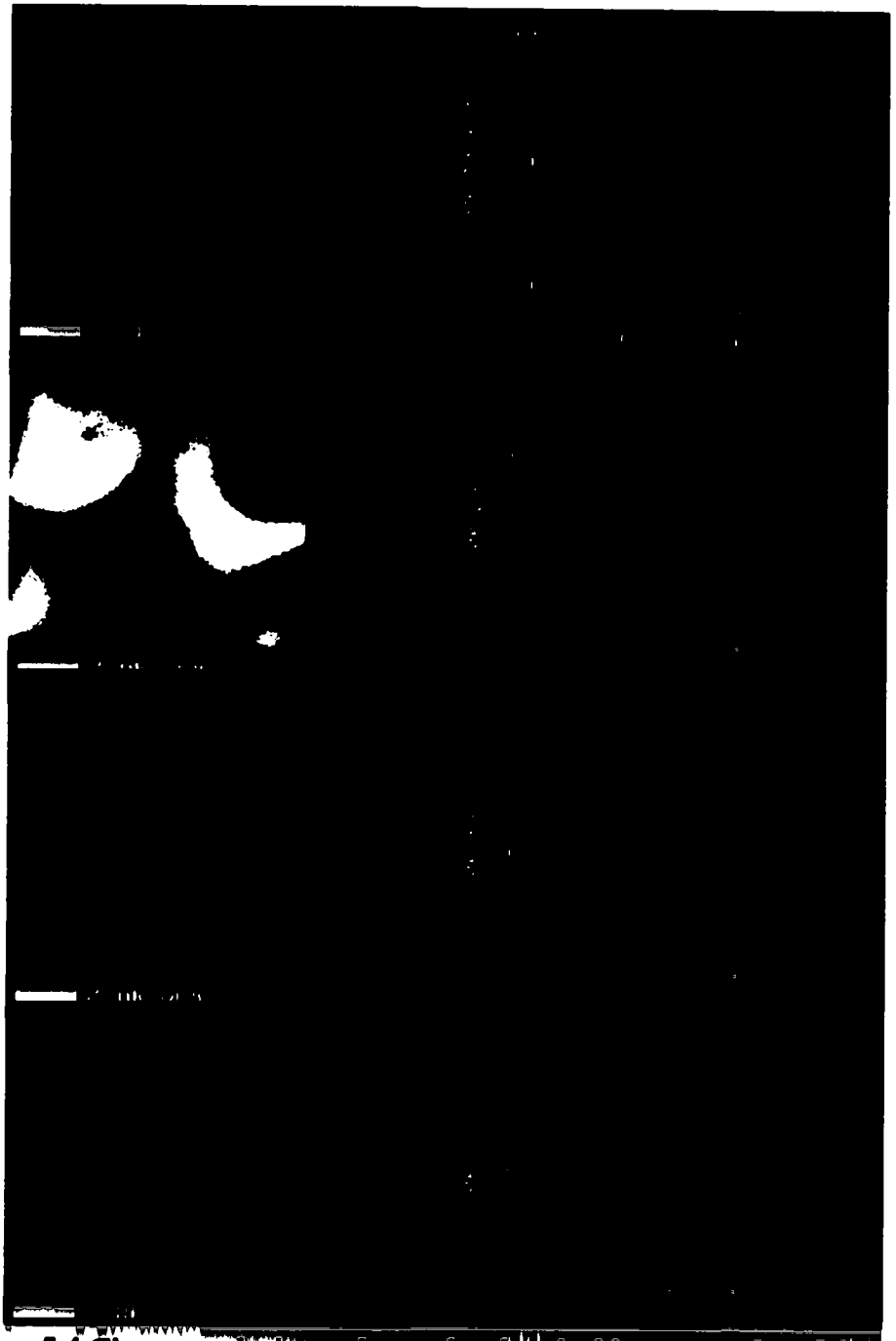

Figure 5.4 Cluster analysis results on the chemical heterogeneity of the HA, used in Figure 5.3. The images indicate the distributions of the different components in the image stacks, with the corresponding spectra on the right.

appear (Jacobsen et al., 2002). Five significant principal components were found in the HA stacks. Trials of different numbers of clusters showed that four clusters sorted the dataset into four regions: a mostly open region with very little optical density (blue region in Figure 5.4), a region enriched in carboxylic carbon (yellow region), a region with relatively more aromatic carbon (red region) and an intermediate region (green) which has no clear concentration of carboxylic or aromatic carbon and is also intermediate in position between that of the yellow and red region. This type of micro-heterogeneity of the HA was observed in all HA used in this study. The yellow region, corresponding to a concentration of carboxylic carbon, is concentrated at the rims of the HA particles, whereas the red region, concentrated in aromatic carbon, is concentrated in the interior of the HA particles. These results show that hydrophilic, carboxylic groups are concentrated at the outside of the HA particles and the hydrophobic, aromatic groups concentrated in the interior of the HA particle.

5.5 CONCLUSIONS

In this study we showed that scanning transmission microscopy, combined with C1s-NEXAFS spectroscopy offers unique possibilities to study humic substances *in situ*, without any extensive isolation procedure and with high spatial resolution. Using multivariate statistical analysis of the HA image stacks, it was found that hydrophilic, carboxylic groups are concentrated at the outside of the HA particles and the hydrophobic, aromatic groups concentrated in the interior of the HA particle. These results show the micro-heterogeneity within HA particles.

Upon reaction with metals, changes in the position of the C 1s(C=O) $\rightarrow 1\pi^*_{C=O}$ transitions (corresponding to the carboxyl functional groups) in the NEXAFS spectra were observed relative to that of HA. Upon reaction of HA with Al(III) no changes in the NEXAFS spectra were observed, indicating that Al(III) interactions with the carboxylic groups of HA are mainly ionic. Upon reaction with Pb(II), Cr(III) and Fe(III), a covalent bond is formed, in the process of which part of the electron density of the carboxylic group is donated to or subtracted from the metals. Upon reaction with Mn(II), a large shift of electron density from Mn(II) to the carboxylic groups was observed, corresponding to a partial oxidation of Mn(II) to Mn(III). Changing the pH of the bathing solution from 4 to 7 also lead to a 0.2 eV shift of the position of the carboxyl peak position to the left, this was explained by protonation of the carboxyl functional groups.

These results show that metal reactions with specific functional groups of HA can be studied with X-ray microscopy and C1s-NEXAFS spectroscopy *in situ* and with a high spatial resolution. It would be interesting to see if changes in the NEXAFS spectra are observed when the HA are reacted with metals such as Fe(II) which might donate some electron density to the carboxylic groups. *Ab initio* calculations to predict shift of this carboxyl peak position upon metal reaction are still largely wanted.

5.5 REFERENCES

Boese, J., A. Osanna, C. Jacobsen and J. Kirz. 1997. Carbon edge XANES spectroscopy of amino acids and peptides. *J. Electron. Spectros. Rel. Phen.* **85:** 9-15.

Buffle, J. and W. Stumm. 1994. General chemistry of aquatic systems, *In*: J. Buffle and RR. DeVitre (eds). Biological regulation of aquatic systems. CRC Press, Boca Raton, Fl.

Cody, G.D., R.E. Botto, H. Ade, S. Behal, M. Disko, S. Wirick. 1995. Inner-shell spectroscopy an imaging of a subbituminous coal: *In situ* analysis of organic and inorganic microstructures using C(1s)-, Ca(2p)-, and Cl(2s)-NEXAFS. *Energy Fuels* **9:** 525-533.

Cody, G.D., H. Ade,, S. Wirick, G.D. Mitchell, A. Davies. 1998. Determination of chemical-structural changes in vitrinite accompanying luminescence alteration using C-NEXAFS analysis. *Org. Geochem.* **28:**441-445.

Davies, G., A. Fataftah, A. Cherkasskly, E. A. Ghabbour, A. Radwan, S. A. Jansen, S. Kolla, M. D. Paciolla, L. T. Sein Jr., W. Buermann, M. Balasubramanian, J.

Budnick and B. Xing. 1997. Tight metal binding by humic acids and its role in biomineralization. *J. Chem. Soc., Dalton Transactions.* **21:** 4047-4060.

Ghabbour, E. A., G. Davies, K. O'Donaughy, T.L. Smith and M. E. Goodwillie. 1998. *In* Humic Substances. Structures, Properties and Uses. Davies, G. and E. A. Ghabbour (Eds.) The Royal Society of Chemistry: Cambridge.

Hitchcock, A.P. and D.C. Mancini. 1994. Bibliography and database of inner shell excitation spectra of gas phase atoms and molecules. *J. Electron. Spec. Rel. Phen.* **67:** 1-132.

Jacobsen C., S. Williams, E. Anderson, M.T. Browne, C.J. Buckley, D Kern, J. Kirz, M. Rivers and X. Zhang. 1991. Diffraction-limited imaging in a scanning-transmission X-ray microscope. *Opt. Commun.* **86:** 351-364.

Jacobsen, C., S. Wirick, G. Flynn, C. Zimba. 2000. Soft X-ray spectroscopy from image sequences with sub-100 nm spatial resolution. *J. Microscopy* **197:** 173-184.

Jacobsen, C., M. Feser, M. Lerotic, S. Vogt, J. Maser and T. Schäfer. 2002. Cluster analysis of soft X-ray spectromicroscopy data. *J. Phys IV France* **1:** 1-3.

Mao J.D., W.G. Hu, K. Schmidt-Rohr, G. Davies, E.A. Ghabbour, B. Xing. 2000. Quantitative characterization of humic substances by solid-state carbon-13 nuclear magnetic resonance. *Soil Sci. Soc. Am.* **64:** 873-884.

Myneni, S.C.B., J.T. Brown, G.A. Martinez, W. Meyer-Ilse. 1999. Imaging of humic substance macromolecular structures in water and soils. *Science* **286:** 1335-1337.

Myneni S.C.B. 2003. Soft X-ray spectroscopy and spectromicroscopy studies of organic molecules in the environment. *In* N.C. Sturchio, P., S.R. Fenter, M.L. Sutton and M.L. Rivers (eds.) Applications of Synchrotron Radiation in Low-Temperature Geochemistry and Environmental Science. Reviews in Mineralogy. Mineralogical Society of America. Washington. D.C.

Neuhausler U., C. Jacobsen, D. Schulze, D. Stott and S. Abend. 2000. A specimen chamber for soft X-ray spectromicroscopy on aqueous and liquid samples. *J. Synchrotron Rad.* **7:** 110-112.

Pearson, R.G. 1963. Hard and soft acids and bases. *J. Am. Chem. Soc.* **85:** 3533-3539.

Plaschke, M., J. Rothe, T. Schafer, M.A. Denecke, S. Pompe and K. Heise. 2002. Combined AFM and STXM *in situ* study of the influence of Eu(III) on the agglomeration of humic acid. *Colloid. Surf. A* **197:** 245-256.

Rothe, J., M.A. Denecke and K. Dardenne. 2001. Soft X-ray spectromicroscopy investigation of the interactions of aquatic humic acid and clay colloids. *J. Col. Interf. Sci.* **231:** 91-97.

Scheinost, A.C., R. Kretschmar, I. Christl and C. Jacobsen. 2001. Carbon group chemistry of humic and fulvic acid: A comparison of C-1s NEXAFS and ^{13}C-NMR spectroscopies. *In* Humic substances: Structure, Modes and Functions. Ghabbour E.A. and G. Davies (eds). The Royal Society of Chemistry, Cambridge, 39-47.

Schnitzer, M. 2000. A lifetime perspective on the chemistry of soil organic matter. *Adv. Agronomy* **68:** 1-58.

Schöll, A., R. Fink, E. Umbach, G.E. Mitchell, S.G. Urquhart and H. Ade. 2003. Towards a detailed understanding of the NEXAFS spectra of bulk polyethylene copolymers and related alkanes. *Chem. Phys. Let.* **370:** 834-841.

Shriver, D.F., and P.W. Atkins. 1999. Inorganic Chemistry. W.H. Freeman and Company, New York, NY.

Sparks D.L. 1995. Environmental Soil Chemistry. Academic Press, Inc. London.

Stevenson, F.J. 1994. Humus chemistry, genesis, composition, reactions. Wiley & Sons Inc.

Stöhr, J. 1992. NEXAFS spectroscopy. Springer-Verslag, Berlin.

Urquhart, S.G., A.P. Hitchcock, A.P. Smith, H. Ade, W. Lidy, E.G. Rightor, and G.E. Mitchell. 1999. NEXAFS spectromicroscopy of polymers: overview and quantitative analysis of polyurethane polymers. *J. Electron. Spec. Rel. Phen.* **100:** 119-135.

Urquhart, S.G. and H. Ade. 2002. Trends in the carbonyl core (C1s, O 1s) to π^* transition in the near edge X-ray absorption spectra of organic molecules. *Chem. Phys. Lett.* **322:** 412-418.

Chapter 6

OVERALL CONCLUSIONS AND RESEARCH NEEDS

The reactions that first row transition metals such as Ni or Zn can undergo in multi-sorbent systems, in which a variety of sorption mechanisms are available for metal uptake, are quite complex. Using novel, state of the art molecular scale spectroscopic and microscopic techniques in combination with macroscopic sorption and desorption studies, fundamental insights into the competitive mechanisms available for metal uptake in multi-sorbent systems were obtained in this dissertation research.

The research findings in this dissertation demonstrated that the presence of ubiquitous coatings such as humic acid and goethite coatings on clay mineral surfaces do affect metal sorption, but do not change the intrinsic metal sorption mechanisms to the underlying clay mineral surface. The effect of 1- and 5-wt % humic acid coatings on the Ni sorption mechanisms to the kaolinite surface was studied at pH 7.5. Special emphasis was placed in this study on getting a better understanding of the competing effects of organic coatings on the formation of stable surface precipitates, since previous research has shown that the incorporation of Ni in stable surface precipitates, in the absence of competing sorbents, lead to a significant reduction in metal bioavailability. It was found that Ni uptake kinetics and capacity increased significantly with increasing amounts of HA coated at the

kaolinite surface. However, the stability of the Ni sorption complex formed decreased with increasing amounts of HA coated at the kaolinite surface. A direct molecular probe, EXAFS spectroscopy, was used to investigate the local bonding environment of the sorbed Ni. EXAFS spectroscopy of the sorption samples revealed that both in the presence and absence of organic coatings, surface precipitates were formed. A nickel hydroxide was formed in the presence of a 5-wt% HA coating, whereas in the presence of a 1-wt% HA coating a more stable Ni-Al LDH was formed.

In another research project, Zn sorption complexes formed at the kaolinite surface, with and without the presence of an iron oxide coating, were studied at pH 5 and 7, using state of the art EXAFS spectroscopy as a molecular spectroscopic tool. It was found that at pH 5, Zn formed inner-sphere sorption complexes mainly with the kaolinite surface Al-OH groups. At pH 7, both the extent of the iron oxide coating and the reaction time determined the Zn sorption complex formed at the goethite-coated kaolinite interface. In the presence of a 6 wt% goethite coating, Zn was incorporated into a Zn-Al LDH surface precipitate. In the presence of a 10 wt% goethite coating, the initial dominant sorption mechanism was the formation of inner-sphere sorption complexes with the surface hydroxyl groups of the goethite coating. With increasing aging time, the inclusion of Zn into a Zn-Al LDH takes over as the dominant sorption mechanism. These results suggest that the formation of precipitate phases at clay mineral surfaces is thermodynamically favored over adsorption to the goethite coating.

There remains a need to use these molecular scale findings on metal sorption mechanisms in competing sorbent systems and implement them into current surface complexation and transport models. Specifically, these studies of metal complexation in multi-sorbent systems suggest that when given enough time, incorporation of many of the first row transition elements into surface precipitates may control the metal speciation at near neutral pH.

My dissertation research primarily utilized well controlled laboratory systems, to systematically study the effects of important reaction variables (pH, extent of coating and metal concentration) on the metal sorption mechanisms in multi-sorbent systems. However, understanding the chemistry of transition metals in natural systems, where reaction variables are not tightly controlled, and predicting the long-term risks to the environment should be one of the ultimate goals of fundamental research. To this end, the effect of *in situ* remediation on the speciation of Zn in a smelter contaminated soil was directly identified using the spectroscopic information gleaned from molecular scale laboratory Zn sorption studies. Comparison of the Zn speciation in a non-treated soil and an aluminosilicate- and compost- treated soil revealed no significant differences in speciation between the treated and non-treated soils 12 yrs after the application of the additives. Using state of the art micro-focused EXAFS spectroscopy, it was found that neo-formed Zn containing surface precipitates, whether a Zn-Al LDH or a Zn-phyllosilicate, made up 60 % of the total Zn fraction in these smelter

contaminated soils. Surface precipitates are therefore much more important in controlling the metal speciation at near neutral pH than traditionally thought. The surface precipitates in this soil formed a unique possibility to study its long term Zn sequestration possibilities, in that the natural pH of the soil was near neutral and high Zn concentrations have been present for at least a century. The fact that the precipitates were not stable when the pH was lowered indicated that no significant stabilization of surface precipitates takes place in natural soil environments. These results reiterate the need for determining important thermodynamic parameters, such as the Gibbs free energy of formation, for the precipitate phases formed in these systems.

Biopolymers (humic substances) are the big unknowns when it comes to understanding metal sorption mechanisms in the environment. Both the macromolecular structure and functional group chemistry of these polymers determines the reactivity toward metals. In an attempt to study for the first time the chemistry of biopolymer-metal interactions *in situ* and with high chemical and spatial resolution, the use of scanning transmission microscopy, combined with C1s-NEXAFS was explored to study these interactions. Preliminary results showed the chemical micro-heterogeneity within nano-sized humic acid (HA) particles in solution. The position of the C 1s(C=O) $\rightarrow 1\pi^*_{C=O}$ transitions in the NEXAFS spectra (corresponding to the electronic transitions in carboxyl functional groups) was sensitive to reactions with metals and could be used to probe the affinity of

different metals for the carboxylic functional groups. Al(III), which is a hard cation, formed an ionic bond with the carboxyl groups, which resulted in no shifts in the carboxyl peak position of the HA C(1s) NEXAFS spectra. Pb(II), Cr(III) and Fe(III), formed covalent bonds with the carboxylic groups. By forming covalent bonds part of the electron density of the carboxylic group (0.2 eV shift) is shared with the metals. Upon reaction with Mn(II), a large shift of electron density from Mn(II) to the carboxylic groups to was observed, corresponding to a partial oxidation of Mn(II) to Mn(III).

These results only revealed a tip of the iceberg of the possibilities of X-ray microscopy and C1s-NEXAFS spectroscopy as *in situ* techniques to study the chemistry of biopolymers. *Ab initio* calculations to predict shifts of this carboxyl peak position upon metal reaction are still needed. One of the many interesting research questions remaining is to study the effect of metals such as Fe(II), which might donate some electron density to the carboxylic groups, on the C1s-NEXAFS spectra. This tool may ultimately be utilized to directly reveal the chemistry of large natural biopolymers, without any pre-extraction and with a high spatial resolution.